Mathematical modeling of free-flooding anti-roll tanks

M.A. van Slooten

Master's thesis

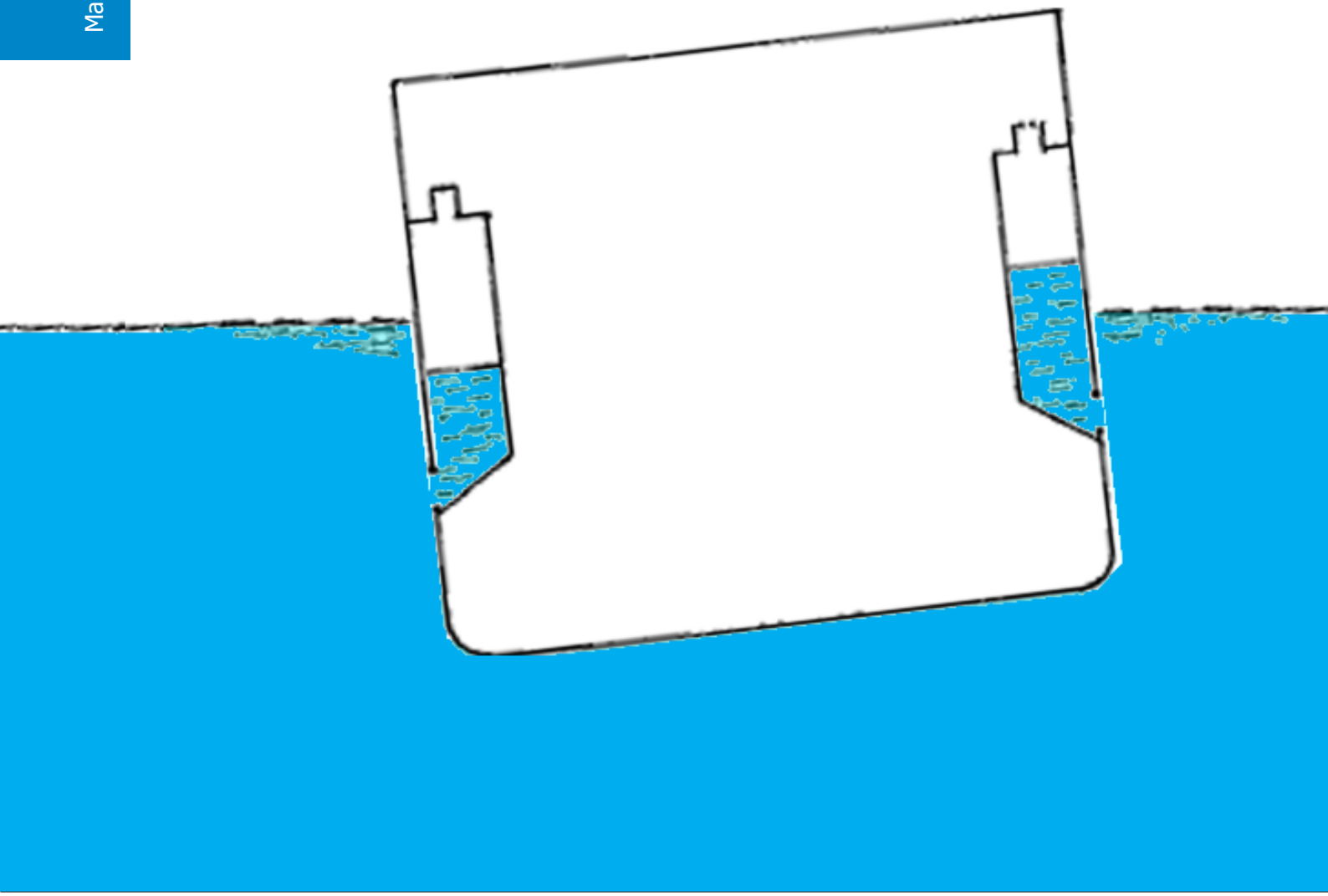

TU Delft Delft University of Technology

Challenge the future

Mathematical modeling of free-flooding anti-roll tanks

by

M.A. van Slooten

in partial fulfillment of the requirements for the degree of

Master of Science
in Marine Technology - Specialisation Ship Hydromechanics

at the Delft University of Technology,
to be defended publicly on Friday April 11, 2014 at 14:00 AM.

Student number:	1283588	
Supervisor:	Prof. dr. ir. R. H. M. Huijsmans	
Thesis committee:	Ir. K. van den Berg,	Vuyk Engineering Rotterdam
	Ir. N. Carette,	MARIN
	Dr. ir. J. A. Keuning,	TU Delft
	Ir. K. Visser SBN-b.d.,	TU Delft

Preface

The thesis project presented in this report has been carried out at Vuyk Engineering Rotterdam. It highlights an understudied topic in the category anti-rolling devices: the modeling of free-flooding anti-roll tanks. As these type of anti-roll devices have only sporadically been considered and applied over the past century, their modeling has hardly been addressed. The findings on the most current mathematical model available are presented here.

I would like to thank my supervisors at Vuyk Engineering Rotterdam, ir. Kuno van den Berg, and at Delft University of Technology, prof. dr. ir. R.H.M. Huijsmans in helping me deciphering all the different components and influences on the mathematical model presented in this report. In that context I must also include ir. Nicolas Carette for his insights into essential conditions for successful simulation of the problem at hand. Besides the members of my thesis committee my special thanks goes out to Elena Stroo-Moredo MSc, who agreed to be my mentor for this project and has taken the trouble to review every scrap of text I have produced. And lastly, the following people have been very important to me: my colleagues at Vuyk Engineering Rotterdam, to whom I could always turn with questions, and of course to all my friends and family, who have supported me throughout my studies.

M.A. van Slooten
Delft, March 2014

Contents

List of Figures

List of Tables

Nomenclature

α	ration of vent or crossover area to tank free surface area
β	ratio of flooding port area to tank free surface area
$\Delta H(_j)$	complex amplitude of differential pressure head across one flooding port
γ	nondimensional half U-tube length
ω	wave frequency
$\overline{GM}_t$	transverse metacentric height
$\overline{U}$	complex air pressure coupling constant
$\overline{V}(_j)$	complex air pressure constant (on one side)
Φ_D	diffraction potential
Φ_I	incident wave potential
Φ_m	radiation potential, m-th mode
$\Upsilon(_j)$	tank water motion (on one side)
Υ_{jo}	tank water level on the opposite side
ξ_m	complex ship motion amplitude, m-th mode
ζ_a	regular wave amplitude
$A(s)$	cross-sectional area of tank at point s on the streamline
A_0	area of free surface in tank
C	dynamic arm of tank moment
C_f	coupling coefficient of tank into ship motion
C_{ad}	effective discharge coefficient for air vent or crossover
C_{cr}	critical linear tank damping coefficient
C_{wd}	effective discharge coefficient flooding port
d_w	distance between flooding port and equilibrium tank water level
d_{ew}	distance between flooding port and still-water line
G_j	complex coefficient of tank transfer function on one side
H_{dyn}	dynamic water pressure head
l_{tk}/b_{tk}	length/width of tank
p_0	equilibrium air pressure in tank
p_u	dynamic air pressure in tank
p_{atm}	atmospheric pressure
R_1	equilibrium pressure in head of water
R_3	dimensional constant for dynamic air pressure analysis

R_Δ linearized discharge coefficient air crossover

s streamline coordinate

T_φ natural period of roll

T_{tk} tank transfer period

v_w instantaneous vertical velocity along the streamline

x_{tk} longitudinal location of centroid of equilibrium tank free-surface, positive to bow

y_{tk} lateral location of centroid of equilibrium tank free-surface, positive to port

Z_{tk} motion of isolated tank

$z_{w,j}$ wave elevation at the flooding port on one side

DoF Degrees of Freedom

1

Introduction

1.1. Background

A growing area in the offshore industry is the development of offshore wind farms. As the demand for clean energy has increased, so did interest in creating energy using wind turbines. Better wind speeds are available offshore compared to on land and complaints from local residents about visual pollution are largely diminished. A high degree of precision is needed to assemble the wind turbine components. It is impossible to position a component in the right place if the ship experiences significant motions. As the offloading of wind turbine components progresses the metacentric height of the ship varies greatly, in turn influencing the ship motions. A way to minimize ship motions in all the loading conditions is attractive as it will extend the operational window of the offshore installation vessel.

A notorious movement for interruption of operations is the roll motion of the ship, which can become very large at resonance frequency, thus the focus for motion reducing methods is usually on reducing the roll motion specifically. The roll motion can be reduced by installing a device, which counteracts the heeling moment with an opposing moment. The possibilities for such a device arranged by type of mass are listed in table 1.1. In recent years there is an increasing interest in the application of free-flooding anti-roll tanks.

In 2009/2010 Vuyk Engineering Rotterdam (VER) performed an investigation into *external* free-flooding anti-roll tanks for the Sea Trucks Group in cooperation with MARIN. The addition of free-flooding anti-roll tanks in the form of sponsons to two existing pipelaying crane ships was studied [1],[2]. In figure 1.1 the sponson is shown. A time domain mathematical model for pure roll (single degree of freedom and a dynamic water pressure based on the velocity head) was developed in Excel with input of ship motions in the form of response amplitude operators (RAOs) from AQWA (3D diffraction program). This model is called the VER Model from here on. The decrease in roll motion was estimated to be about 37% for free-flooding tanks with a capacity of 2.75% of the ship's displacement.

For verification of the results the same ship and lay-out of the free-flooding anti-roll tanks

SOLID	FLUID
wheel	fins or rudder
gyroscope	doughnut tank
unbalanced wheel	U-tube tanks
pendulum	free-surface tanks
rolling ball	free-flooding tanks

Table 1.1: Types of anti-roll systems [3]

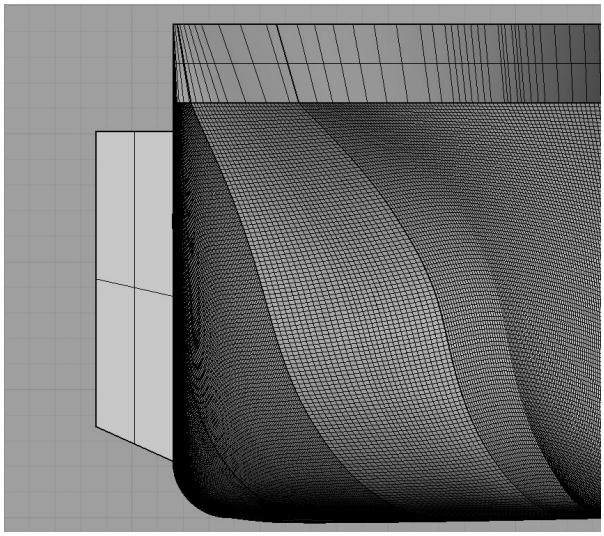

Figure 1.1: External free-flooding anti-roll tanks in the form of sponsons

was revisited at the Maritime Research Institute Netherlands (MARIN) [4],[5]. This study was conducted in Fredyn (3D diffraction) and ReFRESCO (Computational Fluid Dynamics - CFD). Their conclusion was that the damping was well predicted by the VER Model, but that in their model the initial transverse stability ($\overline{GM}_t$-value) was significantly altered by the addition of the anti-roll tanks on the outside of the ship. According to the study the anti-roll tanks only compensate the unfavorable change of stability by the addition of the tanks and do not improve the stability of the ship in the original situation.

On account of these studies the customer was advised not to mount sponsons on the pipelaying vessels, since the investment would be disproportionate to the expected damping of the rolling motion. This result was disappointing, especially in the light that experiments suggest that free-flooding anti-roll tanks are effective roll dampers. It is thought that internal tanks will give better results than external tanks. In figure 1.2 an application of an internal free-flooding anti-roll tank is shown.

1.2. Why free-flooding tanks

One way of stabilizing a ship is by anti-roll tanks. There are three kinds of anti-roll tanks, shown in figure 1.3: the free-surface, U-tube and free-flooding tanks. A free-flooding tank is

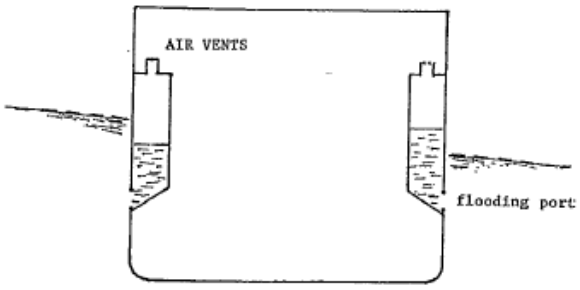

Figure 1.2: Internal free-flooding tanks

considered to resemble a U-tube tank, but with an external crossover duct instead of an internal crossover duct. Of these the free-flooding anti-roll tank is the least known and applied. The reason is that the performance of these tanks is reduced due to a momentum drag penalty incurred at forward speeds. However, at low forward speeds this drag penalty is negligible. If desirable, the tanks could be closed off and emptied for transit.

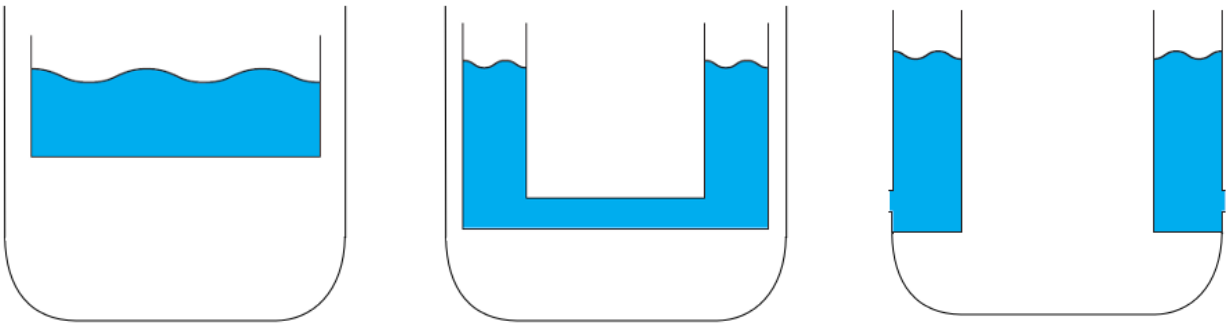

(a) free-surface tank (b) U-tube tank (c) free-flooding tank

Figure 1.3: Types of anti-roll tanks

The reason for choosing anti-roll tanks as a stabilization device for a vessel is, among others, the relatively low cost of building the system and the fact that they continue to work when the vessel is stationary, in contrast to fin-type anti-rolling devices (save for active fin stabilizers). The second is interesting for offshore vessels, which remain stationary or sail at very low speeds in operation. Also, when using free-flooding tanks in operation, the momentum drag penalty incurred at higher forward speeds is avoided. Active fin stabilizers have been heavily developed in recent years and are now more effective at zero speed, but are a lot more expensive than anti-roll tanks.

Offshore installation vessels generally have a broad beam, which is necessary to have enough deck space for the storage of the installation components and generate enough buoyancy and stability during for instance lifting. As the components on board are installed the loading condition of the vessel changes: the vessel sits higher in the water and the metacentric height increases. The metacentric height is inversely related to the roll period, so as the first rises the

second decreases and the natural rolling period comes closer to the range of most commonly found waves. When the wave period is close to the natural rolling period the ship motions are the largest, which is detrimental to the operation. The $\overline{GM}_t$ is generally lowered again by adding water ballast as the operation progresses. To further minimize roll motions during operations anti-roll tanks can be used.

The center part of the vessel is generally occupied by machinery and installation components. U-tube tanks and free-surface tanks both require a considerable amount of space in the center part of the vessel to accommodate the crossover connection. Free-flooding anti-roll tanks do not require a considerable amount of space in the center part of the vessel, but can be built into the sides where, in the case of offshore installation vessels, due to the broad beam plenty of space is available. This makes free-flooding tanks the most suitable for retrofitting existing ships. Of course, free-flooding tanks also have disadvantages. These are highlighted in § 2.2.

1.3. Aims

The basis for this graduation project is the modeling of *internal* free-flooding anti-roll tanks, with as intended result a suitable method or application for use at VER. The goal of this thesis is, therefore, not to develop a complete new theory for predicting the performance of a free-flooding tank, but to find the most suitable analytical mathematical model and develop the practical application in which this theory is applied.

1.4. Programs

AQWA ANSYS AQWA software is an engineering analysis suite of tools for the investigation of the effects of wave, wind and current on floating and fixed offshore and marine structures. This software package is well recognized in the offshore and marine industry. The RAOs in this report are calculated using the 3D diffraction software AQWA-LINE [6] and the time domain simulations are performed using AQWA-NAUT [7].

> [AQWA-LINE] can simulate linearized hydrodynamic fluid wave loading on floating or fixed rigid bodies. This is accomplished by employing three-dimensional radiation/diffraction theory and/or Morison's equation in regular waves in the frequency domain.
>
> The real-time motion of a floating body or bodies while operating in regular waves [or irregular waves] can be simulated with [AQWA-NAUT], in which nonlinear Froude-Krylov and hydrostatic forces are estimated under instantaneous incident wave surface. External forces can be applied to the bodies at each time step imported or defined by a user-written dynamic-link library. The convolution approach is used to account for the memory effect of the radiation force. […] The program requires a full hydrostatic and hydrodynamic description of each structure. This can be transferred directly from a backing file created as a result of an AQWA-LINE analysis.

SCILAB

SCILAB [8] is an open source, cross-platform numerical computational package and a high-level, numerically oriented programming language. It can be used for signal processing, statistical analysis, image enhancement, fluid dynamics simulations, numerical optimization, and modeling, simulation of explicit and implicit dynamical systems and (if the corresponding toolbox is installed) symbolic manipulations. SCILAB is the most complete open source alternative to MATLAB.

The language provides an interpreted programming environment, with matrices as the main data type. By using matrix-based computation, dynamic typing, and automatic memory management, many numerical problems may be expressed in a reduced number of code lines, as compared to similar solutions using traditional languages, such as Fortran, C, or C++.

1.5. Outline

First, publicly available information is explored and assessed in the literature review, chapter 2. Based on the findings in this chapter the most appropriate mathematical model is chosen. The motivation behind this model and its parts is elaborated upon in the chapter on the underlying theory of the model (chapter 3). The problem, as set forth in this chapter, is solved both in the time domain and the frequency domain. The way of solving the problem in both domains is part two of the chapter on theory. The results from the simulations in the time domain and the frequency domain are given in chapter 4. No experiments were performed to actually quantify the outcomes due to time restrictions, so the model is only evaluated upon its accuracy as a mathematical model. Some restrictions to its application are explored here. Finally, in chapter 5, conclusions and recommendations are drawn on the effectiveness of free-flooding tanks and how to improve the results in this report.

2

Literature review

2.1. History

Much has been written about roll and roll stabilization. The term 'roll stabilization' is in fact a misnomer according to Goodrich [2.1], since all ships operating under normal conditions are inherently stable. A device fitted to a ship to reduce the roll should be called a 'roll damper'. However, the term roll stabilization has persisted and is commonly used in the literature concerning roll reduction.

All ships in waves encounter roll motions, but before the industrial revolution roll motions were not considered a problem and therefore did not constitute an important part in ship research. The reason for this is that sails damp the roll motions of the ship, which was the primary means of powering ships in the Age of Sail. At the end of the 19th century motorized vessels started replacing sail driven vessels and due to the differing transverse stability these regularly experienced excessive roll motions.

Froude [2.2] was the first to describe this problem mathematically. He argued that roll motion is a consequence of fluid pressure acting on the hull and not of the impact of waves on the side of the ship, which is a view still held today. The first ship to employ an anti-roll tank (free-surface) was the *HMS Inflexible*. The results of this full scale experiment has been reported by Watts [2.3, 4]. The success was ambiguous: on the one hand the roll motion of the ship was significantly reduced in the resonance region, on the other hand a loss of stability was found outside the resonance region due to the free-surface effect. The free-flooding tanks, which he called sea-ducted tanks, were conceived by Frahm [2.6] in 1911 and he planned to evaluate this concept in future research. Unfortunately, no record of this research can be found. In the 1930's these free-flooding tanks were built into several passenger ferries in Germany (figure 2.1, see Hort [2.7] and Feld [2.8]). There is scant data on the performance of the anti-roll tanks, because passengers insisted that the anti-roll tanks remain in service for their comfort.

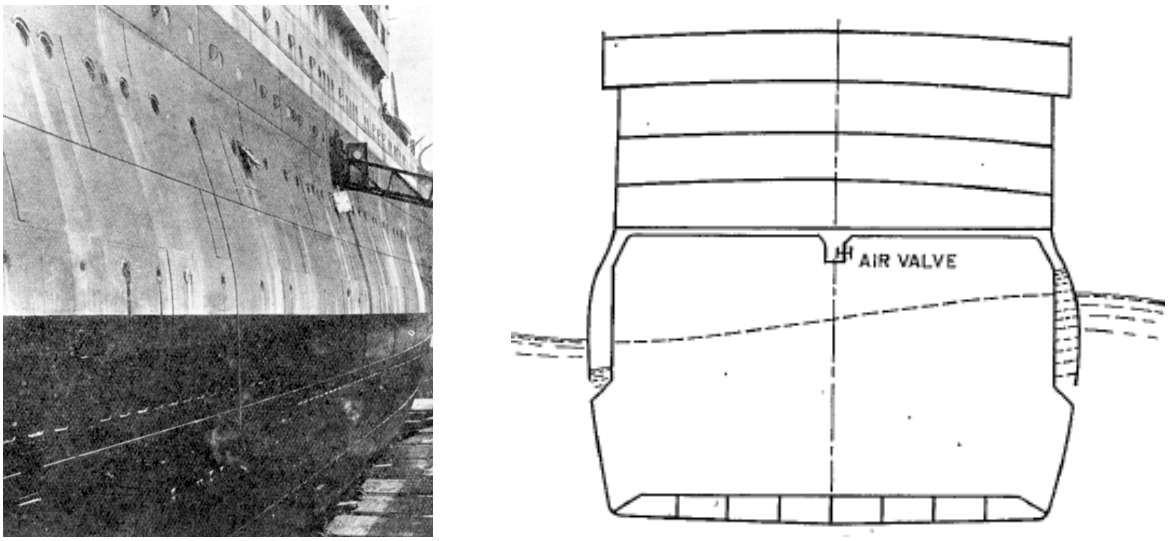

Figure 2.1: Free-flooding anti-roll tanks on the Deutschland [2.5]

Around the same time (1931) free-flooding tanks were retrofitted to 6 US Navy cruisers of the Pensacola and Northampton classes, see figure 2.2. These ships were known for their cruel behavior in rough seas. The free-flooding tanks installed on these war ships did not have an air cross connection constructed between the port and starboard tanks due to space restrictions, thus differing from the original Frahm tanks. Despite initial misgivings the tanks were successful in reducing the roll motion by 30-40% and increasing the roll period by 20%. Unfortunately, even though it is the best documented application of free-flooding tanks, there is not a lot of measured data on these installations as experiments were suspended due to the outbreak of World War II.

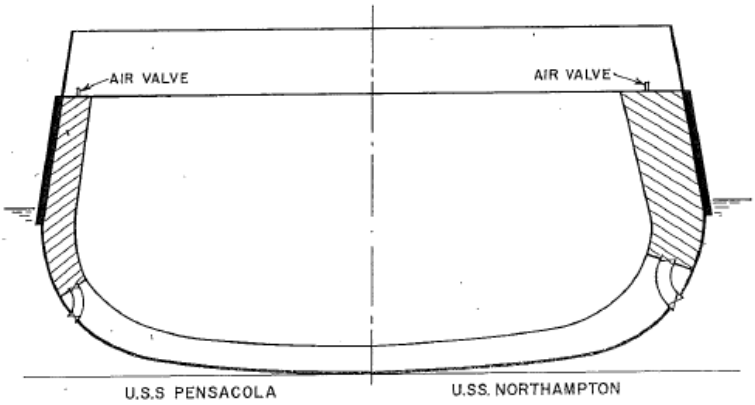

Figure 2.2: Free-flooding anti-roll tanks fitted on the Pensacola and Northampton classes

Even though the free-flooding anti-roll tanks were effective, the system fell into general disuse after these applications. According to Webster et al. [2.9] this is probably due to the reduction in effectiveness under the operating conditions of most ships and the amount of maintenance that the tanks require.

For the next decades not a lot of research is done into free-flooding anti-roll tanks, but only into free-surface and U-tube tanks. At the end of the eighties interest is rekindled for offshore application. No records could be found of actual instances, but variations of free-flooding anti-roll tanks were developed and installed. The best known commercial development from this period is the *Slo-Rol* system by SEATEK Corporation.

The US Navy also renews its interest in free-flooding anti-roll tanks at this time, because retrofitting such a device (without a crossover duct) in an existing (war) ship was the only feasible option. Webster et al. [2.9] concluded that properly designed free-flooding anti-roll tanks can achieve a useful amount of roll stabilization, but that the added resistance penalty they generate could make such systems unattractive for higher ship operating speeds. The free-flooding tanks were never fitted to the object of study (the USN Midway), even though the study did show a possible reduction of the roll motion with 48%.

2.2. Characteristics free-flooding anti-roll tank

The above-mentioned momentum drag is proportional to the ship speed squared and makes the free-flooding anti-roll tank increasingly unattractive with increasing speed. Mostly they are applied in situations where the floating object is stationary. There are also some other disadvantages to free-flooding anti-roll tanks besides the drag penalty, such as high maintenance level due to corrosion of the tank wall by the seawater. On the other hand, anti-roll tanks in general are appreciated for their simplicity, low cost, adaptability to temporary use (close flooding ports or vents) and precisely because they still damp the roll motion at low or even zero speed (Vasta *et al* [2.10]). Moaleji and Greig [2.11] submit that free-flooding anti-roll tanks are ideally suited for multi-hulls, because their side hulls are well separated providing a large lever arm and subsequently less water is required to achieve a given moment.

Possible locations on the hull of the flooding ports of the free-flooding anti-roll tanks, visualized in figure 2.3, are in the bottom of the hull or in the side. If the flooding ports are located in the side of the hull around the water line ventilation can occur for large roll angles.

In contrast to free-surface tanks the free-flooding anti-roll tanks cannot be tuned with water level, but by controlling the air flow between the port and starboard tanks and/or choosing or varying the shape and size of the flooding ports and restrictions/baffles. This limited control can be extended to active control by valves on top of the tanks or a connecting air duct (passive or active control). The active free-flooding tank concept was developed in the early 1960's by Bell and Walker [2.12] (figure 2.4). Air at a low pressure is supplied to a pipe connecting the tops of the tanks, when the ship is on an even keel the water is blown out of the tanks. At low pressure the air pressure can be applied passively or actively. For high pressure air flow the system of anti-roll tanks needs to be specially adapted.

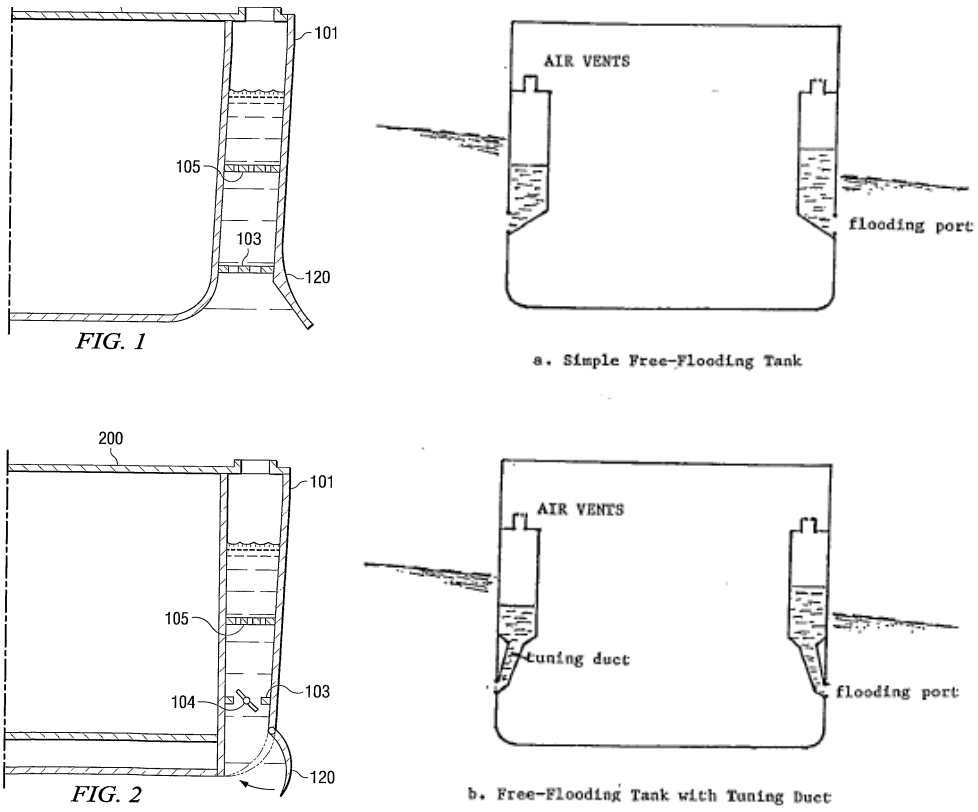

(b)

Figure 2.3: Possible locations and shapes of flooding ports

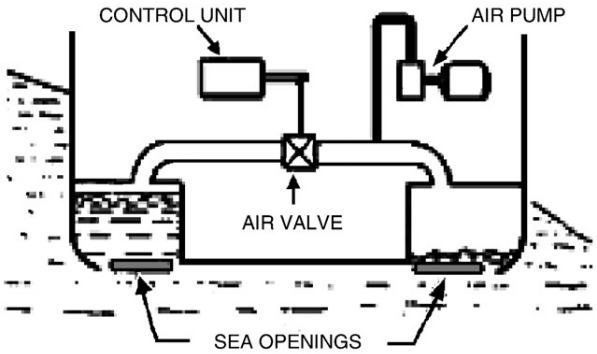

Figure 2.4: Active anti-roll tank

2.3. Mathematical modeling

Of the six degrees of freedom, roll is one of the easiest to control since the hull damping is low and restoring forces are relatively small. The factors that influence roll response of different vessels are (Surendran [2.13]):

- the ratio between the natural period of rolling and the encountering period of wave;
- the shape of the hull, its stability, total weight and buoyancy;
- the wave steepness, h/λ, where h and λ are wave height and length respectively;

- the damping efficiency of the underwater parts of the hull;
- the encountering speed of wave.

Ibrahim and Grace [2.14] give a nice review of the development of modeling ship roll dynamics through the years. From quite early on most authors were in agreement that modeling the roll motion non-linearly was necessary, especially in the resonance region and for large-amplitude motions. However, this is not easy as both the restoring forces and the damping terms are (highly) non-linear. It becomes even more complicated when coupling of the roll motion with other motions is considered.

Authors mostly agree that the roll motion cannot be considered to be uncoupled, but do not agree with what other motion direction the roll motion should be coupled. For example, according to Barr [2.15] it is necessary to consider coupled roll-sway motions in order to predict the rolling motions, which was also adopted by Kleefsman [2.16]. Ibrahim and Grace [2.14] instead look at the coupling with pitch, whilst Dallinga [2.17] argues for the coupling of roll and yaw motions.

The uncoupled roll motion equation is still used regularly by researchers, especially when modeling non-linear large-amplitude motions. Chen *et al* [2.18], for example, reduce a 3DoF model to a 1DoF model by incorporating quasi-static heave dynamics and sway velocity. Taylan set up a non-linear uncoupled mathematical model to predict the roll response, where he alternatively used the Krylov–Bogoliubov asymptotic method [2.19] and the generalized Duffing's method [2.20] as the solution procedure.

Whichever method is used, the nonlinear damping term is the one term which can be varied. The restoring term is generally described by an odd-order polynomial. Cubic and quintic expressions are the most favorable descriptions, but it is not unusual to come across a seventh degree polynomial. The roll damping of the ship can also be estimated:

1. based on experience,
2. based on model or full scale tests,
3. with Ikeda's empirical method as recounted by Himeno [2.21],
4. with a polynomial containing a linear and a non-linear damping term (Taylan [2.20]).

Because of the low roll damping of ships, large responses are experienced under resonance conditions i.e. the amplification factor for roll is high at resonance. Ship roll stabilization has therefore received (and still receives) considerable attention from ship designers. To counter the rolling motion various anti-roll systems were conceived. The different anti-roll systems are categorized neatly on the basis of working principles by Chadwick [2.22], as is shown in table 2.1.

	internal		external	
	acceleration	displacement	acceleration	displacement
fins or rudder			x	
doughnut tank	x			
completely-filled free-flooding tanks	x		x	
free-surface tanks	x	x		
U-tube tanks	x	x		
partially filled free-flooding tanks	x	x	x	

Table 2.1: Working principles of fluid anti-roll systems

The basic principle all anti-roll tank types have in common is the transfer of fluid from starboard to port side and vice versa, with a certain phase lag with respect to the ship's rolling motion; thus, a counteracting moment is provided. Many surveys and comparisons have been executed to establish the most suitable anti-roll device, such as Chadwick [2.23] and Smith and Thomas III [2.24].

Theoretical studies on U-tube tanks are generally based on an equivalent double pendulum theory (Stigter [2.25]): the mass of the tank fluid can be regarded as a second pendulum attached to the pendulum representing the ship, over most of the roll frequency range. The physical behavior of fluid in a free-surface tank is generally classed in the group of shallow water waves (Verhagen and Van Wijngaarden [2.26]). Chu *et al* [2.27] expand this theory since the main stabilizing action is created by a bore traveling up and down the tank's width, which makes the fluid flow essentially non-linear, and the proposed quasi-linear model was deemed insufficiently capable of modeling its behavior.

Interestingly, not all authors agree that free-surface effects due to the fluid motion should also be taken into account for U-tube tanks: Smith [2.24] argues that the free-surface effect in tanks with two small areas instead of one large one (U-tube tanks) is negligible and only the oscillating columns of water provide damping and restoring moments. Gawad [2.28] on the other hand believes that the fluid motion in the tank cannot be neglected, because violent sloshing can occur inside a tank if damping in the tank is low.

From table 2.1 it can be seen that free-flooding tanks incorporate both effects that occur in the U-tube and free-surface tanks, as well as interaction with the environment. It follows that mathematical models for U-tube and free-surface tanks are not directly applicable to free-flooding tanks, which is why Webster et al. [2.9] developed a specific mathematical model for free-flooding anti-roll tanks compatible with contemporary linearized ship motions theory for the response to regular waves. The forces and moments generated by the ship motions and the motion of the fluid in the tank are modeled separately and then combined in a coupled set of equations. This approach was, for example, adopted by Moaleji and Greig [2.29].

2.4. Conclusion

The model for free-flooding anti-roll tanks developed by Webster et al. in 1988 [2.9] is considered to be the most suitable mathematical model.[1] The reasons for this choice are:

- All the working principles of a free-flooding tank, as shown in table 2.1, are included in the model. One such aspect is the acceleration of internal tank water due to unsteady flow, which is not taken into account in the VER Model.
- Tank dynamics are modeled independent of ship dynamics, simplifying the problem to be solved. This is allowed when the relation between the input and output (transfer function) is a linear time-invariant system.
- Air pressure effects for connected tanks and separately vented tanks are included in the model.
- It is the only mathematical model for free-flooding anti-roll tanks to be found in literature. The reason for this is that existing free-flooding anti-roll tank systems have been developed commercially and any modeling and calculations done for the system is subject to professional confidentiality.

[1] Note that sloshing is not included in this model.

2.5. Bibliography literature

[2.1] G. J. Goodrich, *Developmnent and design of passive roll stabilisers,* Transactions - The Royal Institution of Naval Architects (RINA) **111**, 81 (1969).

[2.2] W. Froude, *On the rolling of ships,* Transactions - The Institution of Naval Architects **2**, 180 (1861).

[2.3] P. Watts, *On a method of reducing the rolling of ships at sea,* Transactions - The Institution of Naval Architects **24**, 165 (1883).

[2.4] P. Watts, *The use of water chambers for reducing the rolling of ships at sea,* Transactions - The Institution of Naval Architects **26**, 30 (1885).

[2.5] *Anti-rolling tanks on hamburg-amerika liners.* Brodie Collection, La Trobe Picture Collection, State Library of Victoria (between 1885 and 1946).

[2.6] H. Frahm, *Results of trials of the anti-rolling tanks at sea,* Transactions - The Institution of Naval Architects **53**, 183 (1911).

[2.7] H. Hort, *Beschreibung und versuchsergebnisse ausgef uhrter schiffsstabilisierungsanlagen,* Jarbuch der Schiffbautechnische Gesellschaft (STG) **35**, 292 (1934).

[2.8] E. Feld, *Beitrag zur schlingerd ampufungsfrage unter besonderer berucksichtigung des framschen tanks,* Jahrbuch der Schiffbautechnischen Gesellschaft (STG) **38**, 289 (1937).

[2.9] W. C. Webster, J. F. Dalzell, and R. A. Barr, *Prediction and measurement of the performance of free-flooding ship antirolling tanks,* Transactions - Society of Naval Architects and Marine Engineers (SNAME) **96**, 333 (1988).

[2.10] J. Vasta, J. D. Giddings, J. J. Stilwell, and A. Taplin, *Roll stabilization by means of passive tanks,* Transactions - Society of Naval Architects and Marine Engineers (SNAME) **69**, 411 (1961).

[2.11] R. Moaleji and A. R. Greig, *On the development of ship anti-roll tanks,* Ocean Engineering **34**, 103 (2007).

[2.12] J. J. Bell and W. P. Walker, *Activated and passive controlled fluid tank system for ship stabilization,* Transactions - Society of Naval Architects and Marine Engineers (SNAME) **74**, 150 (1966).

[2.13] S. Surendran and J. Venkata Ramana Reddy, *Numerical simulation of ship stability for dynamic environment,* Ocean Engineering **30**, 1305–1317 (2003).

[2.14] R. A. Ibrahim and I. M. Grace, *Modeling of ship roll dynamics and its coupling with heave and pitch,* Mathematical Problems in Engineering **2010**, unknown (2010).

[2.15] R. A. Barr and V. Ankudinov, *Ship rolling, its prediction and reduction using roll stabilization,* Marine Technology **14**, 19 (1977).

[2.18] S.-L. Chen, S. W. Shaw, and A. W. Troesch, *A systematic approach to modeling nonlinear multi-DOF ship motions in regular seas,* Journal of Ship Research **43**, 25 (1999).

[2.19] M. Taylan, *Solution of the nonlinear roll model by a generalized asymptotic method,* Ocean engineering **26**, 1169 (1999).

[2.20] M. Taylan, *The effect of nonlinear damping and restoring in ship rolling,* Ocean Engineering **27**, 921 (2000).

[2.21] Y. Himeno, *Prediction of Ship Roll Damping-A State of the Art*, Tech. Rep. 239 (University of Michigan, 1981).

[2.22] J. H. Chadwick, *On the stabilization of roll,* Transactions - Society of Naval Architects and Marine Engineers (SNAME) **63**, 237 (1955).

[2.23] J. H. Chadwick, *Ship stabilization in the large: a general analysis of ship stabilization systems*, Tech. Rep. 041-113 (Stanford University, Stanford, California, USA, 1953) for Office of Naval Research (contract N6-ONR-25129).

[2.24] T. C. Smith and W. L. Thomas III, *A Survey of Ship Motion Reduction Devices*, Tech. Rep. Ad-A229-278 (David Taylor Research Center, Ship Hydromechanics Dept., Bethesda, Maryland, 1990).

[2.25] C. Stigter, *Performance of U-Tanks as a Passive Anti-Rolling Device*, Tech. Rep. report no. 81S (Delft Hydraulics Laboratory, TNO, 1966).

[2.26] J. H. G. Verhagen and L. van Wijngaarden, *Non-linear oscillations of fluid in a container,* Journal of Fluid Mechanics **22**, 737 (1965).

[2.27] W. H. Chu, J. F. Dalzell, and J. E. Modisette, *Theoretical and experimental study of ship-roll stabilization tanks,* Journal of Ship Research **12**, 165 (1968).

[2.28] A. F. A. Gawad, S. A. Ragab, A. H. Nayfeh, and D. T. Mook, *Roll stabilization by anti-roll passive tanks,* Ocean Engineering **28**, 457 (2001).

[2.29] R. Moaleji and A. R. Greig, *Roll reduction of ships using anti-roll n-tanks,* in *Proceedings of the 8th International Naval Engineering Conference (INEC2006) or World Maritime Conference, March 2006, London, UK* (Institute of Marine Engineering, Science & Technology (IMarEST), 2006).

3

Theory

3.1. Introduction

The modeling of free-flooding tanks is complex, because of the interaction of the tank fluid with the environment. The amount of water in the tanks varies continuously due to the inflow and outflow of water through the flooding ports. This flow in and out of the tank interacts with the already complex fluid flow around the ship. As a simplification it is assumed that the interaction between the tanks, its neighboring tanks and the ship is small. Also, the actual water flow through the flooding port is not modeled. This requires a multiple domain simulation and falls outside the scope of this thesis.

The basic theory used in this research is the frequency domain, 3DoF model by Webster et al. [9] (from here on shortened to Webster). The model for predicting the performance of free-flooding anti-roll tanks as developed by Webster is derived again to gain insight into the rationale behind the model. For most terms the notation as used by Webster is held, where convenient the notation is adapted. The axis convention as used in this report is shown in figure 3.1.

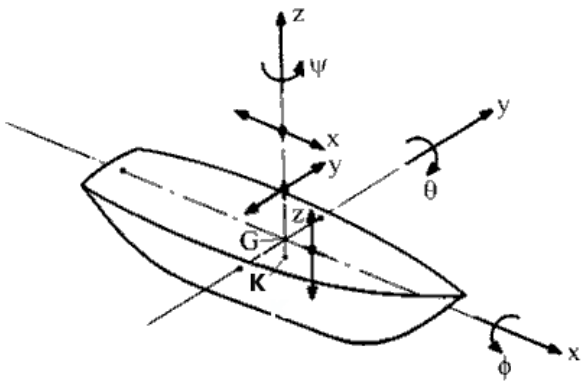

Figure 3.1: Ship axes convention

The prediction model is based on linearized ship motion theory, including several non-linear effects to closer approximate the actual behavior of the water in the free-flooding tanks. Since the application of free-flooding anti-roll tanks is the most interesting for (close to) stationary platforms or vessels, the forward speed is set to zero for now. This means that the wave frequency and the ship motion excitation frequency are equal and terms involving forward speed are omitted from the model.

Temporary separation of tank fluid dynamics from ship dynamics is justified when working in the frequency domain. Transfer functions (a mathematical representation of the relation between the input and output) of each element in the tank and ship dynamics are obtained independently. The tank is given a prescribed motion and forces and moments on the ship by the tank are determined. These forces, moments and transfer functions are combined later on in the process with the ship transfer functions.

Websters model is a 3DoF model for the ship combined with a 1DoF model for the anti-roll tank. In this section the model will be derived in 6DoF for the ship and with the notation as used in AQWA for easier reference as the plot progresses. The main difference between the modeling in AQWA and the modeling by Webster is that AQWA takes as a starting point for the modeling $e^{-i\omega t}$, where Webster uses $e^{i\omega t}$. This is a small but significant difference, because the resulting phases differ by $180°$ and the sign on the velocity terms need to be reversed.

3.2. Mathematical model of tank

The tank is assumed to have two states: an equilibrium state and a dynamic state, see figure 3.2.

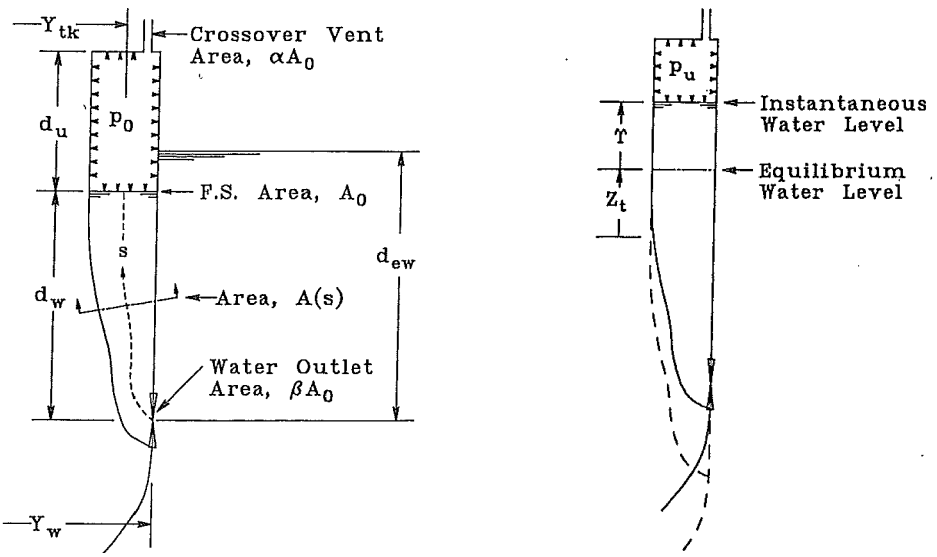

(a) at equilibrium

(b) under dynamic conditions

Figure 3.2: Isolated tank [9]

Assumptions and simplifications:

- incompressible flow
- irrotational flow
- inviscid flow (viscosity is ignored)
- unsteady flow
- the incoming wave has a small slope (small amplitude compared to length)
- the incoming wave is regular
- deep water (> 1000m)
- body has no or small forward speed (a good pipelaying speed is 9 km/day, whilst installation vessels are completely stationary)
- no saturation of the tank occurs
- no ventilation of the flooding port occurs
- sloshing is negligible due to relatively small tank width

The amount of water that flows into the tank must be equal to the water volume increase at the top of the tank (figure 3.3). The volumetric flow rate for incompressible flow is expressed by rate of flow through the port or rise in water level:

$$\begin{aligned} Q &= \beta A_0 C_{wd} \sqrt{2g\Delta H} = A_0 \dot{\Upsilon} \\ \dot{\Upsilon} &= \beta C_{wd} \sqrt{2g\Delta H} \end{aligned} \tag{3.1}$$

with
- A_0 the free surface area of the tank,
- β the size of the flooding port relative to the free surface area,
- C_{wd} the effective discharge coefficient of the flooding port,
- ΔH the differential pressure head over the flooding port [m].

Rewrite to obtain an expression for the water velocity $\dot{\Upsilon}$:

$$|\dot{\Upsilon}|\dot{\Upsilon} = 2g\beta^2 C_{wd}^2 \, \Delta H \tag{3.2}$$

Since the water motion Υ is neither real nor strictly positive (when the pressure head is negative $\Delta H < 0$, outflow from the tank will occur: $\dot{\Upsilon} < 0$), the square of the variable must be described as the absolute value multiplied with the complex value. In order to determine the water velocity at the free surface, the pressure head at the flooding port ΔH needs to be determined.

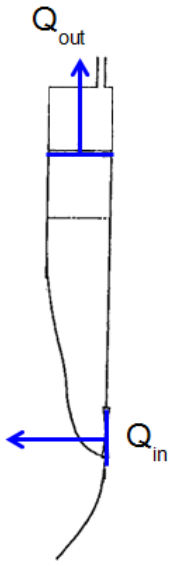

Figure 3.3: Flow rate equality

The differential pressure head over the flooding port is the difference between the external pressure head and the internal pressure head:

$$\Delta H = H_{ext} - H_{int} \tag{3.3}$$

The above equation is the Bernoulli equation in its simplest form, stating that $H_{ext} - H_{int} - \Delta H = 0$ and contains all pressure components. These components depend on the ship/tank motion, the water motion, air pressure in the tank and the incoming wave plus the diffraction and radiation pressures.

Due to the wave(s) in the environment the differential pressure head continuously changes and therewith the volume of water in the tank and subsequently the flow velocity. The consequence is that both the elevation of the water surface and the flow rate are unknown, requiring an unsteady-flow analysis (instead of the commonly used steady-flow analysis).

To determine the internal pressure head the Bernoulli equation for unsteady flow is derived in the z-direction (tank water motion modeled in 1DoF) and integrated over the streamline as drawn in figure 3.2a: from the flooding port at $s1 = 0$ to the internal free surface at equilibrium $s2 = d_w$.

$$H_{int} = \int_{s1}^{s2} \frac{Dw}{Dt} ds = \int_{0}^{d_w} \left[\frac{dp}{\rho g} + \frac{1}{g} \frac{\partial w}{\partial t} ds + d\left(\frac{w^2}{2g}\right) + dz \right]$$

Assume that the flow in the tank is essentially one-dimensional along a vertical streamline. At the free surface $A(s) = A_0$ and at the flooding port $A(s) = \beta A_0$, where β is the ratio of the size of the flooding port to the free-surface area. The instantaneous vertical velocity of the water at position s on the streamline is the sum of the velocity of the tank due to ship motions and the water velocity relative to the tank:

$$w = \dot{Z}_{tk} + \frac{A_0}{A(s)} \dot{\Upsilon}$$

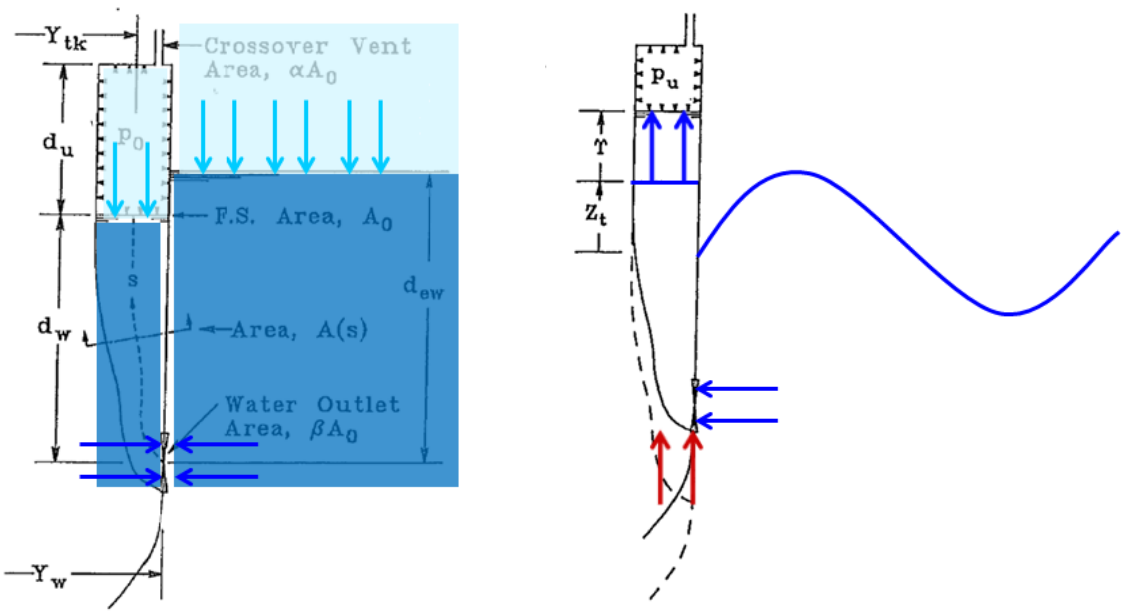

(a) static equilibrium

(b) dynamic equilibrium

Figure 3.4: Pressure head components

$$
\begin{aligned}
H_{int} &= \int_0^{d_w} \left[\frac{1}{g}\frac{\partial w}{\partial t}\, ds + d\left(\frac{w^2}{2g}\right) + \frac{dp}{\rho g} + dz \right] \\
&= \int_0^{d_w} \left(\ddot{Z}_{tk} + \frac{A_0}{A(s)}\ddot{\Upsilon} \right) ds + \frac{(\dot{Z}_{tk} + \dot{\Upsilon})^2 - (\dot{Z}_{tk} + \frac{1}{\beta}\dot{\Upsilon})^2}{2g} + \frac{p_u}{\rho g} + \Upsilon + d_w - 0 \\
&= \frac{\ddot{Z}_{tk} d_w}{g} + \frac{1}{g}\int_s \frac{A_0}{A(s)}\ddot{\Upsilon}\, ds + \frac{\left(1-\frac{1}{\beta}\right)\dot{Z}_{tk}\dot{\Upsilon} + \left(1-\frac{1}{\beta^2}\right)\dot{\Upsilon}^2}{2g} + \frac{p_u}{\rho g} + \Upsilon + d_w
\end{aligned}
$$

Now assuming that the velocities are very small for squared quantities, they may be neglected and the expression for the internal pressure head in equation (3.3) becomes:

$$H_{int} = \frac{p_u}{\rho g} + d_w + \frac{d_w}{g}\ddot{Z}_{tk} + \Upsilon + \frac{\gamma d_w}{g}\ddot{\Upsilon} \tag{3.4}$$

The γ appearing in the above equation is the so-called tank geometry factor and is defined as:

$$\gamma = \frac{1}{d_w}\int_s \frac{A_0}{A(s)}\, ds \tag{3.5}$$

It removes the need to design the exact shape of the tank and replaces it with a shape factor describing the area ratio of the arbitrarily shaped tank relative to a tank with straight walls all along its sides. This means that the tank need not be fully engineered before estimating its performance.

The external pressure head in equation (3.3) may be approximated in the same manner from the flooding port at $s1 = 0$ to the external free surface $s2 = d_{ew}$, but now with all flow

directions included. The velocity terms are expressed in velocity potential Φ (derivation is analogous to H_{int}):

$$H_{ext} = -\frac{1}{g}\frac{d\Phi}{dt} + \frac{\nabla\Phi \cdot \nabla\Phi}{2g} + \frac{p_{atm}}{\rho g} + d_{ew} - Z_{tk}$$

Assuming regular waves with a small slope the velocity of the water is small as the wave passes; the velocities squared are subsequently very small and may be neglected. This leaves only the dynamic pressure due to the waves:

$$H_{ext} = -\frac{1}{g}\frac{d\Phi}{dt} + \frac{p_{atm}}{\rho g} + d_{ew} - Z_{tk} = H_{dyn} + \frac{p_{atm}}{\rho g} + d_{ew} - Z_{tk} \tag{3.6}$$

At static equilibrium the air and water pressures on the inside and outside are in equilibrium: $\frac{p_0}{\rho g} = \frac{p_{atm}}{\rho g} + d_{ew} - d_w$. Combining this relation and equations (3.4) and (3.6) results in the following differential pressure head:

$$\Delta H = H_{dyn} - \frac{p_u - p_0}{\rho g} - Z_{tk} - \frac{d_w}{g}\ddot{Z}_{tk} - \Upsilon - \frac{\gamma d_w}{g}\ddot{\Upsilon}$$

In the above equation Z_{tk} is the collection term for the tank motion in all directions based on the ship motions. Not all ship motions make a significant contribution to the tank motion. Surge is generally small and can be neglected; assuming that the tanks are located midships yaw motions will also be negligible; lastly, the tanks are assumed to have a small width so sloshing and sway motions may also be neglected. The local vertical motion of the tank itself then consists of the contributions of the heave, pitch and roll motions of the ship due to the regular wave:

$$Z_{tk} = \xi_3 - x_{tk}\xi_5 + y_{tk}\xi_4$$

The elaboration on this model is split into the following parts and are treated in the respective subsections:

1. dynamic water pressure (H_{dyn})
2. dynamic air pressure ($\frac{p_u - p_0}{\rho g}$)

Substituting these components into equation (3.3) the differential pressure head for one tank becomes:

$$\Delta H_j = -Z_{tk,j} - \frac{d_w}{g}\ddot{Z}_{tk,j} - (1+\overline{V}_j)\Upsilon_j - \frac{\gamma d_w}{g}\ddot{\Upsilon}_j - \overline{U}\Upsilon_{jo} + \frac{\omega^2}{g}\zeta_a(\Phi_0 + \Phi_7)e^{-i\omega t} + \frac{\omega^2}{g}\sum_{m=1}^{6}\xi_m\Phi_m e^{-i\omega t} \tag{3.7}$$

Combined with the flow equation (3.2) the tank model becomes:

$$\frac{\gamma d_w}{g}\ddot{\Upsilon}_j + \frac{1}{2g\beta^2 C_{wd}^2}|\dot{\Upsilon}_j|\dot{\Upsilon}_j + (1+\overline{V}_j)\Upsilon_j + \overline{U}\Upsilon_{jo} = -Z_{tk,j} - \frac{d_w}{g}\ddot{Z}_{tk,j} + \frac{\omega^2}{g}\zeta_a(\Phi_{0,j} + \Phi_{7,j}) + \frac{\omega^2}{g}\sum_{m=1}^{6}\xi_m\Phi_{m,j}e^{-i\omega t} \tag{3.8}$$

3.2.1. Dynamic water pressure

The modeling of the dynamic water pressure due to the incoming wave, the diffraction and the radiation is treated in this section. This turned out not to be straightforward as panel pressures cannot be exported from AQWA at the present time. In the VER Model the water pressure at the flooding port is estimated with a Froude-Krylov pressure plus a motion pressure in the form of a velocity head. To examine the validity of this approach a forced roll motion is applied to the tank model and its results presented at the end of this section. Two other options, modeling the pressure using the wave elevation or the fluid potentials, are explored first.

Pressure output available from AQWA The following panel pressures excluding the hydrostatic pressure can be obtained from AQWA-LINE (frequency domain):

- output field point pressure (FPNT),
  This is the pressure head at a certain predefined point, including only the height of the undisturbed incoming wave and the diffracted wave.

- the total pressure on a panel (PRPR),
  The total pressure consists of the hydrostatic-varying (i.e. immersion due to motion), radiation (added mass/damping), Froude-Krylov, and diffraction pressures. This pressure is in (kilo)Pascals, so to acquire the total pressure head in meters the panel pressure needs to be divided by ρg.

- the modified and unmodified potentials (PRPT),
  From these unmodified field potentials the total pressure on a panel can be calculated using equation (3.9), which is elaborated in the next paragraph.

The total pressure on a panel cannot be used directly in the model, because the radiation potentials depend on the amplitude of the ship motions. The aim of an anti-roll tank is to reduce the ship motions. If the ship motion is reduced due to anti-roll tank action, the radiation pressure on an element due to ship motions also becomes lower. Consequently, the radiation pressure should be separated from the incoming wave and diffraction pressures. The most direct way to obtain the radiation pressure would be to calculate them directly from the potentials. However, from AQWA only the total pressure on an element or the wave elevation (pressure due to the incoming and diffracted wave) at a certain point on the hull is available. The separate radiation pressures are not given. These can only be determined directly from the potentials.

Modeling of the water pressure in this report The dynamic water pressure head depends on the surrounding field flow velocities. For a stationary ship (no forward speed):

$$H_{dyn} = -\frac{1}{g}\frac{\partial \Phi}{\partial t}$$

The total potential Φ per unit amplitude wave consists of the incident wave, diffraction and radiation potentials (from AQWA [6]). For one regular wave this is:

$$\Phi = (\Phi_I + \Phi_D + \sum_{m=1}^{6} \xi_m \Phi_m) e^{-i\omega t}$$

DELFRAC uses a slightly different definition of the pressure using the potentials than AQWA. According to Pinkster [10]:

$$H_{dyn} = \frac{\omega^2}{g} \left[\zeta_a (\Phi_0 + \Phi_7) + \sum_{m=1}^{6} \xi_m \Phi_m \right] e^{-i\omega t} \tag{3.9}$$

These potentials can be obtained from the diffraction program DELFRAC. In cases where the potentials were unavailable at the time of the simulations the wave elevation given by AQWA-LINE is used (this is clearly stated with the results for those simulations). The wave elevation (indicated with z_w here) consists of the incoming wave and the diffracted wave, radiation is excluded.

Modeling of the dynamic water pressure in the VER Model In the VER Model the dynamic water pressure at the flooding port is modeled with a Froude-Krylov pressure plus the roll submergence and a velocity head. The validity of using the velocity head is explored here.

ship particulars			loading condition			tank particulars						coefficients	
L_{pp}	143	m	m	29210	mt	γ	5.8		m_t	69	t	β	0.28
B	36.8	m	KG	11.926	m	l_{tk}	31.2	m	x_{tk}	0	m	C_{wd}	0.37
H	15.1	m	T	6.45	m	b_{tk}	2.3	m	y_{tk}	17.25	m	α	0.03
			GM_t	9.35	m	A_0	71.7	m^2	d_u	2.55	m	C_{ad}	0.7
			T_φ	11.3	s	d_w	5.45	m	d_{ew}	5.45	m		

Table 3.1: Calculation parameters

At low frequencies (long waves) as $\omega \to 0$, $\omega^2 \approx 0$, the water level should be equal to the motion of the tank as the ship moves so slowly that the water level has time enough to adjust.

$$\Upsilon = y_{tk} \varphi_a = 1.765 \text{ m}$$

In the upper limit the water level indeed goes to 1.77 meters in the simulation. Note that the optimum is still at a period of 10 seconds, where the phase lag with respect to the tank motion is 90 degrees. Even though the water level reaches a higher level, the tank will be less effective due to the different phase shift (not depicted here).

The initial expectation was that the change in water level goes to zero for high frequencies (very short waves) $\omega >$, $\omega^2 \gg$, because the water level does not have time to adjust. However,

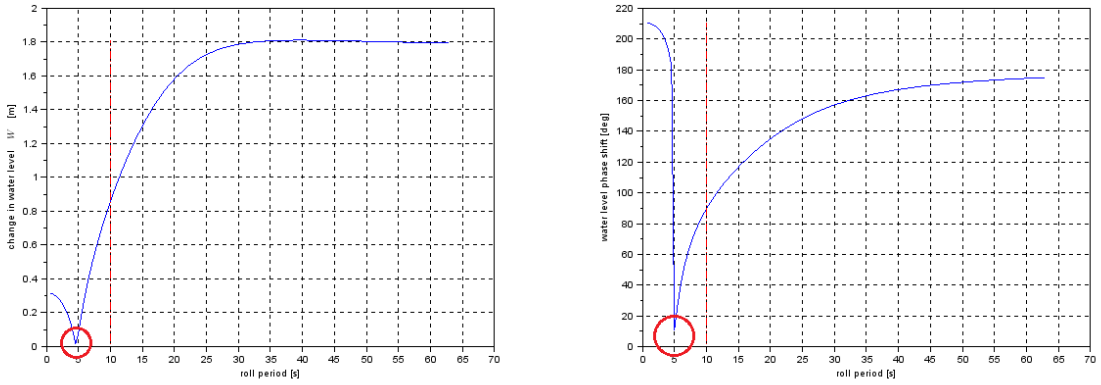

(a) amplitude

(b) phase shift

Figure 3.5: Water level dependence on excitation frequency, fully vented tanks

this is without taking into account the change in water level due to (unsteady) flow acceleration. These scale with ω^2, thus the change in water level does not go to zero for high frequencies. So, the water level should be close to the results of the acceleration terms of the tank and the tank water plus (or rather minus) the hydrodynamic pressure term.

$$\Upsilon = \frac{\frac{\omega^2 d_2}{g} y_{tk}\varphi_a - \frac{\kappa y_{tk}^2 \varphi_a^2}{2}}{\frac{\omega^2 \gamma d_w}{g}} = \frac{y_{tk}\varphi_a}{\gamma}\left(1 - \frac{1}{2}\frac{y_{tk}\varphi_a}{d_w}\right) = 0.373 \text{ m}$$

The water level of the tanks in the model goes to 0.32 m in the lower limit, see figure 3.5, which matches the above calculated value satisfactorily. This figure also shows that for an excitation period of 5 seconds the tank action is (almost) in phase with the ship roll motion, which could lead to amplification of the ship motion. Interestingly the change in water level goes to zero for only one point in the graph. The equation for this cancellation point and the associated roll frequency is:

$$-y_{tk}\varphi_a + \frac{\omega^2 d_w}{g} y_{tk}\varphi_a - \frac{\omega^2}{2g} y_{tk}^2 \varphi_a^2 = 0$$

$$\omega^2 \left(\frac{d_w}{g} - \frac{y_{tk}\varphi_a}{2g}\right) = 1$$

$$\omega = \sqrt{\frac{g}{d_w - y_{tk}\varphi_a/2}}$$

Both the equilibrium water level d_w and the tank arm y_{tk} are constants determined in the design phase, so only the amplitude of forced roll angle is variable. This phenomenon, therefore, does not depend on the natural frequency of the ship or the tank transfer period. With increase of amplitude of forced roll angle, the period at which the water level amplitude goes to zero decreases.

The period at which the change in water level is zero decreases quadratic with roll angle (see figure 3.6). The limit for zero roll angle seems to be a period of exact 5 seconds. This

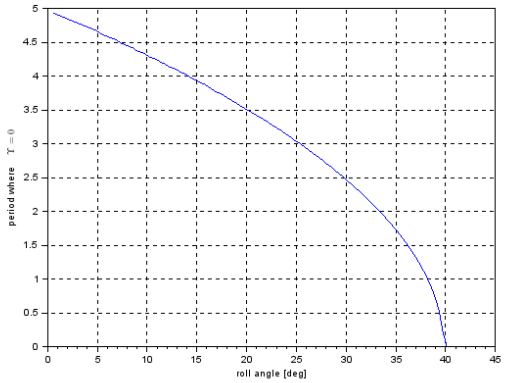

Figure 3.6: Roll period for cancellation point versus forced roll angle amplitude

is in line with the expectation: as the roll angle amplitude goes to zero, the frequency of roll at which the change in water level is canceled out goes to 1.26 rad/s corresponding to a roll period of 5 seconds.

The maximum forced roll angle at which this point exists in this case is around 40 degrees, figure 3.6. The roll frequency quickly rises and goes to infinity as a result of the denominator going to zero: $\varphi_a = \frac{2d_w}{y_{tk}} \frac{180}{\pi} = 40$. For larger forced roll angles the zero point does not exist anymore, because the water acceleration does not become large enough to cancel out the water level change and the velocity pressure.

So the existence of this cancellation point in figure 3.5 can be explained, however, in reality it will never appear. The cancellation point is only present in this graph as a result of modeling the dynamic water pressure using the velocity head and not because it is a physical occurring phenomenon.

Even though the influence of the velocity head turns out to be small, it does present a danger to model the dynamic water pressure using the velocity head, as it can give a non-physical and incorrect result. Because obtaining the velocity head is relatively easy, especially if compared to calculating the pressure using the flow potentials, it is tempting to use it as a simplification of the pressure head problem at the flooding port. However, it can be concluded that it is important to use the velocity head approximation with caution.

3.2.2. Dynamic air pressure

In this subsection the influence of different layouts of the air venting on the pressure head are explored. Four different configurations can be distinguished for the top of the tank, table 3.2 and figure 3.7.

The dynamic air pressure equation is deduced here for a crossover connected tank. The properties of the other air configurations may be inferred from this relation for the air pressure. The homogeneous form for the flow relation of air into and out of a tank is defined according

fully vented	The top of the tank is completely open.
unvented	The top of the tank is completely closed.
separately vented	The tank is connected to the outside air through an air vent.
crossover connected	The tank is connected to the tank on the opposite side by an air duct.

Table 3.2: Passive air configurations

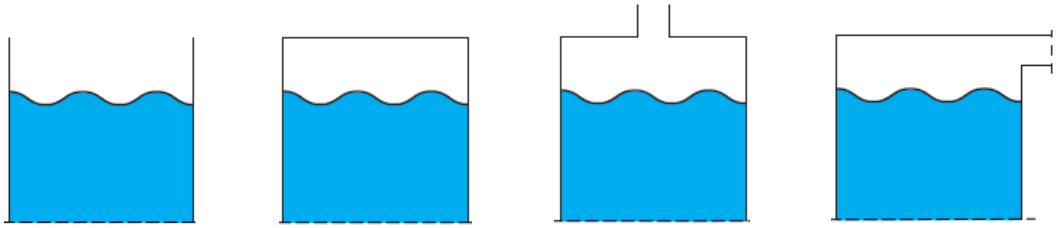

(a) fully vented (b) unvented (c) separately vented (d) crossover connected

Figure 3.7: Passive air configurations

to Rouse [11]:

$$\dot{m}_a = \rho_1 Q = \rho_1 \cdot C_{ad} A_0 \sqrt{\frac{2\Delta p}{\rho_1}} = \alpha C_{ad} A_0 \sqrt{2\rho_1 \Delta p} \tag{3.10}$$

The change in pressure can be described as: $\Delta p = (p_j - p_0) - (p_{jo} - p_0) = p_j - p_{jo}$. Assume isothermal expansion so that $\frac{p_0}{\rho_0} = \frac{p_1}{\rho_1}$. The air mass in one tank under equilibrium conditions is $m_0 = \rho_0 A_0 d_u$. Define the atmospheric pressure R_1, a linearized discharge coefficient R_Δ and a constant describing standard atmospheric conditions R_3 in head of water:

$$R_1 = \frac{p_0}{\rho g} = \frac{p_{atm}}{\rho g} + d_{ew} - d_w$$
$$R_\Delta = C_{ad} \frac{p_1}{\sqrt{|p_j - p_{jo}|}}$$
$$R_3 = \sqrt{2\frac{p_0}{\rho_0}}$$

Substitution of these coefficients into the mass flow equation and its elaboration is given in appendix A. The end result of the derivation is that the air pressure can be expressed using an air pressure constant $\overline{V}$ for the air pressure due to the water level in the tank itself and an air pressure coupling constant $\overline{U}$ to compensate for air crossover effects from the opposite tank:

$$\frac{p_u - p_0}{\rho g} = \overline{V}_j \Upsilon_j + \overline{U} \Upsilon_{jo} \tag{3.11}$$

The definition of the air pressure constants is elaborated upon in the next paragraphs for the air configurations given in table 3.2. The air pressure constants for all air configurations are collected in table 3.3, which can be found beyond the derivation.

Fully vented In the fully vented case both the pressure constant $\overline{V}$ and the pressure coupling constant $\overline{U}$ are zero, since the air pressure is equal to the atmospheric pressure due to the fully open top and there is no interconnection between the tanks.

Unvented The air pressure change as a result of fluctuating water level needs to be taken into account, but there is no air crossover between the tanks: $\overline{V}_j$ is constant and $\overline{U}$ is zero. A significant air "spring constant" is introduced by blocking air flow, which may alter the apparent tank period. Compression of air results in an increase of absolute pressure proportional to the percentage change in volume. The air pressure constant is the ratio of the static pressure head to the height of the tank above the equilibrium water level.

$$R_1 = \frac{p_{atm}}{\rho_w g} + d_{ew} - d_w$$
$$\overline{V}_j = \frac{R_1}{d_u}$$

If the volume of air above the equilibrium water level is small the water level in the tank will hardly vary, because the air pressure in the tank will increase as much as the water pressure. This is in accord with the findings of Webster, who found that the Slo-Rol tanks stopped working when the valves in the crossover duct were closed. This means that anti-roll tanks, if so designed, can be turned off by closing the air vents.

Separate venting In this case the tank is partially vented with an air vent. The amount of air can change, but it cannot flow unobstructed in and out of the tank. The equations for the air pressure now include an air escape and entry coefficient to account for outflow and inflow of air.

$$R_1 = \frac{p_{atm}}{\rho_w g}$$
$$R_{\Delta j} = \frac{C_{ad}}{\sqrt{\frac{|P_j|}{R_1}}} = \frac{C_{ad}}{\sqrt{\frac{|\overline{V}_j \Upsilon_j|}{R_1}}}$$
$$\overline{V}_j = \frac{\omega^2 R_1 d_u + i\omega\, \alpha R_1 R_{\Delta j} R_3}{\omega^2 d_u^2 + \alpha^2 R_{\Delta j}^2 R_3^2}$$

Air crossover connection The tanks are interconnected with an air duct. No external regulation of the air flow is included in this model.

$$R_1 = \frac{p_{atm}}{\rho g} + d_{ew} - d_w$$
$$R_{\Delta j} = \frac{C_{ad}}{\sqrt{\frac{|P_j - P_{jo}|}{R_1}}} = \frac{C_{ad}}{\sqrt{\frac{|2P_j|}{R_1}}}$$

$$\overline{U} = \frac{\alpha R_1 R_\Delta R_3}{d_u} \cdot \frac{2\alpha R_\Delta R_3 - i\omega d_u}{\omega^2 d_u^2 + 4\alpha^2 R_\Delta^2 R_3^2}$$
$$\overline{V}_j = \frac{R_1}{d_u} - \overline{U}$$

		Fully vented	Unvented	Separately vented	Crossover connected
discharge coefficient	R_Δ	0	0	$C_{ad}/\sqrt{\frac{\lvert P_j \rvert}{R_1}}$	$C_{ad}/\sqrt{\frac{\lvert P_j - P_{jo} \rvert}{R_1}}$
air pressure constant	$\overline{V}$	0	$\frac{R_1}{d_u}$	$\frac{\omega^2 R_1 d_u + i\omega\, \alpha R_1 R_{\Delta j} R_3}{\omega^2\, d_u^2 + \alpha^2 R_{\Delta j}^2 R_3^2}$	$\frac{R_1}{d_u} - \overline{U}$
coupling constant	$\overline{U}$	0	0	0	$\frac{\alpha R_1 R_\Delta R_3}{d_u} \frac{2\alpha R_\Delta R_2 - i\omega_e d_u}{\omega_e^2 d_u^2 + 4\alpha^2 R_\Delta^2 R_3^2}$

Table 3.3: Overview of the air constants

3.2.3. Unknown parameters

There are three unknown parameters in the tank model, which are not directly chosen by the tank designer, namely tank geometry factor γ, flooding port discharge coefficient C_{wd} and air discharge coefficient C_{ad}. The tank can be designed such that the tank geometry factor ensures that the tank is tuned to the ship natural rolling period in its most common loading condition by adjusting the tank transfer period (explained in the next paragraph). The other coefficients need to be estimated, determined with model experiments or by other means, such as computational fluid calculations.

Tank transfer period The tank transfer period is the parameter on which the tuning of the tank is based as shown in figure 2.3b. It is defined analogous to the transfer period of a U-tube anti-roll tank. If a ship with a U-tube tank is removed from its upright equilibrium and positioned under a certain roll angle, the water will flow from the higher tank to the lower tank until the level of water in both tanks is equal again. The time it takes to regain an equilibrium water level in the tanks is called the tank transfer period. Now imagine that the free-flooding anti-roll tanks can be thought of as a U-tube tank with an external connection through the surrounding seawater instead of an internal connection tube.

The transfer frequency of a U-tube tank is deduced from the tank equation as done by Stigter [12]. The coupled equation of motion of tank fluid with ship roll motion in still water as given by Stigter:

$$c_1\ddot{\varphi} + c_3\varphi + b_1\ddot{\psi} + b_2\dot{\psi} + b_3\psi = 0$$

with:

- φ roll angle of the ship
- ψ relative roll angle of the tank water:
  angle between bottom plane of tank and a plane through the center points of the free-surfaces of the tanks
- c_1 coupling coefficient of ship inertia into tank fluid motion
- c_3 coupling coefficient of ship spring term into tank fluid motion
- b_1 added mass coefficient of tank fluid
- b_2 damping coefficient of tank fluid
- b_3 spring term coefficient of tank fluid

The tank transfer frequency is defined by the spring term coefficient and the inertia coefficient: $\omega^2 = \frac{b_3}{b_1}$. Developed and translated to the terminology used in this report, the tank transfer frequency becomes:

$$\omega_{tk} = \sqrt{\frac{b_3}{b_1}} = \sqrt{\frac{0.5\rho g w_2 w_3^2 l}{0.5\rho w_2^2 w_3^2 l \int_0^{S_t} \frac{1}{n}\, ds}} = \sqrt{\frac{g}{w_2 l \int_0^{S_t} \frac{1}{n\, l}\, ds}} = \sqrt{\frac{g}{A_0 \int_s \frac{1}{A(s)}\, ds}} = \sqrt{\frac{g}{\int_s \frac{A_0}{A(s)}\, ds}}$$

where $\int_s \frac{A_0}{A(s)}\, ds$ is the effective length of the U-tube tank connection tube. Changing the effective length, either by changing the height of the equilibrium water level or cross section of the tube, changes the transfer frequency of the tank. Translating this to a free-flooding tank, which again is modeled as a U-tube tank with an external tube, using equation (3.5) results in:

$$T_{tk} = \frac{2\pi}{\omega_t} = 2\pi\sqrt{\frac{\int_s \frac{A_0}{A(s)}\, ds}{g}} = 2\pi\sqrt{\frac{\gamma d_w}{g}}$$

According to most authors on anti-roll tanks, the tank transfer period should be equal to or slightly lower than the ship´s natural roll period for optimal performance. Barr and Ankudinov [13], for example, conclude that the tank period should be 6-10% lower than the ship´s natural period for the best performance.

The tank transfer period can be tuned (lengthened) to the ship´s roll period by modifying the geometry of the inlet duct, analogous to the tuning of an internally cross-connected U-tube tank. Since the desired tank transfer period is known, an optimum tank geometry factor can be deduced and used in the mathematical model. The actual shape of the free-flooding tank and inlet duct is not relevant as long as the tank walls are straight around the equilibrium water level. This leaves room for a design that is custom fit, such as the tank shown in figure 3.8.

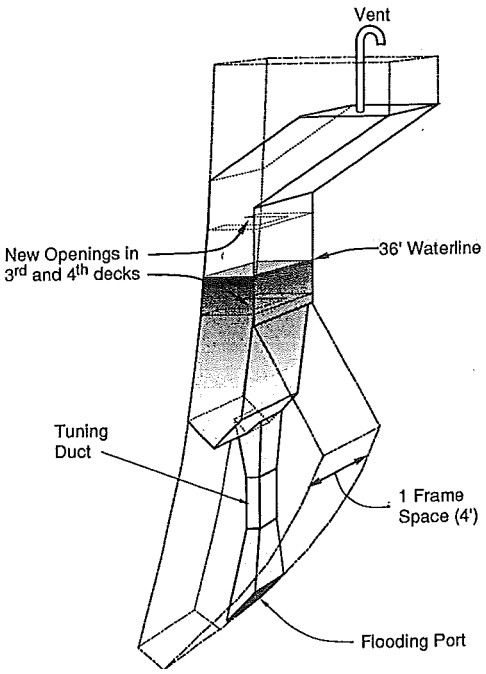

Figure 3.8: Free-flooding anti-roll tank as designed for USS *Midway* [9]

3.3. Time domain

Webster [9] assumes that the system behaves linear, so that the system can be studied in frequency domain. This linear assumption is violated by the non-linear damping in the tanks. In non-linear systems the superposition principle is no longer necessarily valid. However, since the system is only weakly non-linear, the it is likely that a semi-linear approach will also approximate the results of the effect of the anti-roll tank quite well.

This section starts off with the properties of the Webster Model in § 3.3.1 and its solution is derived in § 3.3.2. To determine the properties of the model the situation for a forced roll test with fully vented tanks is evaluated. For the forced roll test the heave and pitch motions will be very small, so these can be neglected and the tank motion will consist of pure roll: $Z_t = y_t\phi$. Also, $\overline{V} = \overline{U} = 0$ as the tank is fully vented. In a forced roll test there is no pressure due to waves, so there is no wave elevation pressure and the dynamic radiation pressure may be neglected for small roll angles. Equation (3.8) gets stripped to:

$$C_1\ddot{\Upsilon} + C_2|\dot{\Upsilon}|\dot{\Upsilon} + \Upsilon = -C_t Z_t \tag{3.12}$$

with:

$$C_1 = \frac{\gamma d_w}{g}$$

$$C_2 = \left(\frac{1}{\beta C_{wd}\sqrt{2g}}\right)^2 = \frac{1}{2g\beta^2 C_{wd}^2}$$

$$C_t = 1 - \omega^2\frac{d_w}{g}$$

Introduce $\Upsilon = x$ and $\dot{\Upsilon} = y$ as functions of time to create the following system of first order equations:

$$\dot{x} = y$$
$$C_1\dot{y} = -x - C_2|y|y - C_tZ_t$$

or

$$\dot{\underline{x}} = \frac{1}{C_1}\left(\begin{bmatrix} 0 & C_1 \\ -1 & -C_2|y| \end{bmatrix}\underline{x} - \begin{bmatrix} 0 \\ C_t \end{bmatrix}Z_t\right) \tag{3.13}$$

Two numerical methods are applied to a forced roll test and a free decay test in SCILAB, as described in § 3.3.2. For application in the diffraction time domain analysis by AQWA-NAUT a Dynamic-Link Library (DLL) has been written in C++. The results of this analysis can be found in § 4.1.2.

3.3.1. Properties of the non-linear system

The problem with non-linear equations such as equation (3.12) is that its properties are not easy to determine. A linear system:

- satisfies the properties of superposition (linearity and homogeneity),
- has one equilibrium point at the origin,
- its stability can be evaluated directly,
- for a sinusoidal input, the output signal only contains one harmonic.

For example, the principle of superposition does not necessarily hold for a forced non-linear system and if the input is sinusoidal the output may contain many harmonics and sub-harmonics with various amplitudes and phase differences. In this section the existence plus uniqueness of equilibrium points and the stability are evaluated for the non-linear system excluding the air pressure and the dynamic pressure head (H_{dyn}).

Equilibrium points In order to determine the number (and approximate location) of the equilibrium points of the non-linear equation a phase plot (figure 3.9) of the problem is constructed. The lines in the figure represent the nullclines. These are curves along which the vector field is entirely horizontal or entirely vertical; it is the boundary where the derivatives to time x' and y' change sign. Intersections between the nullclines represent equilibria of the system. The nullclines can be found by equating the derivative of the system of equations as defined in equation (3.13) to zero:

$$\dot{x} = y = 0 \tag{3.14a}$$
$$\dot{y} = \frac{-x - C_2|y|y - C_tZ_t}{C_1} = 0 \tag{3.14b}$$

So, the x-nullcline is given by $y = 0$ and the y-nullcline is the curve $x = -C_2|y|y - C_tZ_t$. The arrangement of the nullcline curves in figure 3.9 discloses that the solutions circle around one equilibrium point. This cycle represents a linear oscillation.

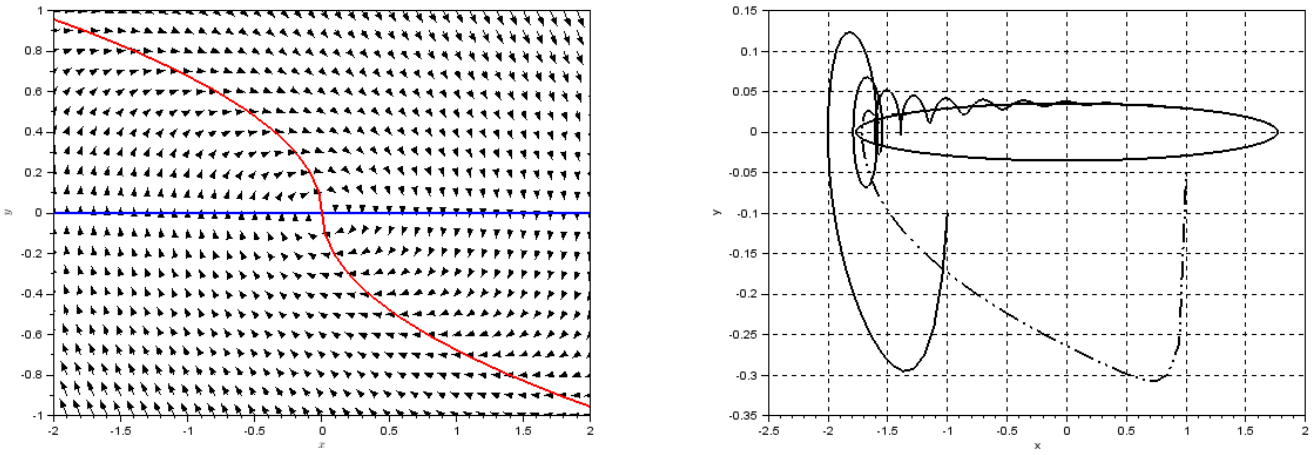

(a) phase plot

(b) trajectory

Figure 3.9: Equilibrium point analysis non-linear equation

In this particular case the only equilibrium point can simply be determined by inserting the result from (3.14a) into (3.14b):

$$\dot{y} = 0 = \frac{-x - C_2|0|0 - C_tZ_t}{C_1} \qquad \Rightarrow \qquad x = -C_tZ_t$$

The equilibrium point is thus $a = (-C_tZ_t, 0)$.

Stability As there is only one equilibrium point, the stability of the system is considered around this point. It is not possible to directly assess the behavior of the non-linear equation, therefore it is linearized in the neighborhood of equilibrium point $a = (-C_tZ_t, 0)$. The linearization of $\underline{\dot{x}}$ is the linear function given by:

$$L(\underline{x}) = f(a) + \frac{\partial f(a)}{\partial(x, y)}(\underline{x} - a)$$

The derivative of the non-linear equation is:

$$\frac{\partial f}{\partial(x, y)} = \frac{1}{C_1}\begin{bmatrix} 0 & C_1 \\ -1 & -2C_2\sqrt{y^2} \end{bmatrix}$$

Around equilibrium point $a = (-C_t Z_t, 0)$:

$$f(a) = \frac{1}{C_1}\begin{bmatrix} 0 \\ C_t Z_t - C_2|0|0 - C_t Z_t \end{bmatrix} = \begin{bmatrix} 0 \\ 0 \end{bmatrix}$$

$$\frac{\partial f(a)}{\partial (x,y)} = \frac{1}{C_1}\begin{bmatrix} 0 & C_1 \\ -1 & 0 \end{bmatrix}$$

The result of linearizing the equations (3.14):

$$\dot{\underline{x}}_L = \frac{1}{C_1}\begin{bmatrix} 0 & C_1 \\ -1 & 0 \end{bmatrix}\begin{bmatrix} x + C_t Z_t \\ y - 0 \end{bmatrix} = \frac{1}{C_1}\begin{bmatrix} C_1 y \\ -x - C_t Z_t \end{bmatrix}$$
$$= \frac{1}{C_1}\left(\begin{bmatrix} 0 & C_1 \\ -1 & 0 \end{bmatrix}\underline{x} + \begin{bmatrix} 0 \\ 1 \end{bmatrix} C_t Z_t\right)$$

The solution of the linearized system is:

$$\frac{dy}{dx} = \frac{1}{C_1}\frac{-x - C_t Z_t}{y}$$
$$C_1 \int y\, dy = \int (-x - C_t Z_t)\, dx$$
$$\frac{1}{2} C_1 y^2 = -\frac{1}{2}x^2 - C_t Z_t x + C = -\frac{1}{2}x^2 - C_t Z_t x - \frac{1}{2}(C_t Z_t)^2$$
$$y = \sqrt{\frac{-x^2 - 2C_t Z_t x - (C_t Z_t)^2}{C_1}} = \sqrt{\frac{(x + C_t Z_t)(-x - C_t Z_t)}{C_1}}$$

The eigenvalues belonging to this system of equations are:

$$A - \lambda I = 0$$
$$\begin{bmatrix} -\lambda & 1 \\ -1/C_1 & -\lambda \end{bmatrix} = \lambda^2 + \frac{1}{C_1} = 0$$
$$\lambda^2 = -\frac{1}{C_1}$$
$$\lambda_{1,2} = \pm\sqrt{\frac{1}{C_1}}\, i = \pm\omega i$$

The solution of the eigenvalues is purely imaginary, signifying that the equilibrium point is a center. The orbits rotate clockwise around the origin, since $\dot{x} > 0$ when $x = 0$ and $y > 0$. The system is stable and periodic with a period $T = \frac{2\pi}{\omega}$. The amplitude of the system oscillation is determined by the initial conditions.

Consequently, it is assumed here that temporarily separating the tank fluid dynamics from the ship dynamics, as stipulated for the frequency domain § 3.1, is still justified for the time domain.

3.3.2. Solving the system

The problem can be solved in the time domain by applying a numerical integrator to solve the system of equations. The most commonly used fixed step methods are evaluated on basis of step size, maximum error and calculation time by introducing a linear test case equation. The reason for using a test equation and not the non-linear equation describing the real problem is that the solution to the non-linear equation is unknown, thus giving no means of determining the error between the approximated value with the numerical method and the real value.

To be able to solve the system of equations with implicit methods such as Backward Euler, the non-linear term needs to be linearized. This is done by taking one of the water velocities in the non-linear term at the old time step n and the other at the new time step $n+1$: $|y_n|y_{n+1}$. In the explicit methods the current estimate for the water velocity at each intermediate time step is used.

As determined in § 3.3.1 only the properties of the linearized problem can be judged. Consequentially, for comparison of the numerical integrators and testing their suitability a linear test case, which is similar to the non-linear problem, needs to be used. The test equation chosen is $C_1\ddot{y} + y = 0$ with the solution $y = \cos(\omega t)$. Since the solution to this linear problem is known, the methods can be evaluated on accuracy by means of the global error. This error consists of all the local errors made over time and thus grows as time progresses, see figure 3.10.

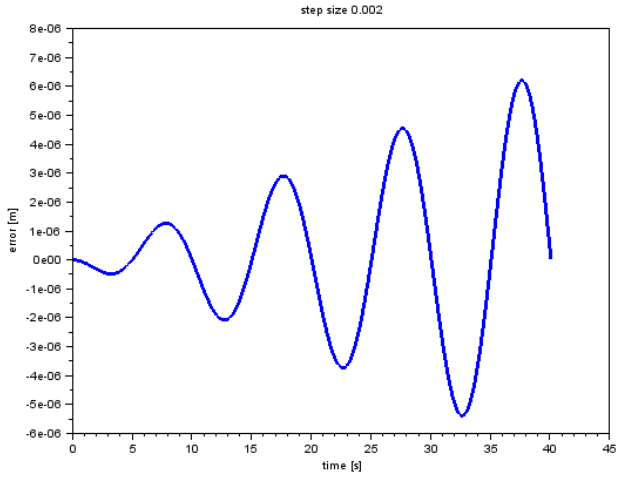

Figure 3.10: Global error for the Modified Euler method

There are many different numerical methods available for solving all kinds of problems. The methods explored in this report are all single-step methods, subdivided in two categories: fixed step methods and variable step methods. Fixed step methods use a constant step size all through the calculation, while variable step methods optimize the step size on the basis of the local truncation error. Fixed step methods are still applied the most frequently, but are slowly replaced by variable step methods.

The most commonly used numerical methods are compared on the produced global error after four periods and their computing times. The numerical method combining a small global error with a short calculation time is considered the optimal choice for use in solving the system of equations.

Fixed step methods

Five fixed step methods have been evaluated on efficiency and accuracy, namely Forward Euler, Backward Euler, Modified Euler, the Trapezoidal method and Runge-Kutta. The step size is inversely related to the computation time, i.e. a long computation time is the result of taking small steps.

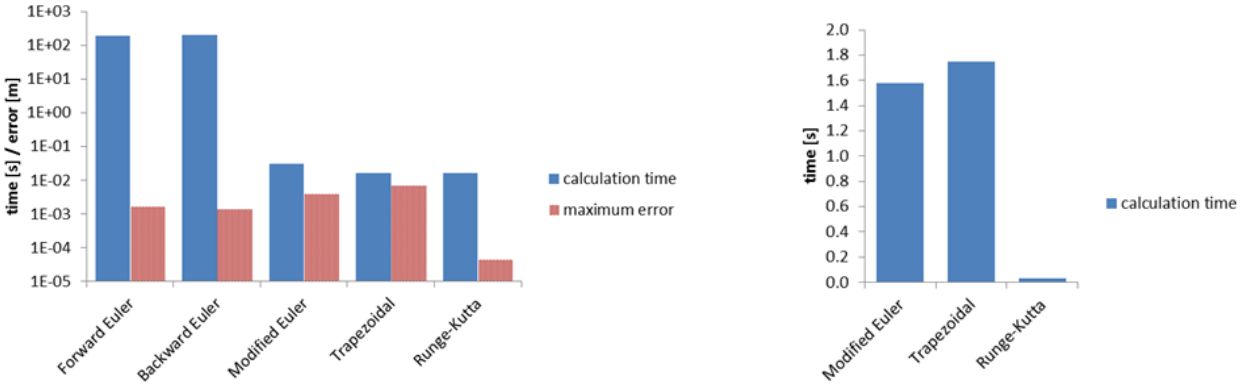

(a) largest possible step size

(b) error same order of magnitude

Figure 3.11: Computation time and error of fixed step methods (visibly smooth and matching the exact solution)

The Forward Euler and Backward Euler methods are notable in figure 3.11a due to the long computing time and relative inaccuracy. These methods are consequently dropped from consideration. Next, the remaining methods are compared on computation time when the global errors have the same order of magnitude (see figure 3.11b). The method combining a short computing time with high accuracy in the category fixed step methods is the Runge-Kutta method.

Variable step methods

These methods are less commonly found, probably because the routine is more complicated. However, they have two significant advantages over fixed step methods:

1. The step size is determined automatically, removing the chance that the result becomes unbounded or inaccurate (especially for the small frequencies).

2. The calculation time is shorter due to the optimization of the step size.

To start with three variable step methods have been evaluated on efficiency and accuracy in figure 3.13a, namely Heun-Euler, Bogacki-Shampine and Runge-Kutta-Fehlberg. It turns out that the time step needs to be extremely small for the Runge-Kutta-Fehlberg method to more or less follow the exact solution, which means that it is unstable for the test case. This instability can be seen in figure 3.12. There are more known instances where the RKF45 method is unstable; a common example of failure of the Runge-Kutta-Fehlberg method is given by Skufca [14]. Due to general problems with the RKF-algorithm an alternative, more stable, 5th order Runge-Kutta method was developed by Cash and Karp [15], called the Cash-Karp method. This method does converge to the exact solution. It follows that the Runge-Kutta-Fehlberg method is dropped from consideration due to the long computing time necessary to gain an acceptable solution (figures 3.13a and 3.13b).

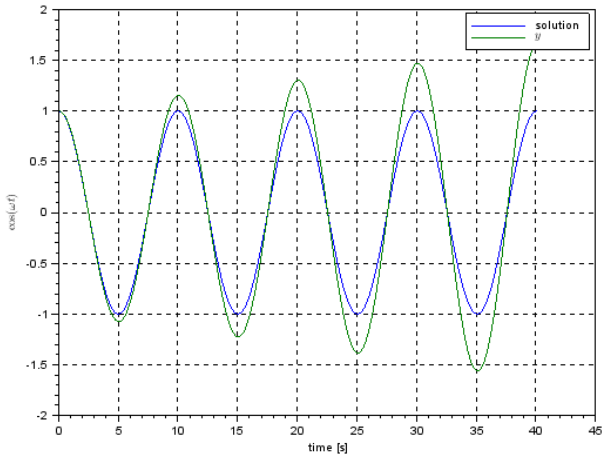

Figure 3.12: Instability of the Runge-Kutta-Fehlberg method

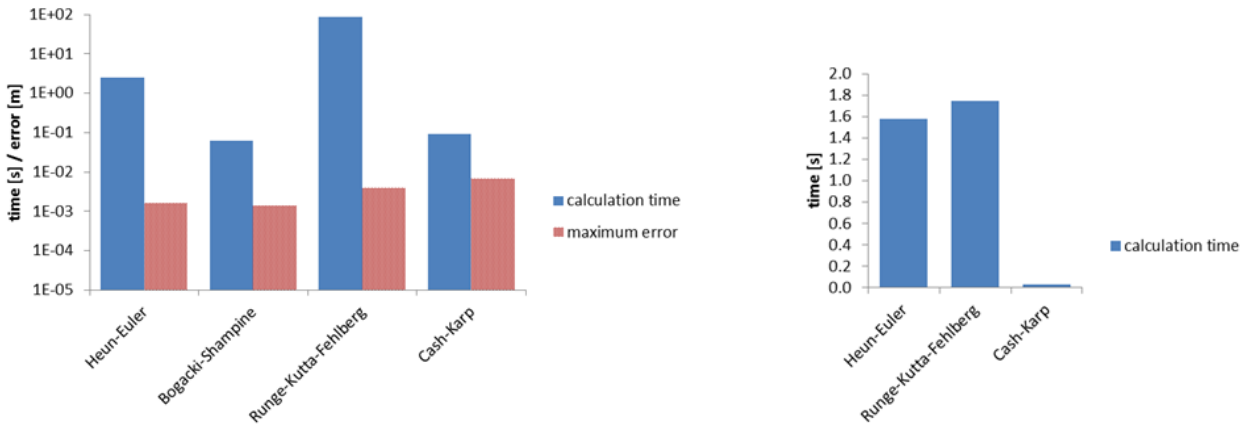

(a) largest possible step size

(b) error same order of magnitude

Figure 3.13: Computation time and error of variable step methods (visibly smooth and matching the exact solution)

For the test case an optimum value for the desired maximum error $\Delta_0 = 1e^{-7}$ was found. Again the remaining methods are compared when the global errors have the same order of magnitude, figure 3.13b. The method combining a short computing time with high accuracy in the category variable step methods is the above introduced Cash-Karp method.

Choice of numerical method

Variable stepping is advantageous over fixed stepping in two ways:

1. no mismatch between wave frequency and time step can occur, because the time step is adjusted automatically;

2. the running time is shorter due to the optimization of the time step.

However, AQWA can only handle fixed steps and one of the objectives is to calculate the ship motions using the time domain solver AQWA-NAUT. For the tank moment calculation routine implemented in AQWA-NAUT the fixed step solver Runge-Kutta is used, since this method combines speed with accuracy in the category fixed step solvers. Variable step methods are included in this report because the optimum step size depends on the wave frequency and for the routine in SCILAB there is no restriction to fixed methods. A mismatch in wave frequency and time step leads to erroneous results. To prevent this from happening a variable stepping method is used for the SCILAB routine.

3.3.3. Coupling with ship motions

The ship is modeled with the equilibrium tank water volume included as if it were frozen water. The excitation forces of the ship come from regular waves.

Ship motions The ship motions can be described as follows:

$$(M + M_a)\underline{\ddot{x}} + C\underline{\dot{x}} + K\underline{x} = \underline{F} \tag{3.15}$$

The ship mass matrix around its center of gravity is defined as:

$$M = \begin{bmatrix} m & 0 & 0 & 0 & 0 & 0 \\ 0 & m & 0 & 0 & 0 & 0 \\ 0 & 0 & m & 0 & 0 & 0 \\ 0 & 0 & 0 & I_{xx} & 0 & -I_{xz} \\ 0 & 0 & 0 & 0 & I_{yy} & 0 \\ 0 & 0 & 0 & -I_{xz} & 0 & I_{zz} \end{bmatrix}$$

Since the ship motions are calculated using linear ship motion theory, they are also sinusoidal, meaning that the system of equations can be simplified to:

$$[-\omega^2(M + M_a) - i\omega C + K]\underline{x} = \underline{F}$$

Tank forces on ship The vertical force exerted upon the ship by a single tank as a result of the changes in water level is:

$$F = -\rho g A_0 \left[1 - \frac{\omega^2 d_w}{g}\right] \Upsilon$$

The summation of this vertical force over all tanks is the heaving force exerted by the tanks on the ship. The tanks are placed in the midship section, where the sides of the ship and the tank are assumed to be vertical in the area of interest around the waterline.

Similarly, a pitching moment is produced by the sum over the tanks of $x_t F$. A small length of the tank plus placement midships in length ensures that the arm of the pitch moment by the tank water is very small and the tank pitch moment consequently does not influence the pitch of the ship. Webster considers the terms due to heave and pitch motions of the ship to be constant and transfers them to the excitation side of the tank equations. This reduces the number of degrees of freedom from six to three. However, it is not much more complex to take these terms into account, so the system of equations is kept in 6DoF.

The relative small width of the tanks also means that phenomena such as sloshing may be neglected. Therefore it is assumed that there is no net lateral force due to a change in water level. The surge, sway and yaw ship motions will not be influenced by these respective forces due to tank water level changes, but only through coupling with the tank roll moment.

And last, the tanks generate a net rolling moment from the summation of the roll moment $y_t F$ over all tanks. The roll moment amplitude for a tank pair (one on port side, another on starboard) can be written as:

$$F_4 = y_t F = -\rho g A_0 \left[1 - \frac{\omega^2 d_w}{g}\right] y_t (\Upsilon_p - \Upsilon_s)$$

The total force exerted on the ship by a tank pair is:

$$F_t = -\rho g A_0 \left[1 - \frac{\omega^2 d_w}{g}\right] \begin{bmatrix} 0 \\ 0 \\ Y_p + Y_s \\ y_t(Y_p - Y_s) \\ -x_t(Y_p + Y_s) \\ 0 \end{bmatrix} \tag{3.16}$$

Assembly of system components The tank motions and force terms are added to the ship motion equations, retaining the algebraic form $Ax = B$:

$$A\underline{x} = \underline{F} + \underline{F}_{tk} \tag{3.17}$$

where A consists of the ship mass plus inertia M, added mass M_a, damping C and restoration K data of the ship, including the equilibrium tank condition. This equation is used in conjunction with the equation for the tank (3.8).

3.4. Frequency domain

Webster approaches the problem in a slightly different way following Blagoveshchensky [16] in order to avoid the quadratic water velocity term. The result is the same system of equations solved from another angle. Starting from equation (3.1):

$$\dot{\Upsilon} = \beta C_{wd}\sqrt{2g\,\Delta H}$$

$$\frac{1}{\sqrt{2g}\,\beta C_{wd}}\dot{\Upsilon} = \sqrt{\Delta H} \qquad \left(\cdot\sqrt{\Delta H}\right)$$

$$\frac{\sqrt{\Delta H}}{\sqrt{2g}\,\beta C_{wd}}\dot{\Upsilon} = \Delta H$$

$$\frac{\sqrt{|\Delta H|}\,e^{i\phi/2}}{\sqrt{2g}\,\beta C_{wd}}\dot{\Upsilon} = \Delta H$$

with $\phi = \arctan\left(\frac{\Im(\Delta H_j)}{\Re(\Delta H_j)}\right)$. The influence of the phase shift in the pressure head on the water level increases as γ gets closer to 1 and β decreases. So, only for very small flooding port sizes combined with a completely straight tank the phase shift plays a role. This means that the effect of the phase shift in the pressure head can be considered negligible, resulting in:

$$\frac{\sqrt{|\Delta H|}}{\sqrt{2g}\,\beta C_{wd}}\dot{\Upsilon} = \Delta H \tag{3.18}$$

Due to the dependence of both sides of the equation on ΔH, the problem needs to be solved iteratively, reevaluating the differential pressure head until an equilibrium is reached. The reason that this exact same approach is not used in the time domain calculations is that the simulations turned out to be unstable (figure 3.14):

1. The solution to the equations (3.7) and (3.18) is unstable if the tank water acceleration terms due to the unsteady flow are included.

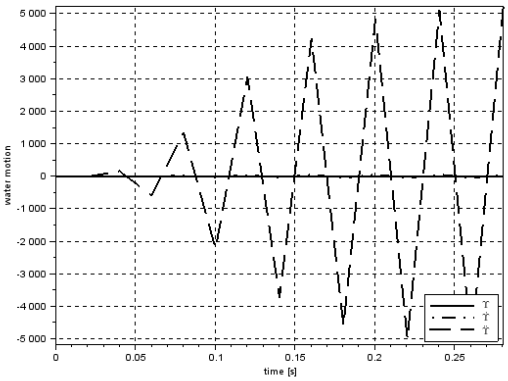

Figure 3.14: Change in water level in the time domain including acceleration terms

If the tank water acceleration terms are omitted from equation (3.7) the solution is stable, but not problem-free as the result is still non-realistic (figure 3.15):

2. The acceleration terms are unrealistically large (especially for high frequencies) and sharply peaked. The velocity curve has a steep slope in the area where the pressure head changes sign, which results in very large accelerations at these turning points.

3. For small frequencies the calculation of the acceleration terms show acceleration oscillations where the water velocity is close to zero.

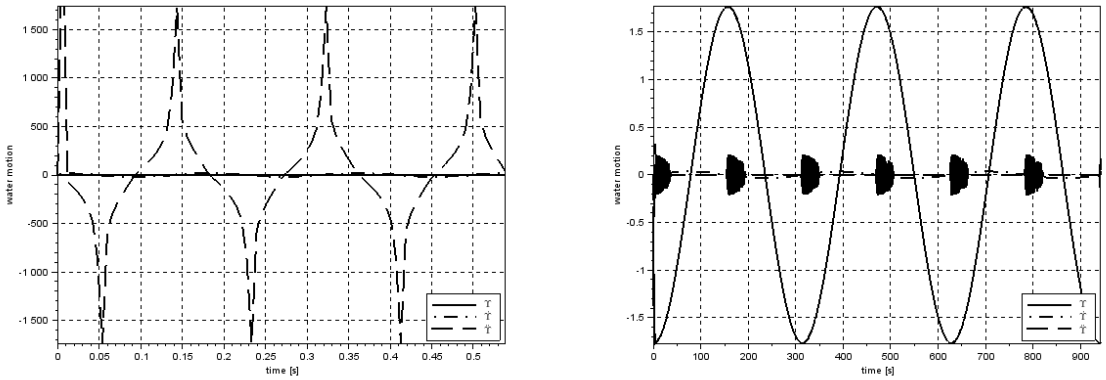

(a) $\omega \gg$ (b) $\omega \ll$

Figure 3.15: Change in water level in the time domain excluding acceleration terms

These problems were resolved by simply redefining equation (3.1) such that the square root of the pressure head is eliminated, as done in equation (3.2).

Additional tank damping From model experiments on Slo-Rol tanks (§ 2.1) Webster found indication of the existence of a small linear component of tank damping alongside the non-linear component for the Slo-Rol tanks. Because the practice for U-tube tanks is to include an experimentally determined linear tank damping in the performance predictions, it is advisable to perform experiments to determine whether a linear tank damping coefficient is applicable for externally connected tanks. The linear tank damping is integrated in the model as follows:

$$\Delta H = \left(\frac{\sqrt{|\Delta H|}}{\sqrt{2g}\,\beta C_{wd}} + 2C_{cr}\sqrt{\frac{\gamma d_w}{g}} \right) \dot{\Upsilon}$$

Since Webster did not find a linear tank damping coefficient in his tests with the tuned free-flooding anti-roll tanks and no further information is known, it is omitted in the model in this report.

3.4.1. Coupling with ship motions

The assumption that a sinusoidal input results in a sinusoidal output for this non-linear equation is considered proven from the results in the time domain section and will be used here to combine the tanks and the tank action with the ship motions in one complete system of equations using the coupling relations established in § 3.3.3. The change in water level can then be described with:

$$\Upsilon = \Upsilon_a e^{-i\omega t},$$

where Υ_a represents the complex amplitude of the tank water motion with respect to the incoming wave. Extending the tank motion in the same way, the tank equation (3.8) changes to:

$$-\omega^2 \frac{\gamma d_w}{g} \Upsilon_{a,j} e^{-i\omega t} - i\omega \frac{\sqrt{\Delta H}}{\sqrt{2g}\,\beta C_{wd}} \Upsilon_{a,j} e^{-i\omega t} + (1 + \overline{V}_j)\Upsilon_{a,j} e^{-i\omega t} + \overline{U}\Upsilon_{jo} e^{-i\omega t}$$
$$= -Z_{tk,j} e^{-i\omega t} + \omega^2 \frac{d_w}{g} Z_{tk,j} e^{-i\omega t} + z_w e^{-i\omega t} + \frac{\omega^2}{g} \sum_{m=1}^{6} \xi_m \Phi_m e^{-i\omega t}$$

The time term $e^{-i\omega t}$ cancels out, transforming the equation from time domain to frequency domain. With the terms rearranged conveniently for the next step:

$$\left(1 - \omega^2 \frac{d_w}{g}\right) Z_{tk,j} - \frac{\omega^2}{g} \sum_{m=1}^{6} \xi_m \Phi_m + \left(1 - \omega^2 \frac{\gamma d_w}{g} + \overline{V}_j - i\omega \frac{\sqrt{|\Delta H|}}{\beta C_{wd}\sqrt{2g}}\right) \Upsilon_{a,j} + \overline{U}\Upsilon_{a,jo}$$
$$= z_{w,j}$$

The associated equation for the pressure head from equation (3.7) is:

$$\Delta H = -\left(1 - \omega^2 \frac{d_w}{g}\right) Z_{tk,j} - \left(1 - \omega^2 \frac{\gamma d_w}{g} + \overline{V}_j\right) \Upsilon_{a,j} - \overline{U}\Upsilon_{a,jo} + z_w + \frac{\omega^2}{g} \sum_{m=1}^{6} \xi_m \Phi_m \quad (3.19)$$

The tank is coupled to the ship motion equations, retaining the algebraic form $Ax = B$ from equation (3.17):

$$A = \begin{bmatrix} A_{11} & A_{12} & A_{13} & A_{14} & A_{15} & A_{16} & 0 & 0 \\ A_{21} & A_{22} & A_{23} & A_{24} & A_{25} & A_{26} & 0 & 0 \\ A_{31} & A_{32} & A_{33} & A_{34} & A_{35} & A_{36} & C_f & C_f \\ A_{41} & A_{42} & A_{43} & A_{44} & A_{45} & A_{46} & C_f y_t & -C_f y_t \\ A_{51} & A_{52} & A_{53} & A_{54} & A_{55} & A_{56} & -C_f x_t & -C_f x_t \\ A_{61} & A_{62} & A_{63} & A_{64} & A_{65} & A_{66} & 0 & 0 \\ -\frac{\omega^2}{g}\phi_1 & -\frac{\omega^2}{g}\phi_2 & \left(C - \frac{\omega^2}{g}\phi_3\right) & \left(Cy_t - \frac{\omega^2}{g}\phi_4\right) & -\left(Cx_t + \frac{\omega^2}{g}\phi_5\right) & -\frac{\omega^2}{g}\phi_6 & G_p & \overline{U} \\ -\frac{\omega^2}{g}\phi_1 & +\frac{\omega^2}{g}\phi_2 & \left(C - \frac{\omega^2}{g}\phi_3\right) & -\left(Cy_t - \frac{\omega^2}{g}\phi_4\right) & -\left(Cx_t + \frac{\omega^2}{g}\phi_5\right) & +\frac{\omega^2}{g}\phi_6 & \overline{U} & G_s \end{bmatrix}$$

$$x = \begin{bmatrix} \xi_1 \\ \xi_2 \\ \xi_3 \\ \xi_4 \\ \xi_5 \\ \xi_6 \\ \Upsilon_p \\ \Upsilon_s \end{bmatrix} \qquad B = \begin{bmatrix} F_1 \\ F_2 \\ F_3 \\ F_4 \\ F_5 \\ F_6 \\ z_{w,p} \\ z_{w,s} \end{bmatrix} \tag{3.20}$$

with $C = \left[1 - \frac{\omega^2 d_w}{g}\right]$, $C_f = \rho g A_0 \left[1 - \frac{\omega^2 d_w}{g}\right]$ and G_j is the collection term for the tank water dynamics:

$$G_j = 1 - \omega^2 \frac{\gamma d_w}{g} + \overline{V}_j - i\omega \frac{\sqrt{|\Delta H|}}{\beta C_{wd}\sqrt{2g}} \tag{3.21}$$

The complex motion amplitudes ξ_m and the complex excitation force and moment amplitudes F_m have been divided by the wave amplitude ζ_a to achieve the normalized form per amplitude wave. The system of equations can be extended to include multiple tank pairs.

The system of equations cannot be solved directly, since the coefficients involving tank dynamics are interdependent due to their non-linear nature, but needs to be solved iteratively. With a trial solution for the response vector x the air pressure head in equation (3.11) is estimated with which the complex air constants $\overline{V}$ and $\overline{U}$ are determined from table 3.3. The differential pressure head ΔH (equation (3.19)) is updated with this result and thence the complex coefficients of tank transfer function, equation (3.21). The system of equations (3.20) is solved and compared with the result from the previous iteration. The process is repeated until the desired tolerance requirement has been met.

4

Results

In this chapter the results of the various simulations are presented and discussed. The chapter starts of with an overview of the particulars of the case presented and follows through with the results from different simulations.

The mathematical model in chapter 3 is based on a regular wave input. However, the expected ship motions are best estimated with a viscous damping based on an irregular wave spectrum. The viscous damping in the frequency domain is therefore iteratively adjusted to give a more realistic result for the RAOs and the expected tank performance. The time simulations are only based on regular wave input, because it is laborious to create a frequency response spectrum from the time simulations and produces no additional information with respect to the frequency domain analysis of the expected tank performance.

A frequency domain simulation gives the most useful information for engineering purposes as it directly shows the expected motion responses of the ship over a whole range of wave frequencies. Its results can be found in § 4.2. To verify the frequency domain model, direct and indirect time domain simulations with AQWA-NAUT are explored in § 4.1. To check these time domain results and specify points of interest a time domain simulation in SCILAB is utilized. The input for the time domain simulations are the RAOs and the wave loads on the vessel.

Lastly the results are compared in the discussion with one another based on simulation type, air vent configuration and other noteworthy aspects. Also, a parameter study is performed into different parameters in the tank model. This gives an indication of how tank performance can be optimized, because the tank moment is directly dependent on the tank water level, see equation (3.16).

The method used to define the effectiveness of the anti-roll tanks in the previous studies cited in this report is to find the roll response at the resonance frequency in beam seas for the stabilized and the unstabilized ship and determine the percentage reduction in roll motion. This gives largest roll reduction feasible by the anti-roll tanks, but may not lead to the most effective system in all conditions, see Chaplin [17]. However, for ease of comparison in this report the tank performance is defined by the roll response at resonance frequency.

The ship The ship used in this report is the pipelaying crane vessel Jascon 18 of the Sea Trucks Group. The principle ship particulars and used loading condition for this vessel are given in table 4.1.

ship particulars			loading condition		
L_{pp}	143	m	m	29210	mt
B	36.8	m	KG	11.93	m
H	15.1	m	T	6.45	m
			GM_t	9.35	m
			T_φ	11.3	s

Table 4.1: Ship particulars and loading condition

Ship viscous damping In AQWA a linear(ized) (viscous) damping value can be added manually to the simulation. Viscous damping is the damping of the motions due to skin friction, eddies, lift, forward speed and, if present, bilge keels and other appendages. Viscous damping is always present, but only manifests itself when wave potential damping is small. The wave damping of all motion is generally much larger than the viscous damping, except for the roll motion. With roll a significant viscous damping influence can be felt, because its radiation damping is small.

The amount of damping for a ship is expressed with the the non-dimensional damping coefficient κ, which is the ratio of the actual damping to the critical damping: $\kappa = \frac{c}{c_{cr}} = \frac{c}{2\sqrt{k(m+m_a)}}$. If the damping coefficient is too small, the roll angles in the vicinity of the resonance frequency will not have realistic values. For the Jascon 18 the roll angle at resonance would be $33°$, which is extreme. To get realistic roll motion angles at resonance frequency extra damping needs to be added to the simulation.

The amount of added damping is estimated here using Ikeda's Method for Rectangular Barges [18]. The viscous damping determined with Ikeda's method is frequency independent, but proportional to the roll motion amplitude. The anti-roll tanks reduce the roll motion of the ship, in turn reducing the amount of viscous damping present. By recalculating the estimated amount of viscous roll damping after the effect of the anti-roll tanks has been encompassed, a better prediction of the performance of the tanks can be made.

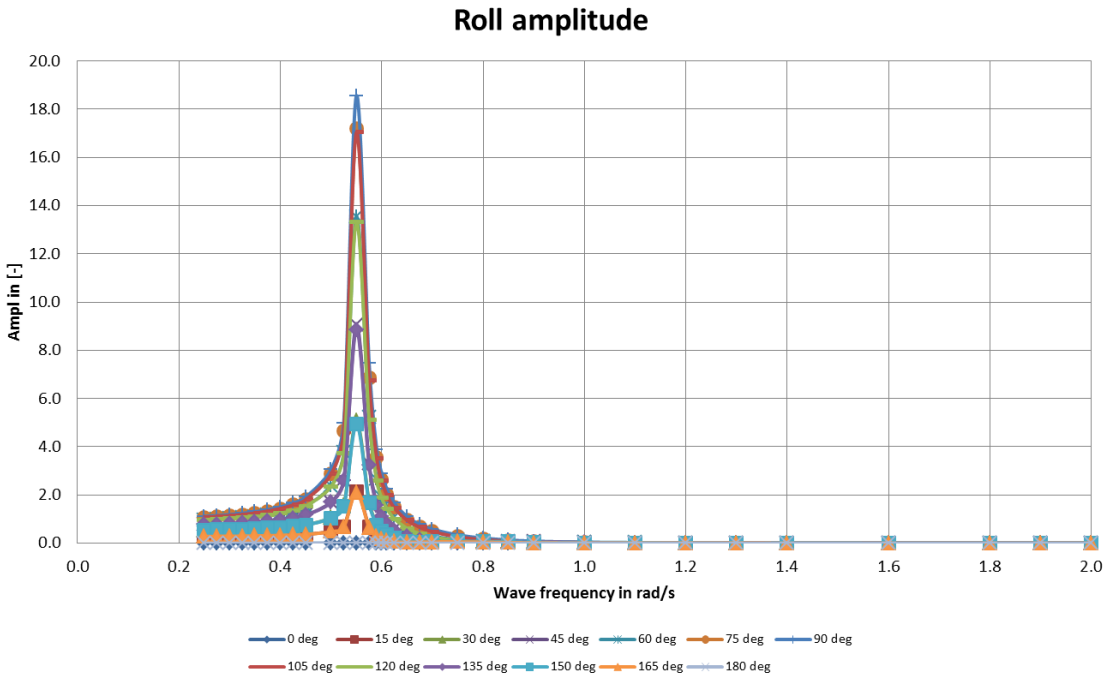

(a) RAOs excluding viscous damping

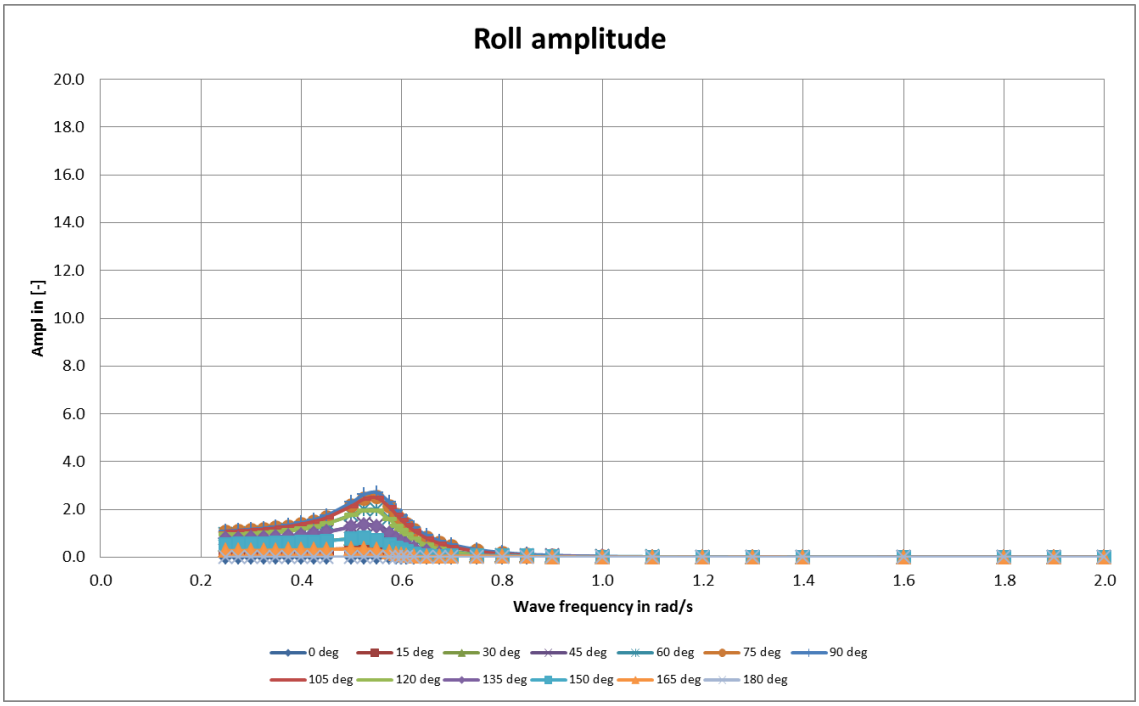

(b) RAOs including viscous damping

Figure 4.1: RAOs of roll with and without viscous damping

The tanks The tanks in general are designed to take up a maximum of 3% of the displacement and occupy a maximum of one third of the vessel length. The tanks have an assumed permeability of 100% as used by VER in their earlier calculations. The flooding port size is defined as a ratio in relation to the tank free-surface area as indicated in figure 3.2: βA_0. The sides of the ship and the free-flooding tanks are assumed to be vertical around the waterline. Below this area the geometry may vary. If the tanks are straight all the way down to the bottom, the tank geometry factor $\gamma = 1$, if the tanks are shaped the geometry factor increases. For the tanks as "designed" for the Jascon 18 the geometry factor is $\gamma \approx 6$.

The dimensions and parameters of the tank as used in this chapter are given in table 4.2. Where not specifically mentioned the tanks are fully vented in the calculations. For ease of comparison with the VER Model later on the size of the flooding port β used in their calculations is adopted. The value of the effective discharge coefficient C_{wd} for the untuned tank is taken as advised in Ruponen [19]. The tuned tank has a pipe connecting the flooding port with the actual tank. Pipes have a discharge coefficient dependent on length and flooding port size [20] for which a good estimate can be made in the design stage. For this study the pipe is not actually designed, so no good estimate can be made. In absence of experimental values the effective discharge coefficient and the other unknown parameters (α and C_{ad}) are assumed to be the same as for the tuned free-flooding tank from Webster. Coincidentally, thence the effective discharge coefficient for the tuned and untuned tank are the same.

γ	5.8		m_t	69	t	β	0.22
l_t	31.2	m	x_t	0	m	C_{wd}	0.37
b_t	2.3	m	y_t	17.25	m	α	0.03
A_0	71.7	m^2	d_u	2.55	m	C_{ad}	0.7
d_w	5.45	m	d_{ew}	5.45	m		

Table 4.2: Particulars for isolated free-flooding tank

Influence of tank water mass on natural period of roll In the VER research into *external* free-flooding tanks the change in shape of the hull on the outside meant a significant change in transverse metacentric height and consequently in the natural period of roll [1]. This change in natural period of roll can result in a completely different response of the ship. Since the tanks are open to the sea, the change in transverse metacentric height is caused by the loss of buoyancy (reduction of waterline area). Only the mass of water up to equilibrium level is considered; the change in mass of water in the tanks due to ship motions is not taken into account. The virtual reduction in metacentric height and the resulting change in natural period

of roll is estimated using the following equations:

$$KB' \approx KB + 0.55 \cdot \frac{2m_{tk}}{\rho C_w L_{pp} B}$$

$$BM' = \frac{I_T - \frac{l_{tk} b_{tk}^3}{12}}{\frac{m - m_{tk}}{\rho}}$$

$$d\overline{GM}_t = KB' + BM' - KG$$

$$T_\varphi = 2\pi \sqrt{\frac{k_{\varphi\varphi}^2}{g\overline{GM}_t}}$$

The guideline for fluid anti-roll devices is to use a tank water mass of 2-3% of the ship mass. In the VER project 2.75% was present in a tank with straight sides over the entire tank height ($\gamma = 1$ or untuned). The tuned tank ($\gamma = 6$) with the same free surface area only carries 0.5%. From figure 4.2 it can be seen that the change in metacentric height varies up to about 10%. As a result the ship's natural roll period can shift from about 11.3 seconds to about 10.7 seconds for a tank mass of 4.5% of the ship mass for this particular ship. This is not a

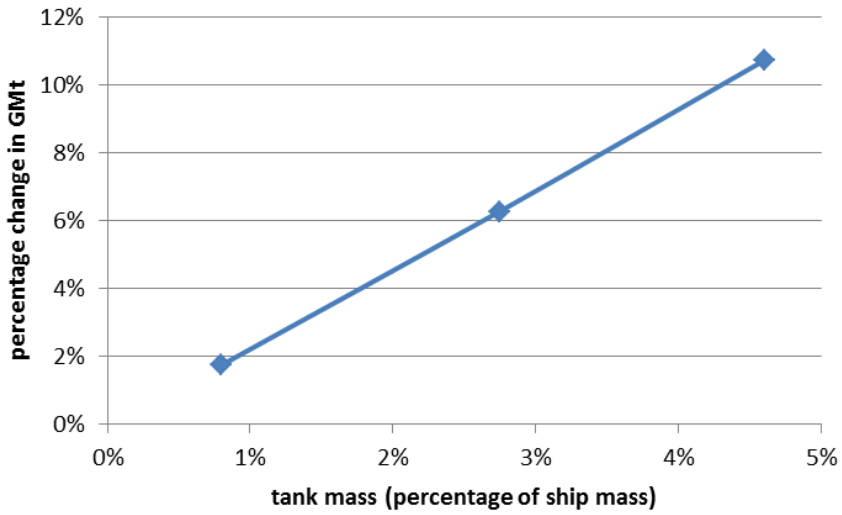

Figure 4.2: Influence of loss of buoyancy on the metacentric height

4.1. Time domain

Forced roll and free decay analysis were performed before venturing into solving the system excited by a regular wave. The time domain simulation is performed in both SCILAB and AQWA-NAUT. The aim is to have an extension to the AQWA suite to calculate the tank performance. In order to check the results obtained in AQWA-NAUT, a SCILAB program specifically created to mimic the calculations from the AQWA-NAUT time simulation is written.

The tank dynamics cannot be added directly into the simulation, because AQWA-NAUT itself cannot be altered. However, a force/moment can be applied on the center of gravity

through an external Dynamic Link Library (DLL). The function of a DLL is to import/export functions and data to/from a program without changing the core program. The moment generated by the tank as a result of the change in water level is fed to AQWA-NAUT through this DLL. The DLL is created here using C++.

For the time domain simulation the Webster Model is adhered to as described in § 3.3. Because the response at the resonance frequency is by far the largest, it is the primary focus of interest and therefore only the response at resonance is shown in this report. The response is including the dynamic radiation pressure calculated with the potentials as shown in equation (3.9).

The input regarding tank parameters and settings for the calculations is collected in an excel sheet. From this excel sheet the variables are imported in SCILAB. The tank is "tuned" to the ship natural period of roll by adapting the tank geometry factor through the equation:

$$\gamma = \frac{g}{d_w} \cdot \left(\frac{T_\varphi}{2\pi}\right)^2$$

Even though the area of the tank varies with the height; it is not dependent on the height:

$$\int_0^{d_w} A(s)\,ds = A(s)\Big|_0^{d_w} d_w = V$$
$$\int_0^{d_w} \frac{1}{A(s)}\,ds = \frac{d_w}{A(s)|_0^{d_w}}$$

This means that the required free surface area of tank for a certain mass of seawater (% of displacement) can be calculated based on the tank geometry factor and the equilibrium water height:

$$\gamma d_w = \int_0^{d_w} \frac{A_0}{A(s)} ds = \frac{A_0 d_w}{A(s)|_0^{d_w}}$$
$$A_0 = \frac{\gamma d_w A(s)|_0^{d_w}}{d_w} = \frac{\gamma V}{d_w} = \frac{\gamma m_t}{\rho d_w}$$

Input definition One of the initial encountered problems was that the shape of the curves is not physically correct as can be seen in figures 4.3 and 4.4: for a sinusoidal input the output should also be sinusoidal even if the equations are non-linear. This turned out to be a limitation in both SCILAB and AQWA-NAUT: the input needs to be declared as a complex number (as a sinusoidal with a certain phase) in order for the numerical computing environment to take into account any phase shifts between the input and the output. If the phase is not explicitly declared the program will treat all the variables as reals and ignore phase shifts, giving a non-physically correct output. Consequently, the input needs to be described in the form $Ae^{i\omega t}$ and cannot be declared as $A\cos(\omega t)$ or $A\sin(\omega t)$.

In AQWA-NAUT this is problematic, because even though complex numbers are used in the main routine, only real values are imported into the DLL. So the phase of inputs is only

introduced into the non-linear tank equation for the terms that are independent of the tank position and velocity.

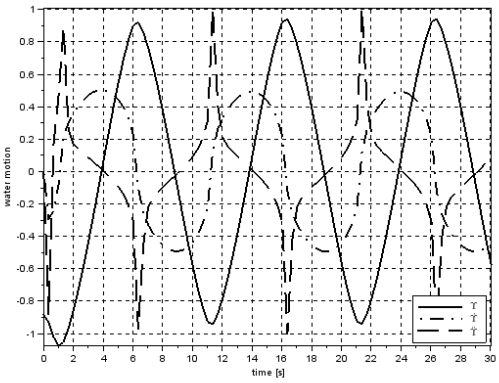

Figure 4.3: Non-physical result SCILAB

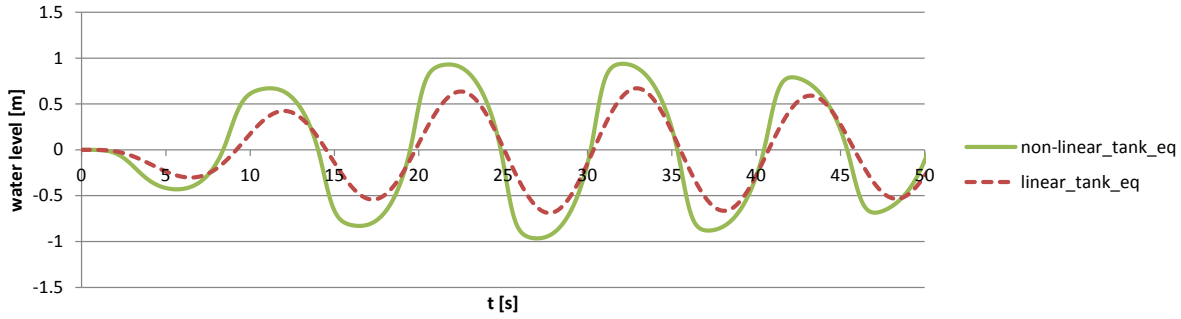

Figure 4.4: Non-physical result AQWA-NAUT

4.1.1. indirect AQWA-NAUT simulation

Next the option to add the effect of the tank moment indirectly to the time simulation was explored. Instead of calculating the tank moment directly during the time simulation, the tank damping is estimated using a free decay test on the ship motion data and an equivalent damping is determined. This equivalent damping is used to estimate the tank moment acting on the ship. The equivalent tank damping is only related to the roll angle of the ship, its mass and transverse metacentre; greatly reducing the number of variables. Also, the phase dependency vanishes, removing the problem in the previous section with missing phase values.

In this section the free decay analysis is explained and performed on the ship excluding viscous damping to try to estimate the tank damping as accurately as possible. The tank moment based on the equivalent damping is fed into AQWA-NAUT and the result from the time simulation is shown.

Free decay analysis

The equivalent damping coefficient of the tank can be determined with a free decay analysis. A free decay test takes place in still water. The ship is given a displacement in a certain direction (in this case an initial roll angle since the aim of the anti-roll tanks is to reduce the roll motion), is released and starts rolling. These motions decay and die out, since there is no external exciting force acting on the ship. The time it takes for the motion to die out and the decrease in maximum motion value are an indication for the damping the tank generates. Since the only motion of interest is the roll motion, the equations of motion (3.15) can be reduced to one equation describing a pure roll motion:

$$(I_{xx} + m_{a44})\ddot{\varphi} + C_{44}\dot{\varphi} + K_{44}\varphi = F_4 + M_{tk}$$

A free decay test takes place in still water, so the exciting force F_4 is zero. The input for the free decay is a starting position. The test is performed for several initial roll angles; in this case 5, 10, 15 and 20 degrees were applied. Viscous damping of the roll motion is not taken into account, in order to try and capture purely the tank damping. At each time step the position of the tank is estimated using the acceleration and velocity from the previous time step:

$$\ddot{\varphi}_n = \frac{M_{tk} - K_{44}\varphi_n - C_{44}\dot{\varphi}_n}{I_{xx} + m_{a44}}$$

$$\dot{\varphi}_{n+1} = \dot{\varphi}_n + h_{n+1}\ddot{\varphi}_n = \dot{\varphi}_n + h_{n+1} \cdot \frac{M_{tk} - K_{44}\varphi_n - C_{44}\dot{\varphi}_n}{I_{xx} + m_{a44}}$$

$$\varphi_{n+1} = \varphi_n + h_{n+1} \cdot \frac{\dot{\varphi}_n + \dot{\varphi}_{n+1}}{2}$$

with:

$$M_{tk} = -\rho_w g A_0 \left(1 - \frac{\omega^2 d_w}{g}\right) y_t(\Upsilon_j - \Upsilon_{jo})$$

In appendix C damping of the roll motion is described using a linear and a quadratic damping coefficient (courtesy of MARIN). However, the curve in figure 4.5b is not straight as in the appendix, but curved strongly. This shows that the tank damping is indeed non-linear. This non-linear curve cannot be approximated by the general approach using a linear plus a quadratic coefficient, instead we opted for a regression analysis in order to describe the curve more accurately. It was found that the non-linear data set can best be described with a third degree logarithmic equation:

$$b_0 + b_1 \ln(\varphi) + b_2 \ln^2(\varphi) + b_3 \ln^3(\varphi)$$

With the damping curve equation and the known roll motion amplitude of the ship including viscous damping (4.8 degrees in this case) the equivalent damping coefficient of the free-flooding tank can be determined. Note that the curve equation is expressed in radians for the reason that the roll angle in the AQWA-NAUT calculation is in radians. The equivalent damping coefficient can be used as an alternative input into AQWA-NAUT instead of the direct calculation of the tank moment in the DLL.

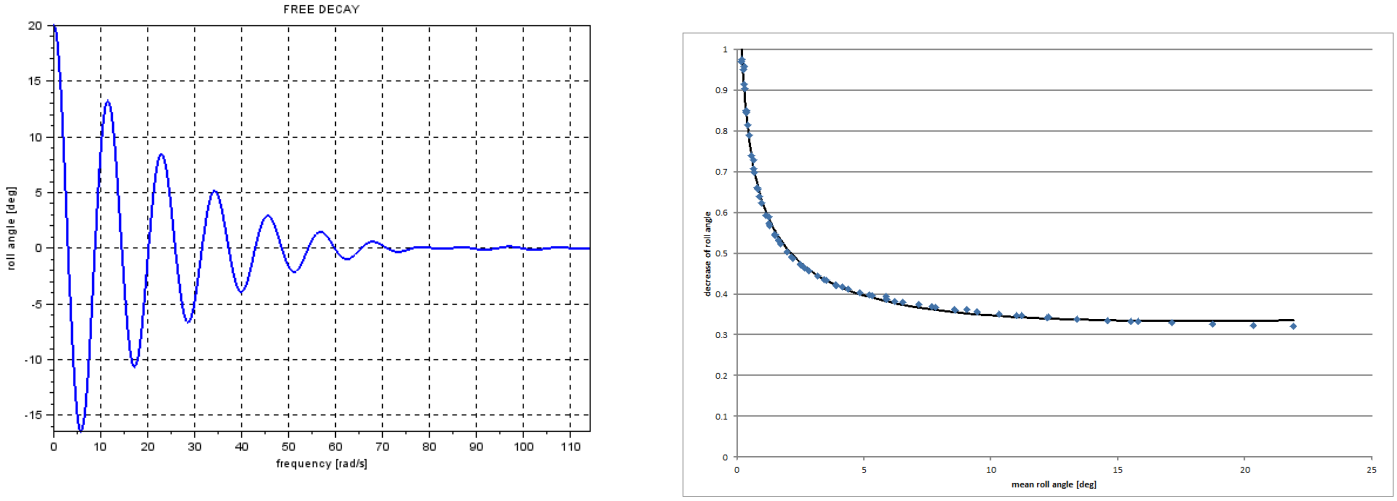

(a) tank & water motion

(b) equivalent damping coefficient

Figure 4.5: Free decay test

Solution convergence Figure 4.6a (created using a fixed step Runge-Kutta solver) shows that a minimum number of steps needs to be taken per period in order to achieve a converged solution for the free decay test. In order to average this number of steps per period the overall tolerance level of the simulation must be set appropriately. There is a trade-off between accuracy and computing time (figure 4.6b). An overall tolerance level of $1e^{-12}$ is chosen as the optimum between computing time and accurate decrease in peak values.

Results of the indirect time simulation

The tank moment for the indirect time simulation is based on the equivalent damping coefficient and the roll velocity (see appendix C):

$$M_{tk} = -\frac{c_{eq}}{\pi\omega} g\, m\overline{GM}_t \cdot \dot{\phi}$$

This moment is applied to the center of gravity of the ship. The resulting time plot is shown in figure 4.7. The indirect time simulation seems to work rather well, but nothing can be said about tank water levels or other values of design interest. The reduction of roll angle is from 4.8 degrees to 3.8 degrees; this is a reduction of 21%.

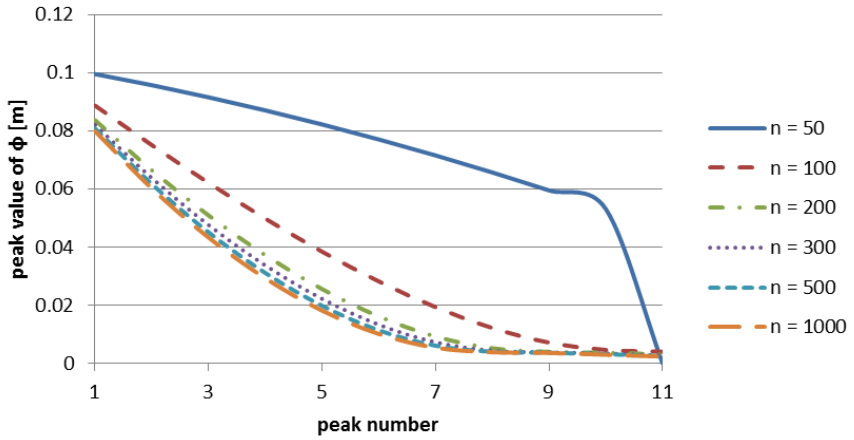

(a) Free decay peak values versus number of steps per period

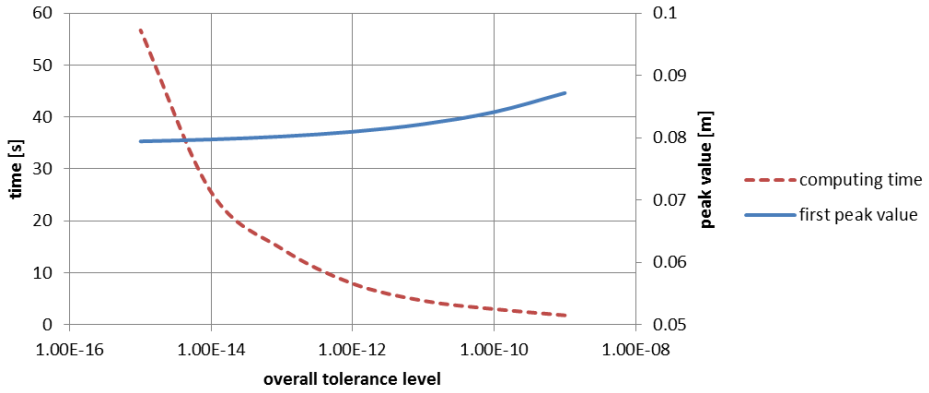

(b) First peak value versus accuracy

Figure 4.6: Trade-off between accuracy and computing time (free decay test)

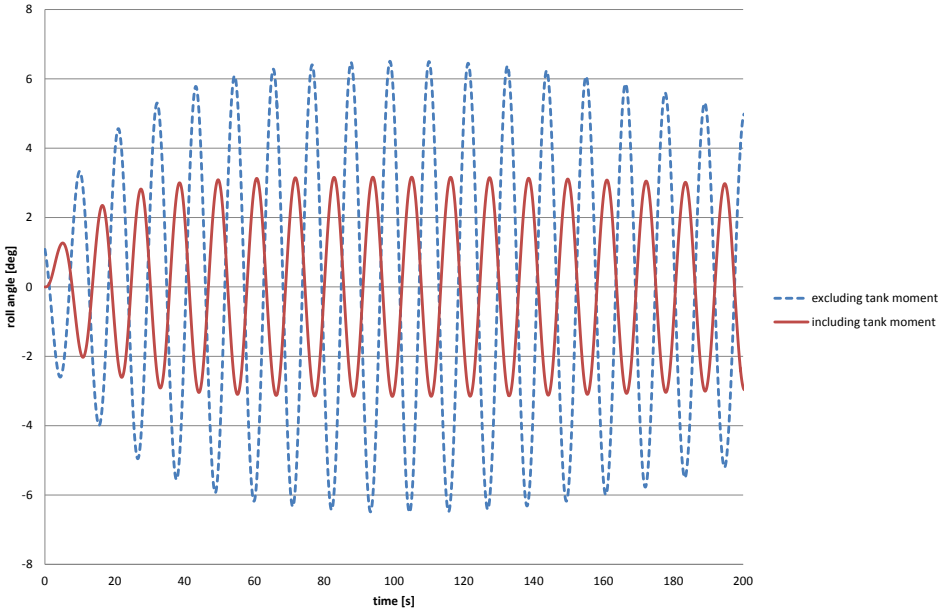

Figure 4.7: Time simulation of equivalent damping (AQWA-NAUT)

4.1.2. direct AQWA-NAUT simulation

The magnitude roll motion with free-flooding anti-roll tanks is significantly lower on average than the motion without tanks: the motion is reduced by about 43% by the anti-rolling tanks in this case. Looking at output for the variables in the tank equation, the water level in the tanks stood out (figure 4.8b). The water level should oscillate around the equilibrium level, which is indicated in the figure by a water level of zero. This is not the case; the water level in both tanks has the same offset (about -4.5m) around which it oscillates. This was not the only difficulty encountered with the time simulation in AQWA-NAUT. The limitations found with the DLL in AQWA are:

1. Only the real parts of the complex numbers are imported into the user_force routine, which is not a problem when solving a linear equation, but only when solving a non-linear equation the neglected phase differences influence the shape of the result curve. This is (partially) resolved by the externally introduced terms, which are defined with a phase angle.

2. The panel pressure at the inflow of the tank cannot be used to determine the dynamic pressure component, because:

   - it cannot be input directly from AQWA into the DLL,
   - it is not a global variable allowing it to be called in the user_force routine (only the density, gravity acceleration and water depth are defined on a global level).

3. It is very hard to pinpoint the cause of a problem in the calculation, such as the offset in the tank water levels in figure 4.8b, because the calculation for the most part takes place in a black box to which the user has no access.

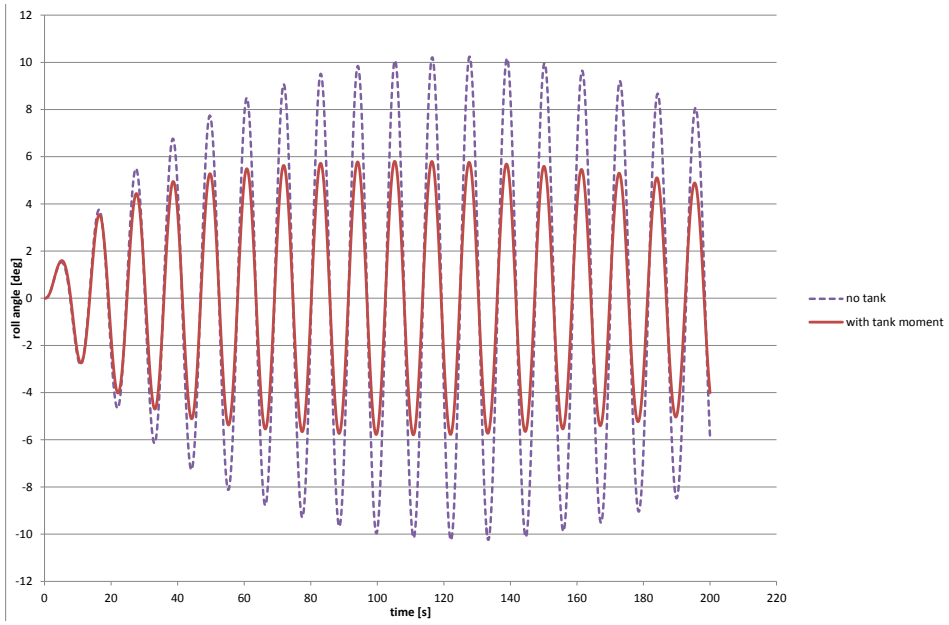

(a) Motion of the ship with and without tank action

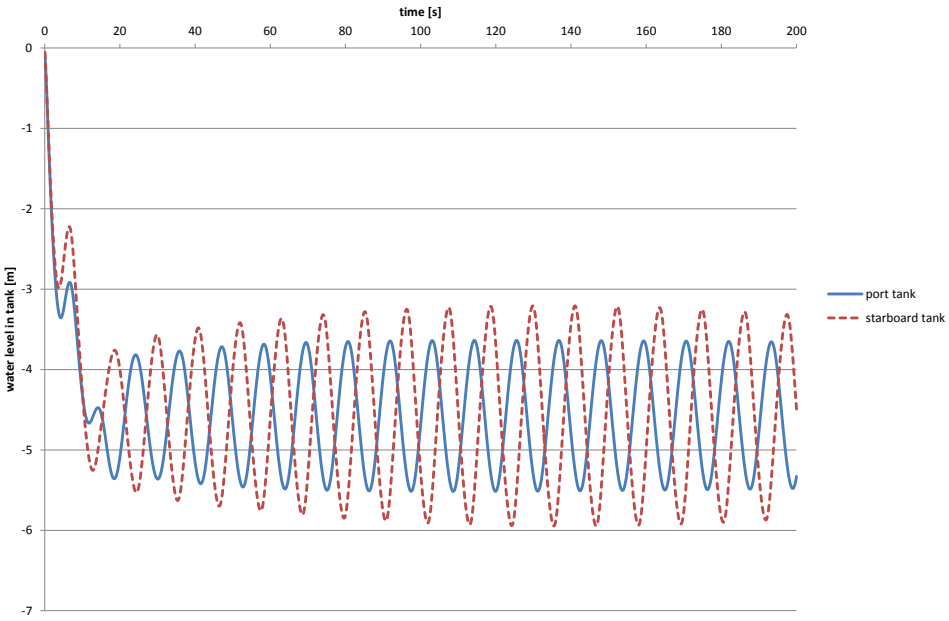

(b) Water level in the tanks

Figure 4.8: Motion of the ship and tank water levels (AQWA-NAUT)

4.1.3. SCILAB simulation

In order to check the results from the AQWA-NAUT simulation a simple time simulation program was written in SCILAB, based on the assumption that linear theory applies even though the tank equation is weakly non-linear. What is neglected is the fact that a displacement during a previous time interval influences the motions not only during this interval, but also in all later time intervals. In other words, the system in SCILAB does not have a form of "memory" in contrast to the system in AQWA-NAUT.

As mentioned in the chapter introduction it is of importance to check the non-dimensional damping coefficient κ for the roll motion. Besides the unrealistic roll angles one would determine when viscous damping is excluded, it is imperative to include an appropriate amount of viscous damping in order for the SCILAB time simulation to converge. The damping coefficients for a small selection of ships including the Jascon 18 is given in table 4.3.

	L/B	B/T	damping coefficient κ	
			excl. viscous damping	incl. viscous damping
Jascon 18	3.9	5.7	0.02	0.09
ship 1	3.9	5	0.03	0.10
ship 2	2.2	14	0.09	-

Table 4.3: Non-dimensional damping coefficient

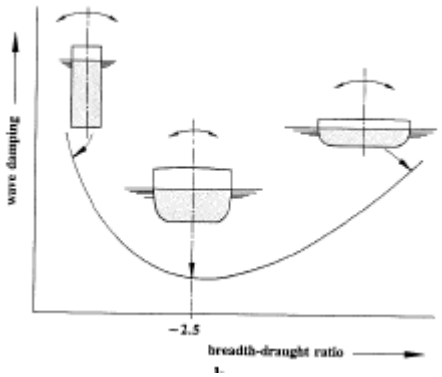

Figure 4.9: Wave potential damping on roll motion

Ship 2 has a much larger B/T ratio than the other two ships. From figure 4.9 it can be seen that the wave potential damping for roll is much larger for this ship than for the other two, which is why its damping coefficient is already sufficiently large. The other two require the manual addition of viscous damping. On the basis of a small selection of ships no specific limit for the damping coefficient could be found.

The time simulation results at a frequency of 0.55 rad/s for the Jascon 18 with a tuned tank in beam waves (coming in from starboard) are given in figure 4.10. The simulation is including radiation pressure. The roll reduction is 26%. The water levels in the SCILAB simulation

oscillate nicely round the equilibrium water level, confirming that the offset in the AQWA-NAUT simulation is an irregularity.

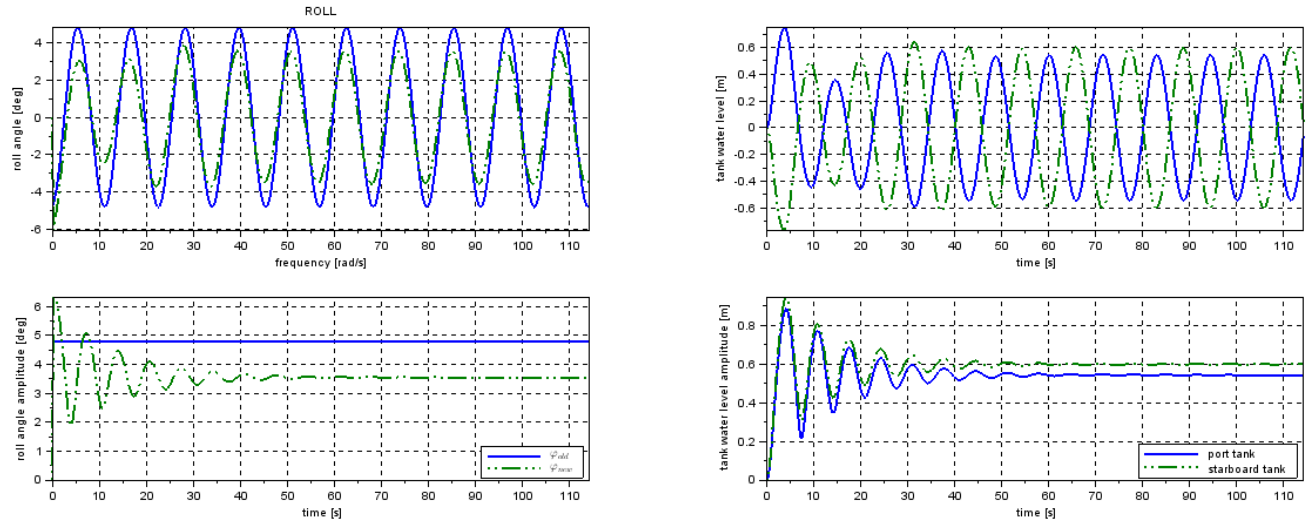

(a) roll motion

(b) tank water level

Figure 4.10: Time simulation tuned tank (SCILAB)

Solution convergence Even though the step size is automatically determined in the variable step routine, a qualitative measure is incorporated in the calculation through an overall tolerance level. This tolerance level is used to adjust the time step to where the difference between the fourth and fifth order approximations in the Cash-Karp method meets the tolerance criterium. Figure 4.11 shows the trade off between accuracy of the calculation and the computing time for the tuned and the untuned tank. Based on this information the overall tolerance level is set at $1e^{-9}$ for the wave excited calculations in SCILAB.

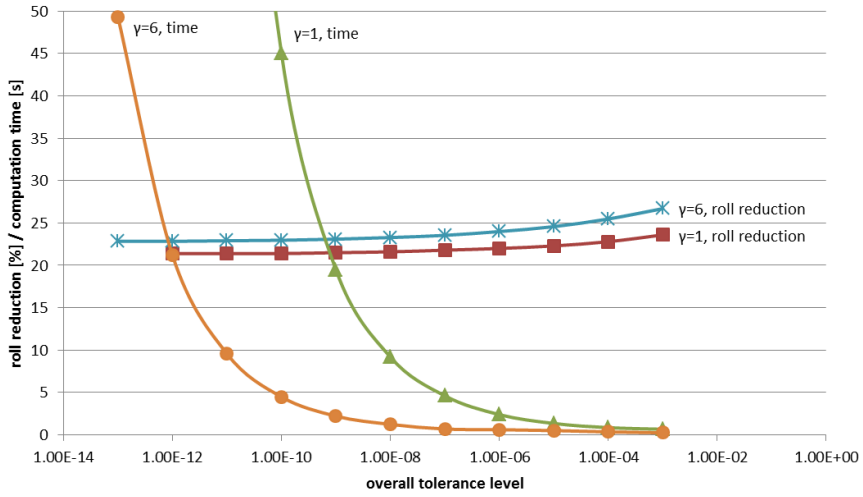

Figure 4.11: Trade off between accuracy and computing time (wave excited simulation)

4.2. Frequency domain

The normalized results from the SCILAB simulation in the frequency domain are given in this section. The tolerance for the tank water level in the frequency domain simulation is set at a thousandth of the absolute value. All attempted cases converge for this value. Should a case not converge for all frequency/direction combinations a log file is created, which contains the information on the non-converged frequency/direction combinations. A log file is also created when saturation or ventilation of the tank occurs.

4.2.1. Regular wave response

In this section the results for a tuned tank are shown with viscous damping including the correction step for the viscous damping based on the motions damped by the free-flooding tanks. The value for the viscous damping of the roll motion without tanks is iteratively determined to be 17% the critical damping for a regular wave amplitude of 1m. As a result of the damped motions the viscous damping of the roll motion is reduced from 17% of the critical damping to 12%. The expected response of the ship is given in figure 4.12b; the roll motion in beam seas is reduced from an amplitude of 4.8 degrees to 3.8 degrees, which is a reduction of 27%.

The tank action depends on both the change in metacentric height, shifting the ship's natural period, and a stabilizing moment. If the tank action depended only on the first, figure 4.12b would merely show a shift of the roll motion peak response to a different wave frequency. The change in natural roll period is not very large for this particular vessel and does not have a discernible influence. The response curve does broaden a little, but the free-flooding tanks seem to have hardly any effect on the roll motion aside the resonance frequency.

Compare figure 4.12b with the RAOs in figure 4.13, which is damped with the viscous damping value for the original roll RAO; it is clear that the performance of the tank would be overestimated if the viscous damping would not be adjusted to the new ship roll motion.

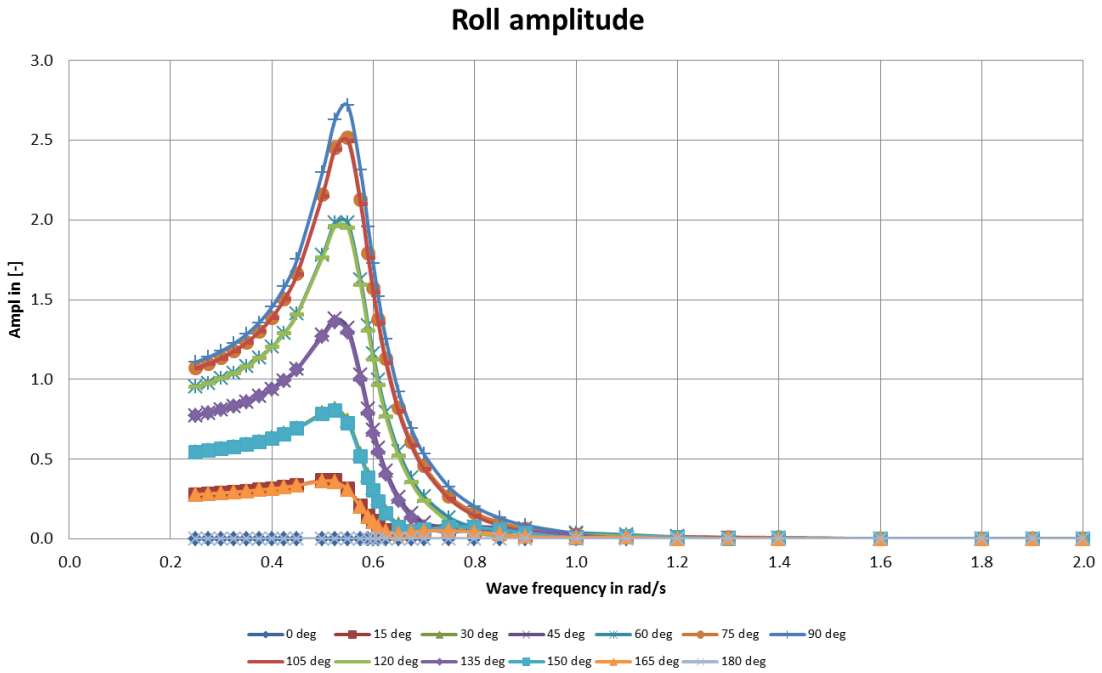

(a) excluding tank action (viscous damping: $0.17C_{cr}$)

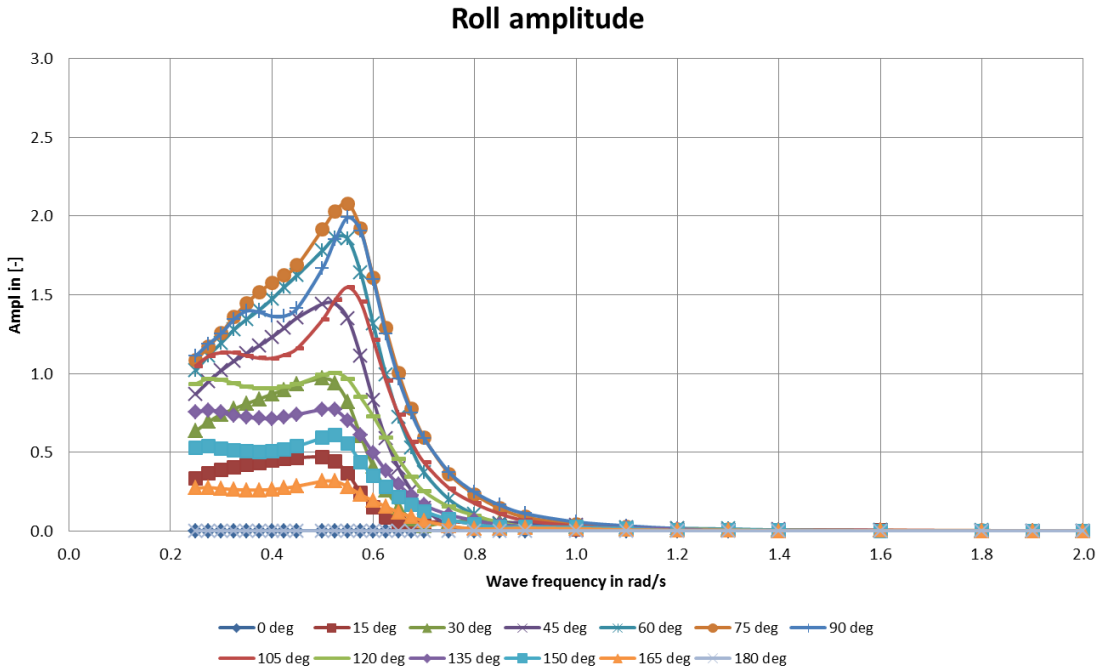

(b) including tank action (viscous damping: $0.12C_{cr}$)

Figure 4.12: RAOs for roll with the tuned tank in a regular wave

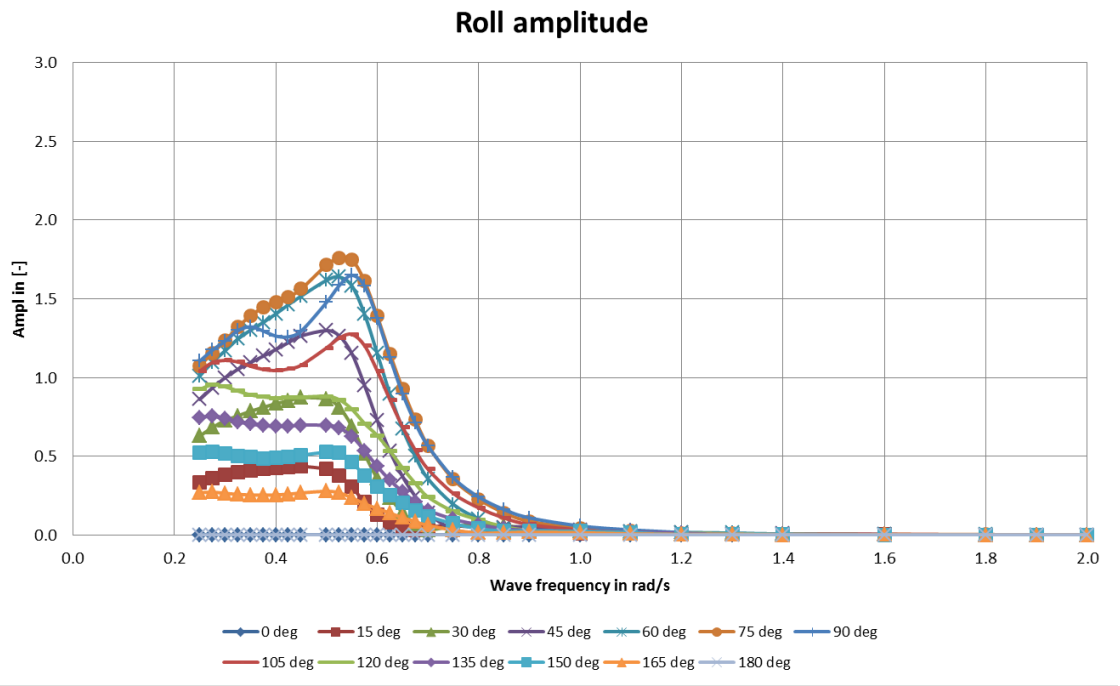

Figure 4.13: Overdamped RAOs for roll with the tuned tank in a regular wave ($0.17C_{cr}$)

Coupling of the tank action into other motions Webster [9] stipulated that the free-flooding tanks influenced the roll motion in particular and had a small effect on the sway and yaw motions, whilst not having a significant effect on the heave and pitch motions. These effects are found to be slightly different in the results as presented in appendix D. The anti-roll tank seems to have no significant effect on the surge, sway and yaw motions, while the heave and pitch motions are slightly influenced. These last two are a result of the heave force and pitch moment of the tank. The influence is small and may be neglected. For the Jascon 18 there is no coupling of the sway and yaw motions with the roll motions. Away from resonance the anti-roll tanks seem to have no effect on any of the motions.

4.2.2. Irregular wave response

In this section only the results are shown for the motion of interest: roll. The amount of added damping is estimated here using Ikeda's Method for Rectangular Barges [18] and the significant wave height in irregular waves. The value for the viscous damping of the roll motion for this particular ship is iteratively determined to be 12% of the critical damping in an irregular JONSWAP wave spectrum with a significant wave height of 2.5 meters.

The expected response of the ship is given in figure 4.14b; the roll motion is reduced from an amplitude of 6.7 degrees to 4.7 degrees, which is a reduction of 30%.

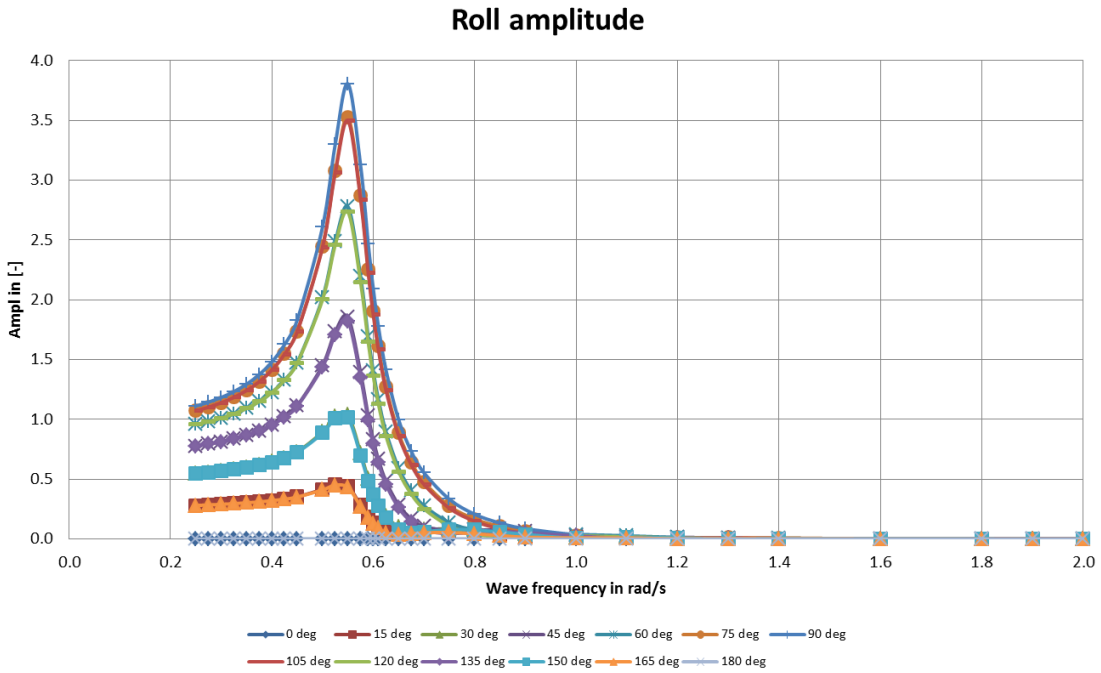

(a) excluding tank action (viscous damping: $0.12C_{cr}$)

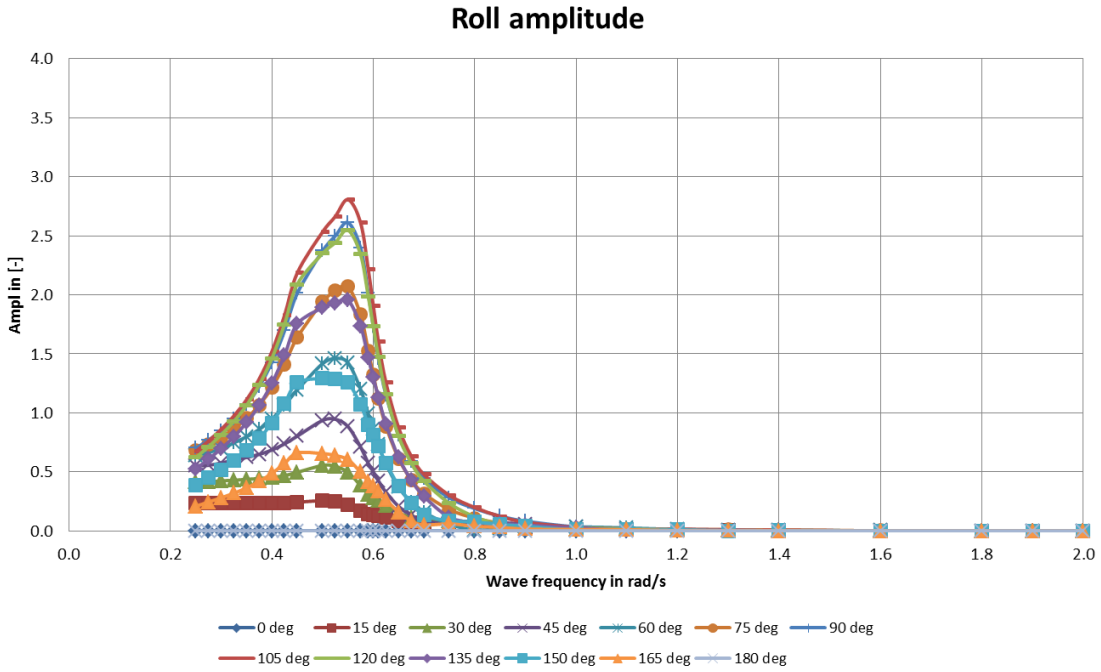

(b) including tank action (viscous damping: $0.08C_{cr}$)

Figure 4.14: RAOs for roll with the tuned tank in an irregular wave spectrum

4.3. Discussion of results

The results are in a regular wave with an amplitude of 1 meter and beam seas condition (wave coming in from starboard at $90°$ in the model).

4.3.1. Linearization of model

Webster in effect linearizes the mathematical model by computing the system of equations in a non-dimensional format (per one meter wave amplitude). However, if the model is computed without dividing through the wave height the tank performance is clearly non-linear with respect to wave height, as can be seen in figure 4.15. It is inversely and non-linearly related to wave height and not linearly increasing. The shape of the curve is the same as found for the damping curve derived from the free decay analysis in § 4.1.1. This means that the RAOs given in § 4.2 are only valid for a wave amplitude of one meter. Because of this result all the tank performances given in this chapter are based on actual peak roll angles for a wave amplitude of one meter and not on the RAO peak.

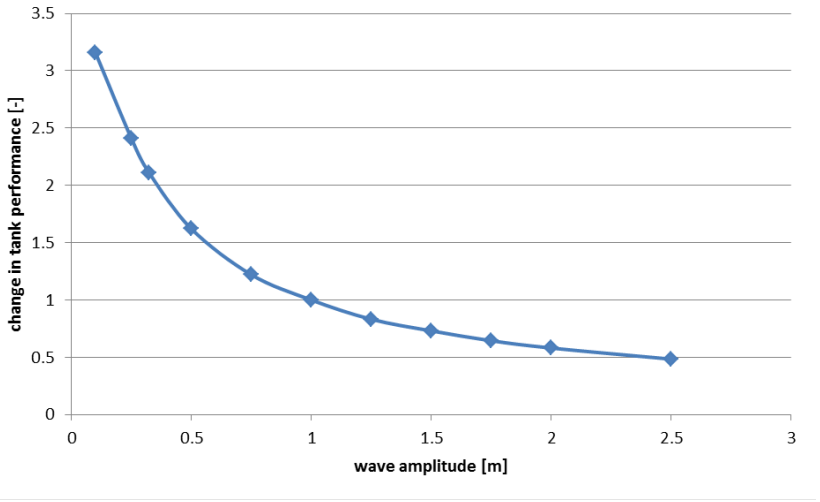

Figure 4.15: Tank performance for different wave heights

4.3.2. Comparison of simulation types

The simulations are compared for a tuned tank with a flooding port size ratio of 0.22 to the free surface area. The original roll peak is 4.8 deg.

The results from the frequency domain simulation and the direct time domain simulations correspond to each other. Even for the direct AQWA-NAUT simulation, even though, the returned water levels are incorrect. Compared to the reduction in the direct AQWA-NAUT and SCILAB wave excited simulations the equivalent damping seems to underestimate the damping of the roll motion by the free-flooding tanks only slightly. Nevertheless, indirect AQWA-NAUT simulation is really only useful if the roll angle data from the actual free decay test of the ship is available, because that includes the viscous damping.

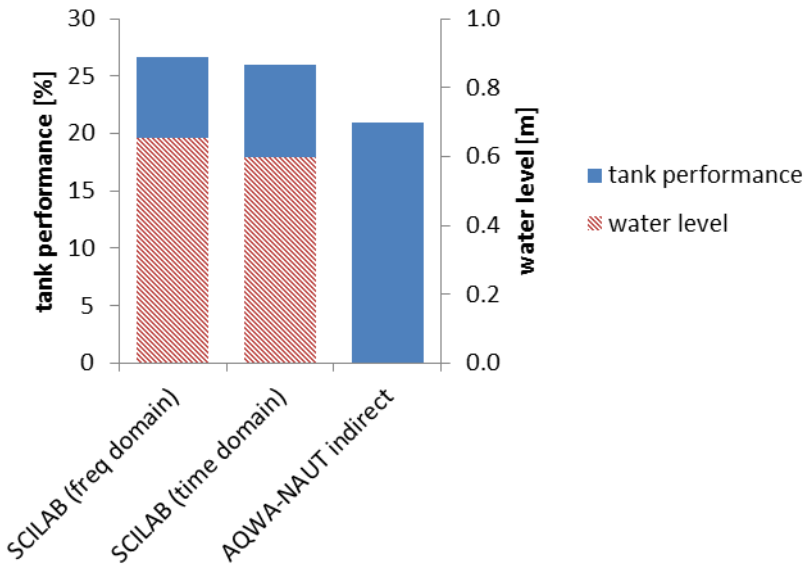

Figure 4.16: Comparison of time and frequency domain simulation results

4.3.3. Comparison of Webster Model with VER Model

In this section several tank designs are evaluated and compared to the results from the study by VER in 2009.

In the VER Model with external free-flooding tanks a roll amplitude reduction of 37% was found for a tank with $\gamma = 1$ and a flooding port size of 22% of the free surface area [2]. The layout of the tank is shown in figure 4.17a. This external tank is moved to the inside for evaluation with the Webster Model. Due to this move the flooding port is transferred from the bottom of the tank to the side.

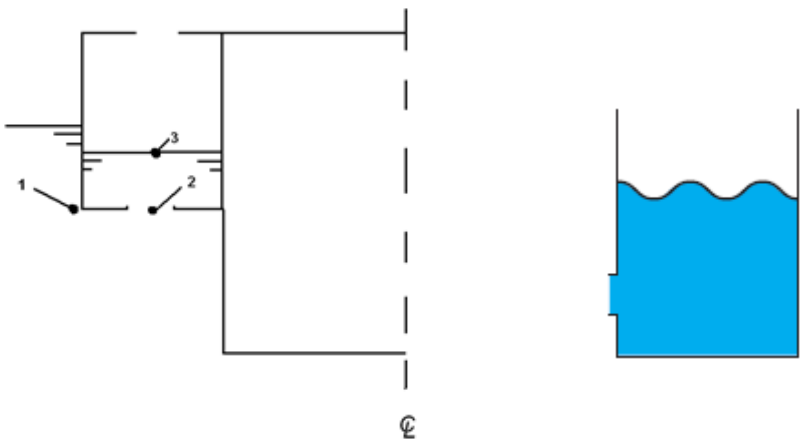

(a) External free-flooding tank used in the VER Model

(b) Internal free-flooding tank used in the Webster Model

Figure 4.17: The tanks used for comparison of modeling

The tank in the VER Model has an equilibrium water level of 2 meters. With this equilibrium water level the inlet duct for a tuned tank needs to be unrealistically small to fit a geometry factor of 16 plus the flooding port starts ventilating, which is not included in the model. In reality the tuned tank needs more space under water to incorporate the shaping of the inlet duct plus a straight section under the free surface, so the tank performance of the tuned tank cannot be evaluated for an equilibrium water level of 2 meters.

The external water pressure head for the simulations is approximated using the wave elevation, because the potentials at the higher located flooding port were not available at the time (i.e. no radiation pressure included in the Webster Model). The tank with $d_w = 2$ shows the best performance, however it should be noted that this tank will start ventilating at a static roll angle of 7 degrees. For this or larger angles the tank effectiveness will decrease. The tank performance is higher than that of the tank with a lower set flooding port (figure 4.16) as a result of the higher external pressure from the wave elevation. The wave elevation at the flooding port decreases as it is set lower in the hull (increasing d_{ew}).

In the VER Model the roll reduction was estimated to be 37% for externally added free-flooding anti-roll tanks, in the Webster Model the internal free-flooding tanks are expected to damp the roll motion with 32%. One of the differences is that in the VER calculations steady flow is assumed, whilst Webster assumes quasi-steady flow. It was found that including the unsteady terms ($\ddot{Y}$ and $\ddot{Z}_{tk}$) in the model reduces the expected tank moment. The other difference between the models is the modeling of the pressure head at the flooding port: Froude Krylov head plus velocity head versus wave elevation. Compared to the VER Model the tank performance is estimated to be about 5% lower. Since there is no experiment data available, it is not possible to conclude which of the two models gives a better estimation of the tank performance, but it is plausible that the Webster Model comes closer because it takes unsteady behavior of the tank water into consideration.

4.3.4. Comparison of air configurations

The results in the fully vented, the separately vented and the crossover connected case are essentially equal, figure 4.18. The choice between the three configurations can therefore be based entirely upon construction considerations, since air vent size has a nearly negligible effect on the performance of the tanks (also see figure 4.27).

The unvented tank can be considered a fully vented tank if the height of the plenum is sufficiently large. As the height of the plenum is reduced, the roll reduction goes to zero. For a plenum height d_u of 0.7 meters the roll reduction is a mere 0.5%. It is advantageous therefore to minimize the height of the plenum and install an air vent with a valve in order to close off the tank effectively turning it into an unvented tank. This way the tanks can be shut off. Fully vented the water level comes up to 0.6 meters in the simulation, so the plenum height cannot be reduced much further than 0.7 meters.

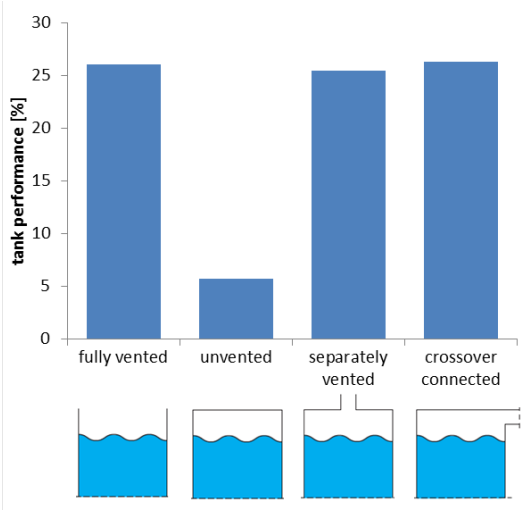

Figure 4.18: Comparison of frequency domain results for different air configurations

It can be concluded that only for greatly restricted air flow or a small plenum height there is an effect of air pressure on the tank water level, else the effect is so small that it might as well be neglected. This is in line with the conclusions drawn by Webster who stated that the part of the theory describing the effects of air pressure might as well not have been present even though it yields reasonable results compared for the physical model.

4.3.5. Influence of radiation pressure

The expectation was that the radiation pressure would have a larger influence on the tank performance for ship 2 than for the Jascon 18, because the motion of the second ship is damped in addition with viscous damping. As can be seen in figure 4.19 the radiation pressure head has less influence on the tank performance of ship 2 (6%) than on the Jascon 18 (14%). However, the order of magnitude remains the same, so it is permissible to neglect radiation pressure if no data is available. This entails that the free surface height from AQWA may be used as input in the model if the potentials are unavailable.

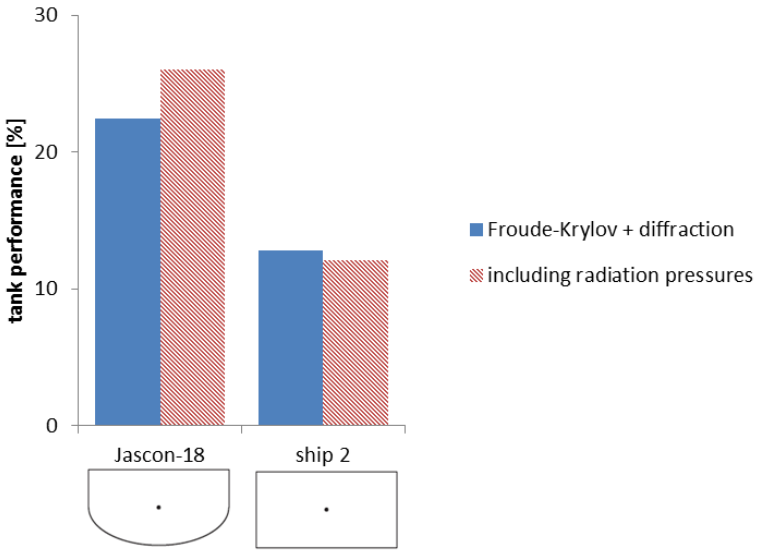

Figure 4.19: Influence of pressure head components on tank performance

4.3.6. Influence of tank parameters on tank performance

The tank parameters are determined in the design stage and cannot be readily adapted once the tank has been built. This means that in the design stage a good deal of thought needs to be put into working conditions and loading conditions.

On the subject of the design of the tank the conclusions of the influence of tank parameters are the following. Even though for this particular ship there seems to be no advantage of the tuned tank over the untuned tank, the tank performance can be optimized by thorough inlet design. The flooding port size and duct shape have a great influence the tank transfer period and the effective discharge coefficient.

Tank transfer period

The tank transfer period is sensitive to the geometry factor and the equilibrium water level (figure 4.20). The tank transfer period can be adjusted by changing the equilibrium water height in the tank, for example by adjusting the location of the flooding port, or the geometry factor by tuning. If the tanks would be actively controlled, the tank transfer period could also be adapted by changing the air pressure in the tanks, effectively changing d_w. Adapting the tank transfer period does not alter the magnitude of the water level much, but does influence the phase shift, positioning the tank moment more or less favorably with respect to the heeling moment. Figure 4.21 shows that the tank moment for the tuned tank lags with $90°$ when the wave excitation period is equal to the ship natural roll period, at this point the tank will damp the roll motion the most. For this particular ship the difference in tank performance is small even though the tank transfer period is heavily influenced, because the difference in phase lag between the untuned tank and the tuned tank is small (see figure 4.22).

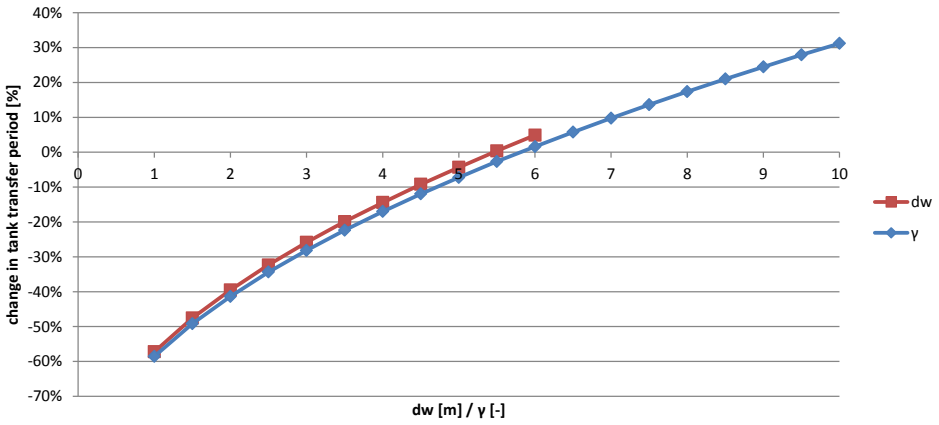

Figure 4.20: Influence of d_w and γ on the tank transfer period

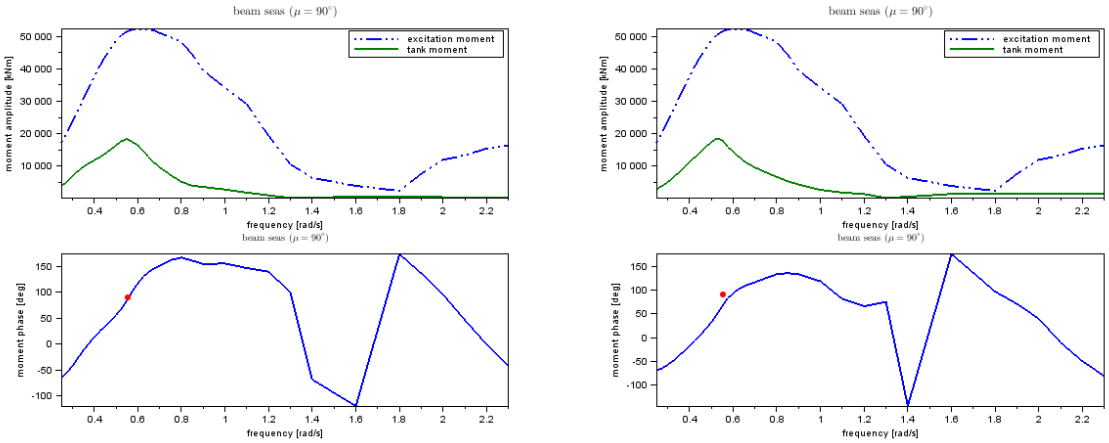

(a) $\gamma = 6$ (b) $\gamma = 1$

Figure 4.21: Tank moment amplitude and phase

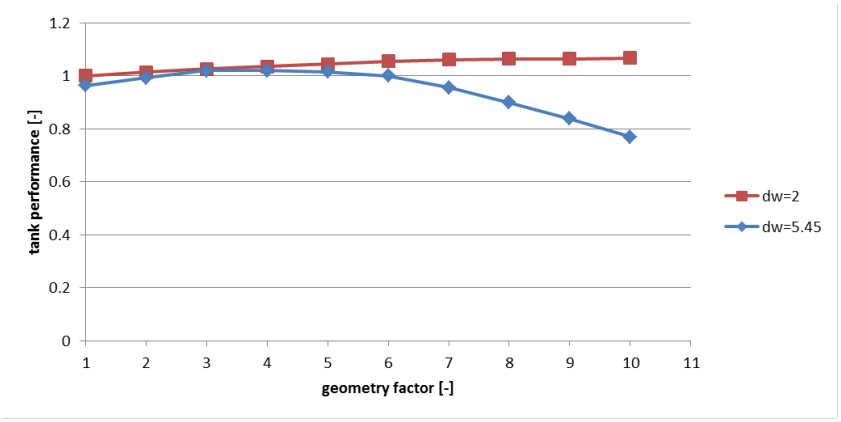

(a) Influence of equilibrium water height

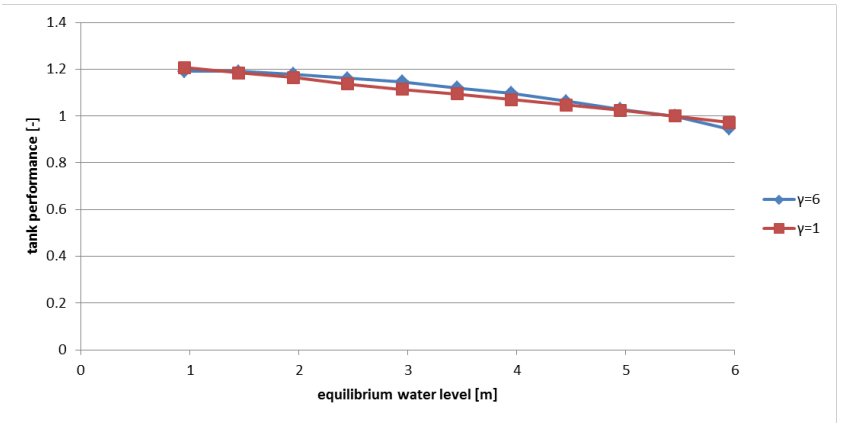

(b) Influence of tank geometry factor

Figure 4.22: Influence of tank transfer period on tank performance

For the aircraft carrier studied by Webster the theoretical difference in performance was significant. The performance difference between an untuned and a tuned tank is probably dependent on the location of the roll peak relative the location of the maximum wave potential

damping. The wave potential damping for the aircraft carrier is presumably lower as its natural roll period lies higher at 15.7 seconds versus 11.3 seconds for the Jascon 18. It must also be noted that the maximum roll angle of the aircraft carrier is likely much larger than the maximum roll angle of the Jascon 18 as its metacentric height is only half as high. The last has a maximum roll angle of only 4.8 degrees, which means that a round off error has a much greater influence on the results. In conclusion, for the Jascon 18 tuning has a small effect, but no general conclusion can be drawn on whether tuning for other vessels is necessary in order to optimize performance.

Free surface area

Figure 4.23 shows a linear association of the tank free surface area with the tank performance. This means that if the performance is calculated for only two area sizes a good estimation can be given. The maximum free surface area depends on the space available in the ship. The change in free-surface effect has not been taken into account in this influence evaluation.

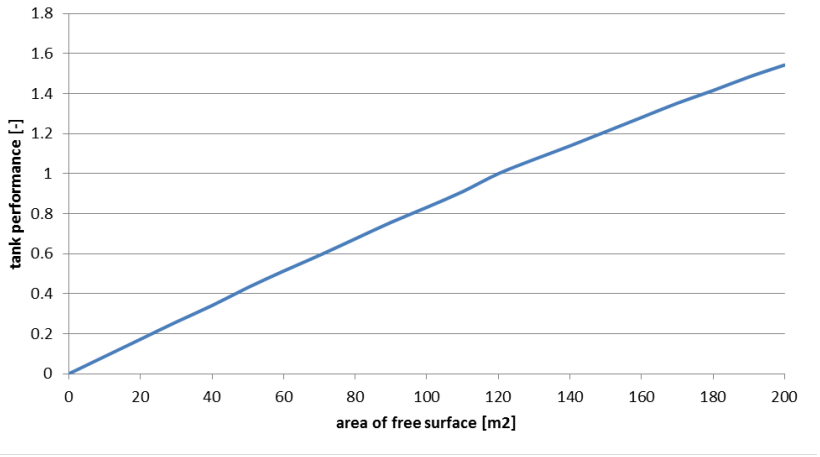

Figure 4.23: Influence of free surface area on tank performance

Inlet coefficients

The non-dimensional flooding port size β (figure 4.24) influences the flow rate and thus directly the attained water level. Although it is treated separately here, it is linked to the tank geometry factor, see equation (3.5): $A(s = 0) = \beta A_0$.The relationship between the flooding port size and tank performance is non-linear. The increase in tank performance levels off as the size of the flooding port increases. This effect is more pronounced with the lower viscous damping as used for the evaluation of the tank performance in irregular waves. Any construction issues have not been taken into account, but in the design a trade off between pipe design, tank geometry factor and flooding port size exists.

The effective discharge coefficient C_{wd} (figure 4.25) influences the roll damping less strongly than the flooding port size, but still significantly. The parameter depends on the size of the flooding port and the shape of the duct behind it. For the untuned tank the discharge coefficient is more or less constant, but the effectiveness of the tuned tank can be optimized through the

inlet design. The determination of this coefficient is treated more extensively in the introduction of this chapter where the choice for the tank parameters in this report is elaborated upon.

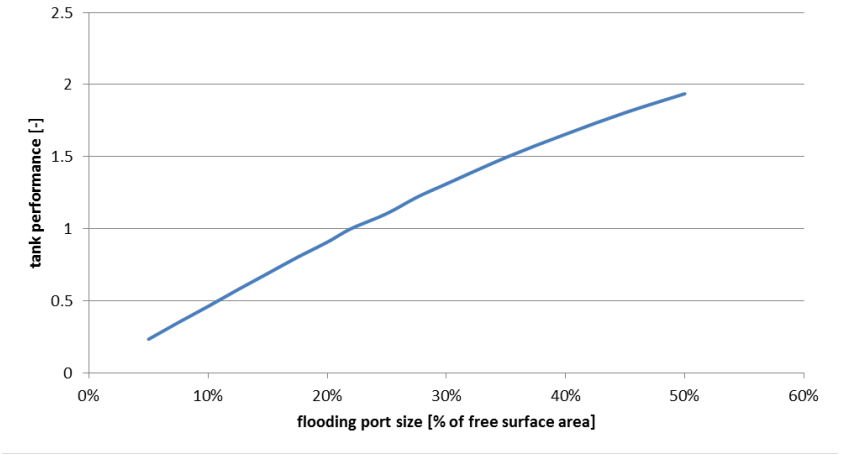

Figure 4.24: Influence of flooding port size on performance

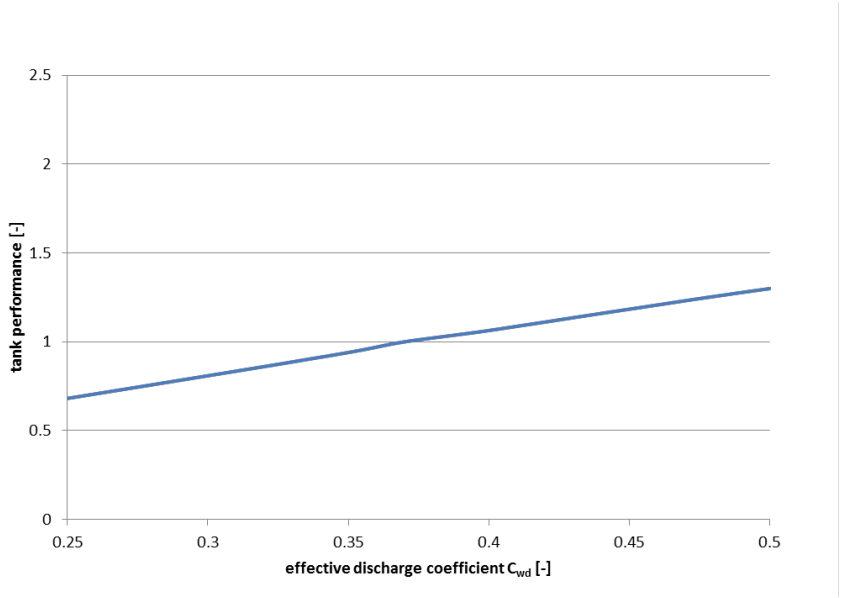

Figure 4.25: Influence of flooding port discharge coefficient on water level

Air vent coefficients

The vent coefficients α (dimensionless vent size) and C_{ad} (air discharge coefficient) of course only play a role in the case of separate venting and not in the fully vented case. The comparison given in this paragraph cannot entirely be justified, because the air discharge coefficient depends to a large extent on the vent size. Unfortunately, since the Webster Model does use the two coefficients separately, they need to be defined independently in order to get a result.

Despite of the interdependency of the vent size and the discharge coefficient an attempt is made here to at least give a quantitative indication of the effect of the vent size α. The size of the vent has a significant influence on the water level up to about 1.5% of the free surface

area with the air discharge coefficient set at 0.7; for larger vent sizes the behavior will not differ from the fully vented case ($\alpha = 1$).

The air discharge coefficient is found to vary between 0.19 and 1.25 according to Kinsman [21] and these limits are also held here. It seems that the value chosen by Webster (0.7) lies in the middle of the range and should be a safe estimated value for the effective discharge coefficient.

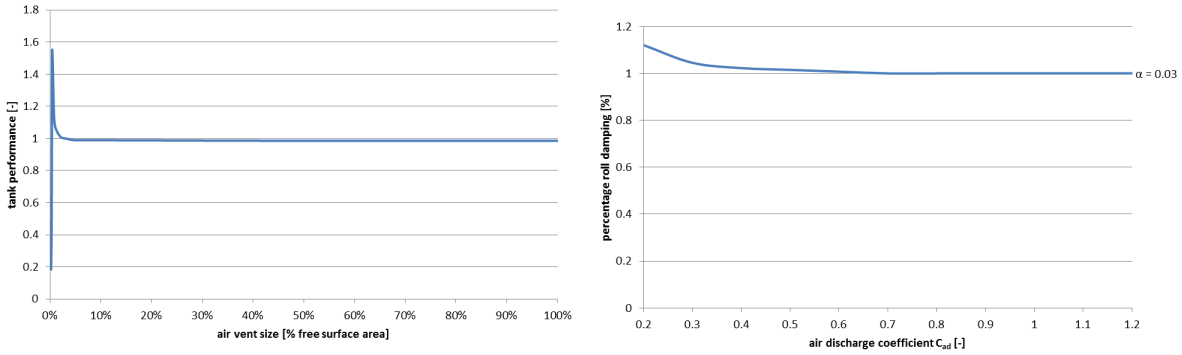

(a) dimensionless size of vent α

(b) air discharge coefficient C_{ad}

Figure 4.26: Influence of air coefficients on tank performance

From figure 4.27 it is clear that the effect of the air pressure on the tank water level is minimal unless the lower limit is approached, where uncertainties in the correctness of the values are large. This means that, unless αC_{ad} is very small, exact values for the vent coefficients are not important to obtain a good indication of tank water level and the generated tank moment. This is in line with the conclusion that there is a negligible effect of passive air pressure on the tank performance. It is adequate to use estimated values in the tank model. In combination with the results in figure 4.18 it can be said that the design of air vents is secondary to the design of the water inlet.

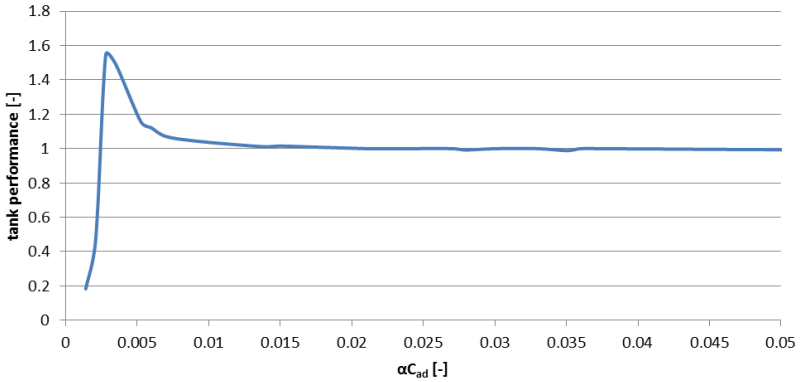

Figure 4.27: Influence of combined air vent coefficients αC_{ad} on tank performance

5

Conclusions and recommendations

5.1. Conclusions

A roll reduction of 30% may be expected in irregular waves for this particular vessel for a peak roll angle of 6.7 degrees in beam seas. This maximum roll angle is small, which means that the uncertainty in the tank performance is relatively large.

The tank performance is non-linearly related to the differential pressure head over the flooding port and therewith directly with the incoming wave height. Consequently the ship response should not be defined using RAOs, but using the actual predicted roll angle.

The tank performance for the frequency domain and time domain simulations in SCILAB agree as essentially the system of equations is solved in the same way. If the radiation pressure is not taken into account the tank performance can differ with a few percent from the tank performance calculated including the radiation pressure, however, the order of magnitude remains the same. This means that the wave elevation at the flooding port from AQWA (Froude-Krylov plus diffraction) obtains sufficient information on the pressure head to give a good indication of the tank performance.

For a time simulation the equations of motion and tank equation should be integrated simultaneously and interactively. In the AQWA-NAUT time simulation this is not possible and results are considered unreliable. An indirect time simulation in AQWA-NAUT using tank damping values from a theoretical free decay analysis differs significantly from the estimated tank performance by SCILAB. It is possibly a good alternative if experimental values from a free decay test of the actual ship are available.

The parameters influencing tank performance are identified for design purposes. Even though for this particular ship there seems to be no advantage of the tuned tank over the untuned tank, the tank performance can be optimized by thorough inlet design. The flooding port size and duct shape have a great influence the tank transfer period and the effective discharge coefficient. Fitting a valve on the air vent or in the crossover connection between the tanks enables a shutdown of the tanks, if the height of the tank above equilibrium water level is

sufficiently small. Otherwise the air pressure has a negligible effect on the tank performance and the most convenient configuration for construction may be selected.

5.2. Recommendations

The coupled ship and tank model explored in this report has been verified as far as feasible. To validate these calculations it is advised to perform experiments. Webster found a good correlation between the model and experiments.

Design aspects have not been taken into consideration in this report, while they are essential for the determination of the expected tank performance. One of the important aspects lacking in the results is a good estimate of the effective discharge coefficient for the tuned tank.

The SCILAB time domain simulation presented in this report simply solves the equations of motion and the tank equation separately at each time step. If more extensive calculations in time domain are desired, it is advisable to at least include the influence of the motions from the previous time intervals (”memory”) plus retardation functions. It might also be of interest to include a non-linear restoring and damping moment to closer approximate the roll behavior of the ship.

A possible improvement on the frequency domain simulation is a multi-domain simulation where the interaction between the tank and the ship directly depend on each other. The differential pressure head over the flooding port can then be determined directly at the joint boundary of the domains.

Bibliography

[1] *Free-flooding Anti-roll Tanks - feasibility study*, Tech. Rep. 09.185 R01 - Rev B1 (Vuyk Engineering Rotterdam B.V., 2010).

[2] *Free-flooding Anti-roll Tanks - preliminary tank dimensions*, Tech. Rep. 09.185 R02 - Rev B (Vuyk Engineering Rotterdam B.V., 2010).

[3] J. H. Chadwick, *On the stabilization of roll,* Transactions - Society of Naval Architects and Marine Engineers (SNAME) **63**, 237 (1955).

[4] *Anti Roll Tank System for Offshore Crane/Pipelay Vessel - phase 1*, Tech. Rep. 24001-100 (Maritime Research Institute Netherlands (MARIN), 2010).

[5] *Anti Roll Tank System for Offshore Crane/Pipelay Vessel - phase 2*, Tech. Rep. 24001-300 (Maritime Research Institute Netherlands (MARIN), 2010).

[6] *AQWA-LINE User Manual*, ANSYS, Inc., release 14.5 ed. (2012).

[7] *AQWA-NAUT User Manual*, ANSYS, Inc., release 14.5 ed. (2012).

[8] Wikipedia, the free encyclopedia (2014).

[9] W. C. Webster, J. F. Dalzell, and R. A. Barr, *Prediction and measurement of the performance of free-flooding ship antirolling tanks,* Transactions - Society of Naval Architects and Marine Engineers (SNAME) **96**, 333 (1988).

[10] J. A. Pinkster, *Low Frequency Second Order Wave Exciting Forces on Floating Structures*, Ph.D. thesis, Delft University of Technology (1980).

[11] H. Rouse, *Elementary Mechanics of Fluids* (Wiley, New York, 1946).

[12] C. Stigter, *Performance of U-Tanks as a Passive Anti-Rolling Device*, Tech. Rep. report no. 81S (Delft Hydraulics Laboratory, TNO, 1966).

[13] R. A. Barr and V. Ankudinov, *Ship rolling, its prediction and reduction using roll stabilization,* Marine Technology **14**, 19 (1977).

[14] J. D. Skufca, *Analysis still matters: A surprising instance of failure of Runge–Kutta–Felberg ODE solvers,* SIAM review **46**, 729 (2004).

[15] J. R. Cash and A. H. Karp, *A variable order Runge-Kutta method for initial value problems with rapidly varying right-hand sides,* ACM Trans. Math. Softw. **16**, 201 (1990).

[16] S. N. Blagoveshchensky, *Theory of Ship Motions*, edited by L. Landweber, Vol. 2 (Dover Publications, New York, 1962) translated from the 1st Russian edition by T. Strelkoff and I. Strelkoff.

[17] P. D. Chaplin, *The effectiveness of roll stabilisers,* The Naval Architect **2**, 33 (1972).

[18] Y. Ikeda, T. Fujiwara, and T. Katayama, *Roll damping of a sharp-cornered barge and roll control by a new-type stabilizer,* in *Proceedings of the 3rd International Offshore and Polar Engineering Conference* (1993) pp. 634–639.

[19] P. Ruponen, *Progressive Flooding of a Damaged Passenger Ship*, Ph.D. thesis, Helsinki University of Technology, Espoo, Finland (2007).

[20] *IMO Resolution A.266(VIII) SLF50/10,* (2007).

[21] R. G. Kinsman, *Outlet Discharge Coefficients of Ventilation Ducts*, Master's thesis, McGill University, Montreal (1990).

[22] W. H. Press, S. A. Teukolsky, W. T. Vetterling, and B. P. Flannery, *Numerical Recipes in C++: The art of scientific computing*, 2nd ed. (Cambridge University Press, New York, 2002).

A

Dynamic air pressure

Substituting the atmospheric pressure R_1, the linearized discharge coefficient R_Δ and the standard atmospheric conditions R_3 into equation (3.10), the mass flow becomes:

$$\dot{m}_a = \alpha A_0 \cdot C_{ad} \sqrt{\frac{p_1}{|p_j - p_{jo}|}} \cdot \sqrt{\frac{|p_j - p_{jo}|}{p_1}} \cdot \sqrt{2\rho_1(p_j - p_{jo})} = \alpha A_0 R_\Delta \sqrt{2\frac{\rho_1}{p_1}}\,(p_j - p_{jo})$$
$$= \alpha A_0 R_\Delta \sqrt{2\frac{\rho_0}{p_0}}\,(p_j - p_{jo}) = \frac{\alpha R_\Delta m_0}{d_u p_0} \sqrt{2\frac{p_0}{\rho_0}}\,(p_j - p_{jo}) = \frac{\alpha R_\Delta R_3 m_0}{d_u p_0}\,(p_j - p_{jo})$$

Net air mass Δm extracted from the starboard tank is the integral over time of the mass flow:

$$p_0 \frac{\Delta m}{m_0} = \frac{\alpha R_\Delta R_3}{d_u} \int_{-\infty}^{t} (p_j - p_{jo})\, dt \tag{A.1}$$

The mass density is:

$$\rho = \frac{M_0 - \Delta M}{A_0(d_u - \Upsilon_j)} = \rho_0 \frac{1 - \Delta M/M_0}{1 - \Upsilon/d_u}$$

Linearize this mass density around $a = 0$. The general formula for linearizion is $L(x) = f(a) + f'(a)(x - a)$.

$$x = \frac{\Delta M}{M_0}$$
$$f(x) = 1 - x \quad \Rightarrow \quad f(0) = 1$$
$$f'(x) = -1 \quad \Rightarrow \quad f'(0) = -1$$
$$L_1(x) = 1 + (-1) \cdot (x - 0) = 1 - x = 1 - \frac{\Delta M}{M_0}$$

$$
\begin{aligned}
x &= \frac{\Upsilon_j}{d_u} \\
f(x) &= \frac{1}{1-x} \qquad \Rightarrow \qquad f(0) = 1 \\
f'(x) &= \frac{1}{(1-x)^2} \qquad \Rightarrow \qquad f'(0) = 1 \\
L_2(x) &= 1 + 1 \cdot (x - 0) = 1 + x = 1 + \frac{\Upsilon_j}{d_u}
\end{aligned}
$$

$$
L(x) = L_1(x) \cdot L_2(x) = \left(1 - \frac{\Delta M}{M_0}\right)\left(1 + \frac{\Upsilon_j}{d_u}\right) = 1 - \frac{\Delta M}{M_0} + \frac{\Upsilon_j}{d_u} - \frac{\Delta M}{M_0} \cdot \frac{\Upsilon_j}{d_u}
$$

$$
\rho_j = \rho_0 \left(1 - \frac{\Delta M}{M_0} + \frac{\Upsilon_j}{d_u}\right) \quad \Rightarrow \quad p_j = p_0 \left(1 - \frac{\Delta M}{M_0} + \frac{\Upsilon_j}{d_u}\right)
$$

$$
\frac{\Delta M}{M_0} = 1 + \frac{\Upsilon_j}{d_u} - \frac{p_j}{p_0} \tag{A.2}
$$

Substitute (A.2) into (A.1) and convert the air pressures into equivalent water heads:

$$
\begin{aligned}
\frac{\Delta M}{M_0} p_0 &= \left(1 + \frac{\Upsilon_j}{d_u} - \frac{p_j}{p_0}\right) p_0 = p_0 - p_j + \frac{\Upsilon_j p_0}{d_u} \\
&= \frac{\alpha R_\Delta R_3}{d_u} \int_{-\infty}^{t} (p_j - p_p)\, dt \\
p_j - p_0 &= \frac{\Upsilon_j p_0}{d_u} - \frac{\alpha R_\Delta R_3}{d_u} \int_{-\infty}^{t} (p_j - p_{jo})\, dt \\
\frac{p_j - p_0}{\rho g} &= \frac{\Upsilon_j}{d_u} \frac{p_0}{\rho g} - \frac{\alpha R_\Delta R_3}{d_u} \int_{-\infty}^{t} \left(\frac{p_j - p_0}{\rho g} - \frac{p_{jo} - p_0}{\rho g}\right) dt
\end{aligned}
$$

Substituting $P_j = \frac{p_j - p_0}{\rho g}$ and $R_1 = \frac{p_0}{\rho g}$ in the above air pressure equation for simplicity, results in:

$$
\begin{aligned}
P_j &= \frac{R_1}{d_u} \Upsilon_j - \frac{\alpha R_\Delta R_3}{d_u} \int_{-\infty}^{t} (P_j - P_{jo})\, dt \\
P_j + \frac{\alpha R_\Delta R_3}{d_u} \int_{-\infty}^{t} P_j\, dt &= \frac{R_1}{d_u} \Upsilon_j - \frac{\alpha R_\Delta R_3}{d_u} \int_{-\infty}^{t} P_{jo}\, dt
\end{aligned}
$$

with the newly defined atmospheric pressure in head of water $R_1 = \frac{p_0}{\rho g}$. As an example, the air pressure head is derived for separate venting. Since the tanks are not interconnected in

the separate venting case, the coupled air pressure term P_{jo} drops out:

$$P = \frac{R_1}{d_u}\Upsilon + i \cdot \frac{\alpha R_\Delta R_3}{d_u} \cdot \frac{P}{\omega}$$

$$\left(1 - i \cdot \frac{\alpha R_\Delta R_3}{\omega\, d_u}\right) P = \frac{R_1}{d_u}\Upsilon$$

$$\frac{\omega\, d_u - i\,\alpha R_\Delta R_3}{\omega\, d_u} \cdot P = \frac{R_1}{d_u}\Upsilon$$

$$P = \frac{R_1}{d_u}\Upsilon_j \cdot \frac{\omega\, d_u}{\omega\, d_u - i\,\alpha R_\Delta R_3} \cdot \frac{\omega\, d_u + i\,\alpha R_\Delta R_3}{\omega\, d_u + i\,\alpha R_\Delta R_3}$$

$$= \frac{R_1}{d_u} \cdot \frac{\omega^2 d_u^2 + i\omega\, d_u\, \alpha R_\Delta R_3}{\omega^2\, d_u^2 + \alpha^2 R_\Delta^2 R_3^2} \cdot \Upsilon$$

$$= \frac{\omega^2 R_1 d_u + i\omega\, \alpha R_1 R_\Delta R_3}{\omega^2\, d_u^2 + \alpha^2 R_\Delta^2 R_3^2} \cdot \Upsilon = \overline{V}\Upsilon$$

If the coupled air pressure term does not drop out, equation (3.11) (applying linear assumptions) reduces to:

$$P_j = \overline{V}_j \Upsilon_j + \overline{U}\Upsilon_{jo}$$

B

Numerical methods

The two numerical methods (Runge-Kutta and Cash-Karp), which were found to be the most suitable for computing the time domain problem in § 3.3.2, are described in this appendix section.

B.1. Fixed step method (Runge-Kutta)

A numerical method is an iterative method for the approximation of the solution of an ordinary differential equation. One of many numerical methods is the explicit recursive Runge-Kutta method (often abbreviated to RK4). This method is first order, which means that a second order differential equation needs to be simplified to contain only first derivatives in order to be able to implement the RK4 method. The initial value problem should be specified as follows:

$$\dot{x} = f(t, x), \quad x(t_0) = x_0$$

From this initial value vector x_0 the approximation of $x(t_{n+1})$ is calculated at a brief time later ($t_{n+1} = t_n + h$, where h is the step size) by adding the weighted average of four increments to the value at the present time x_n:

$$\begin{aligned} t_{n+1} &= t_n + h \\ x_{n+1} &= x_n + h\left(\frac{1}{6}k_1 + \frac{1}{3}k_2 + \frac{1}{3}k_3 + \frac{1}{6}k_4\right) \\ k_1 &= f(t_n, x_n) \\ k_2 &= f\left(t_n + \frac{h}{2}, x_n + \frac{h}{2}k_1\right) \\ k_3 &= f\left(t_n + \frac{h}{2}, x_n + \frac{h}{2}k_2\right) \\ k_2 &= f\left(t_n + h, x_n + hk_3\right) \end{aligned}$$

where x_{n+1} is the approximation of $x(t_{n+1})$. The k_i-terms are estimated slopes of the function at the specified time. Multiplied with the size of the interval this gives an increment to the value

at the present time. Basically, the RK4 method takes a trial step to the midpoint of the time interval twice and then uses the values at both the beginning and the midpoint to compute the "real" step across the whole interval.

In the implementation of the method in the calculations the generalized form of the RK4 is used. It is given by:

$$x_{n+1} = x_n + h\sum_{i=1}^{m} b_i k_i$$

$$k_i = f(t_n + c_j h, x_n + h\sum_{j=1}^{m} a_{ij}k_j)$$

$$= \frac{1}{C_1}\left(\begin{bmatrix} 0 & C_1 \\ -1 & -C_2 \left| y_n + h\sum_{j=1}^{m} a_{ij}k_j \right| \end{bmatrix} \underline{x} - \begin{bmatrix} 0 \\ C_3 \end{bmatrix} Z + \begin{bmatrix} 0 \\ 1 \end{bmatrix} H_{dyn}\right)$$

The coefficients a, b and c can be arranged in a schematic called the Butcher tableau:

c_1	a_{11}	a_{12}	a_{13}	a_{14}	=	0	0	0	0	0
c_2	a_{21}	a_{22}	a_{23}	a_{24}		1/2	1/2	0	0	0
c_3	a_{31}	a_{32}	a_{33}	a_{34}		1/2	0	1/2	0	0
c_4	a_{41}	a_{42}	a_{43}	a_{44}		1	0	0	1	0
	b_1	b_2	b_3	b_4			1/6	1/3	1/3	1/6

For the first order system of equations as given in equation (3.13) the Runge-Kutta algorithm remains unchanged, the variables are simply replaced by vectors.

B.2. Variable step method (Cash-Karp)

The Cash-Karp method is an extended Runge-Kutta method and thus structured and solved in the same way. The difference is that both a fourth and fifth order method are used to estimate the truncation error at each time step. This truncation error is compared to a desired maximum error Δ_0. If the truncation error is larger than the desired error the calculation step is repeated with a smaller step size until the error condition is met. The solution is then set to the fifth order approximation and the next time step is then initiated. The implementation of the varying step size has been taken from Press [22]. The Butcher tableau for the Cash-Karp method is:

0	0					
1/5	1/5	0				
3/10	3/40	9/40	0			
3/5	3/10	-9/10	6/5	0		
1	-11/54	5/2	-70/27	35/27	0	
7/8	1631/55296	175/512	575/13824	44275/110592	253/4096	0
	37/378	0	250/621	125/594	0	512/1771
	2825/27648	0	18575/48384	13525/55296	277/14336	1/4

The first row of the b-coefficients is the fourth order approximation to the system (b_i^*) and the second row the fifth order approximation (b_i). The difference between the two (local error) can be described with:

$$\Delta = \sum_{1}^{6} (b_i - b_i^*) k_i$$

For the simulations other than the test case a desired maximum error, relative to the dependent variables and the system of equations, is defined in order to keep the factional errors constant.

$$\Delta_0 = max\left[eps\left(|\underline{x}| + |h\,\underline{\dot{x}}|\right)\right]$$

where eps is the overall tolerance level. The recommended time step for the next calculation step is:

$$h_{new} = \begin{cases} 0.9h_{old}\left|\frac{\Delta}{\Delta_0}\right|^{0.2} & \Delta \geq \Delta_0 \\ \\ 0.9h_{old}\left|\frac{\Delta}{\Delta_0}\right|^{0.25} & \Delta < \Delta_0 \end{cases}$$

It is advisable to put in a safety factor of 0.9 in the step size change, because the estimates of error are only indicative and not exact.

C

Theory of decay analysis

From the recorded decay curves of the various decay/free extinction tests the damping coefficients may be derived from the decrease of motion amplitude for two successive oscillations. Also the natural periods may be derived from the tests.

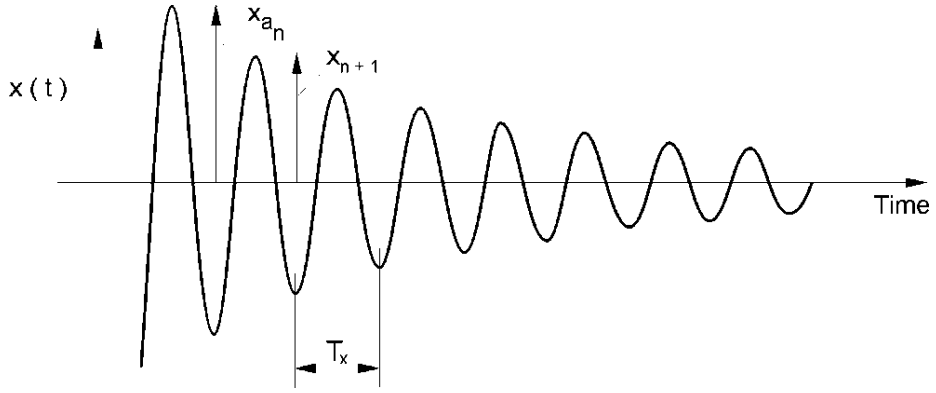

x(t) = time history of motion x

x_{a_n} = motion amplitude of n-th oscillation

T_ϕ = natural period of motion x.

If the motion x(t) during a free extinction test is described by:

$$a_x . \ddot{x} + b_x^{(1)} . \dot{x} + b_x^{(2)} . \dot{x} . |\dot{x}| + c_x . x = 0$$

where:

a_x = total mass (ship mass + added mass) in mode x

$b_x^{(1)}$ = linear damping coefficient in mode x

$b_x^{(2)}$ = quadratic damping coefficient in mode x

c_x = restoring coefficient in mode x

the linear and quadratic damping coefficients are found in the following way:

When the decrease of motion amplitude divided by the mean motion amplitude is plotted versus the mean motion amplitude the damping coefficients are determined by:

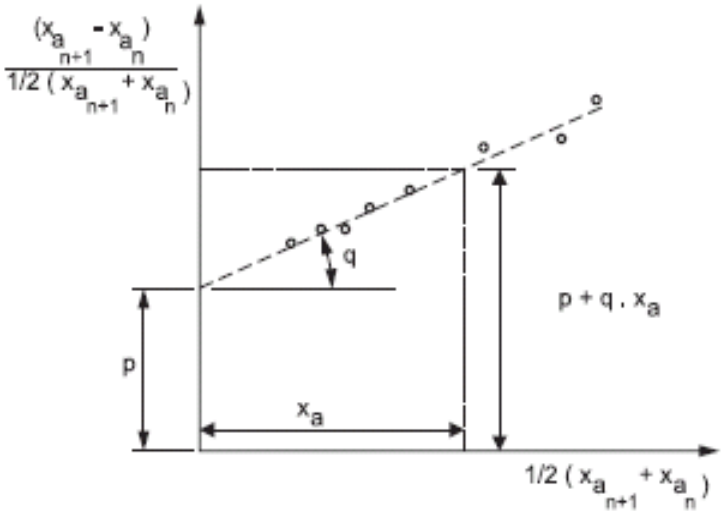

$$b_x^{(1)} = 2 . p . \frac{a_x}{T_x} \qquad b_x^{(2)} = \frac{3}{8} . q . a_x$$

In order to be able to determine the values p and q a line has been fitted through the data points found from the decay tests.

The equivalent linearised damping at a particular amplitude x_a follows from the effective "p" value at that amplitude according:

$$b_x = \frac{(p + q . x_a)}{2\pi} . b_{CR} = \frac{(p + q . x_a)}{2\pi} . 2 . \sqrt{a_x . c_x} = \frac{(p + q . x_a)}{2\pi} . \frac{T_x}{\pi} . GM . \Delta . g$$

In the above T_x denotes the roll period and GM.Δ.g the restoring term in roll (the product of transverse GM and displacement weight Δ.g in kN).

D

RAOs for all motion directions

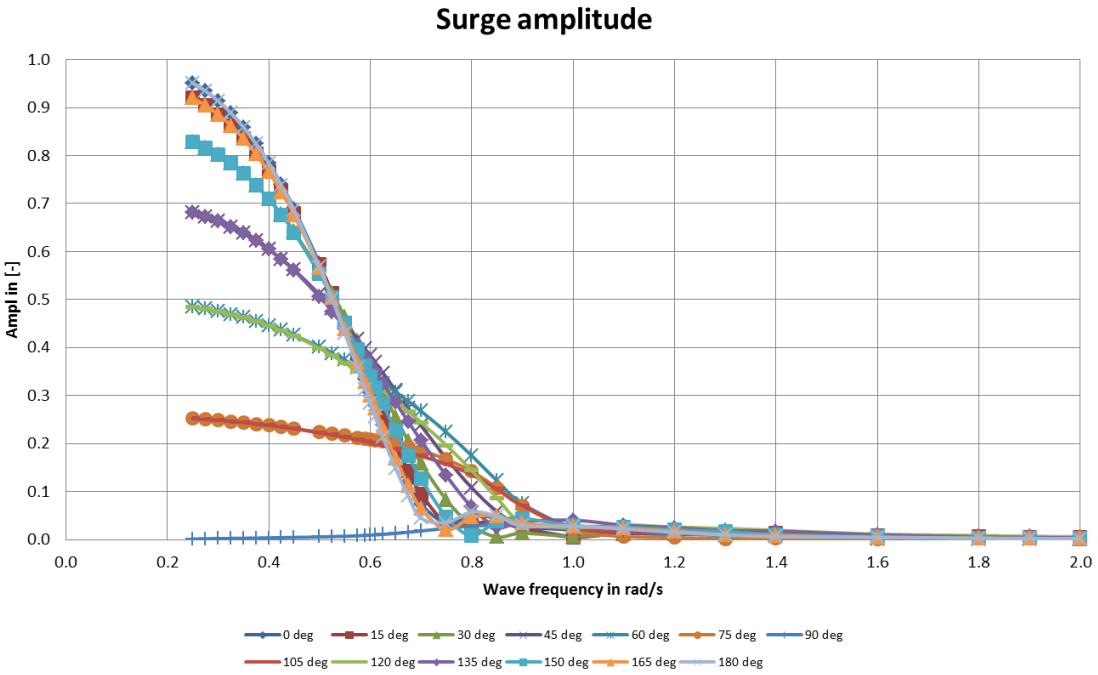

(a) excluding tank action

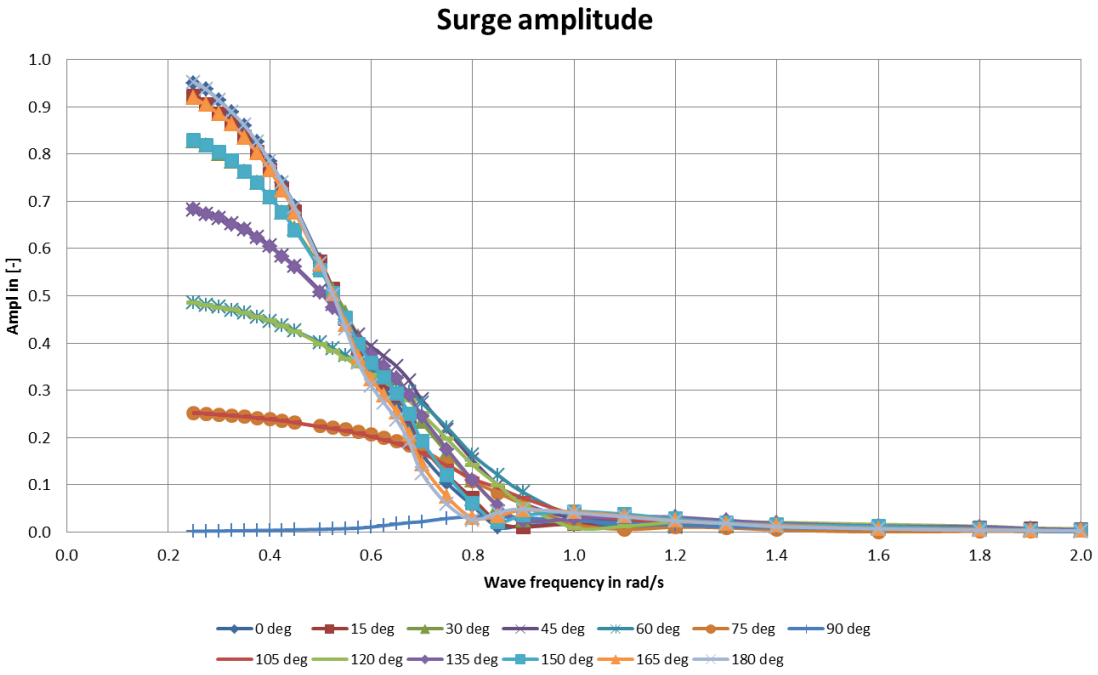

(b) including tank action

Figure D.1: RAOs for surge with the tuned tank in a regular wave

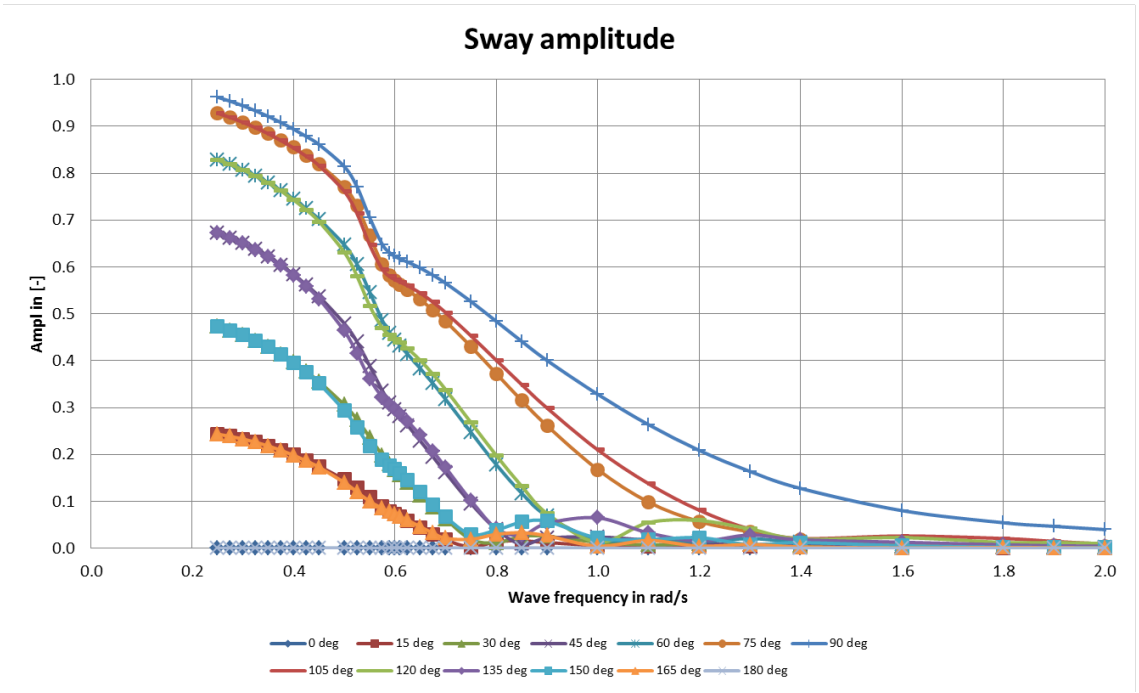

(a) excluding tank action

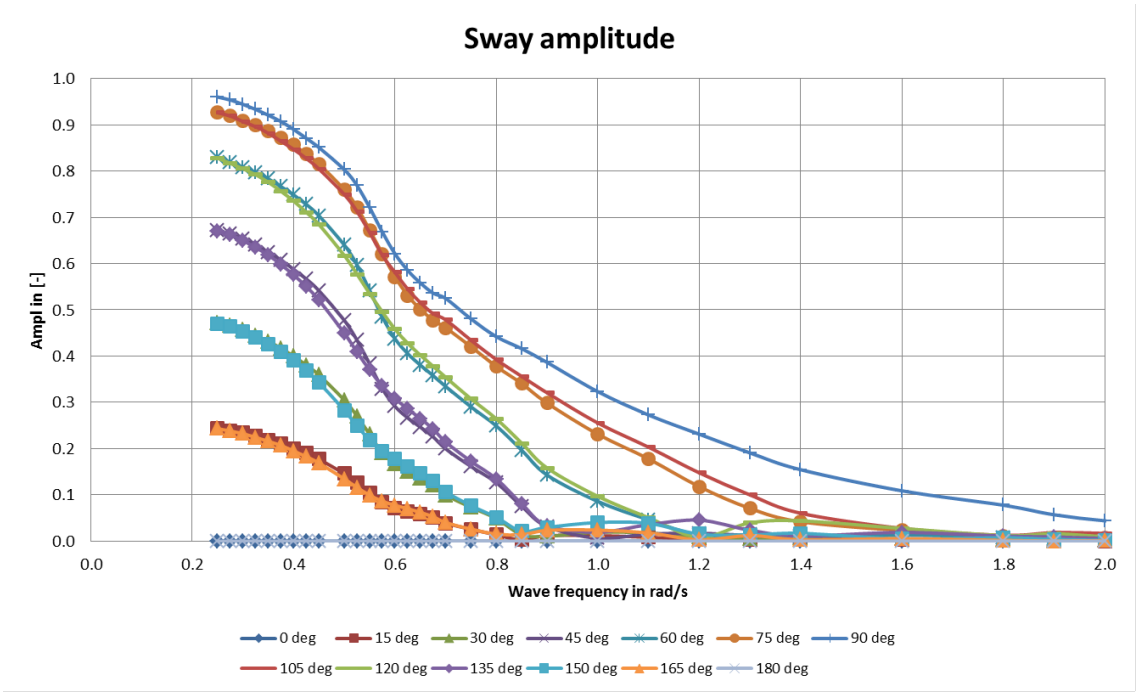

(b) including tank action

Figure D.2: RAOs for sway with the tuned tank in a regular wave

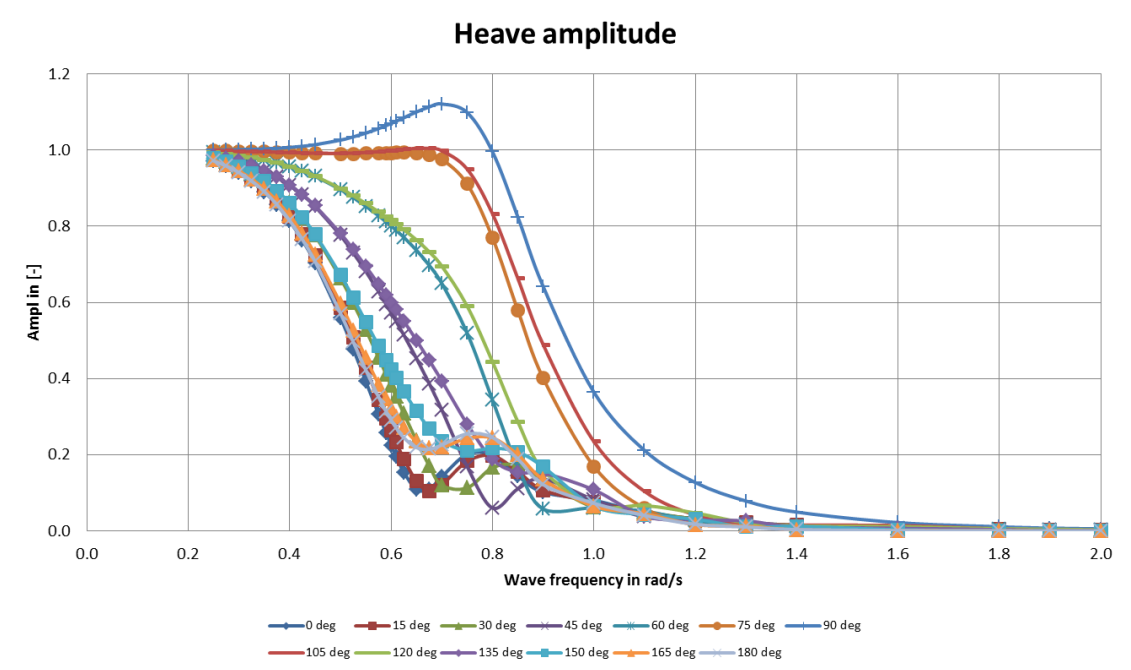

(a) excluding tank action

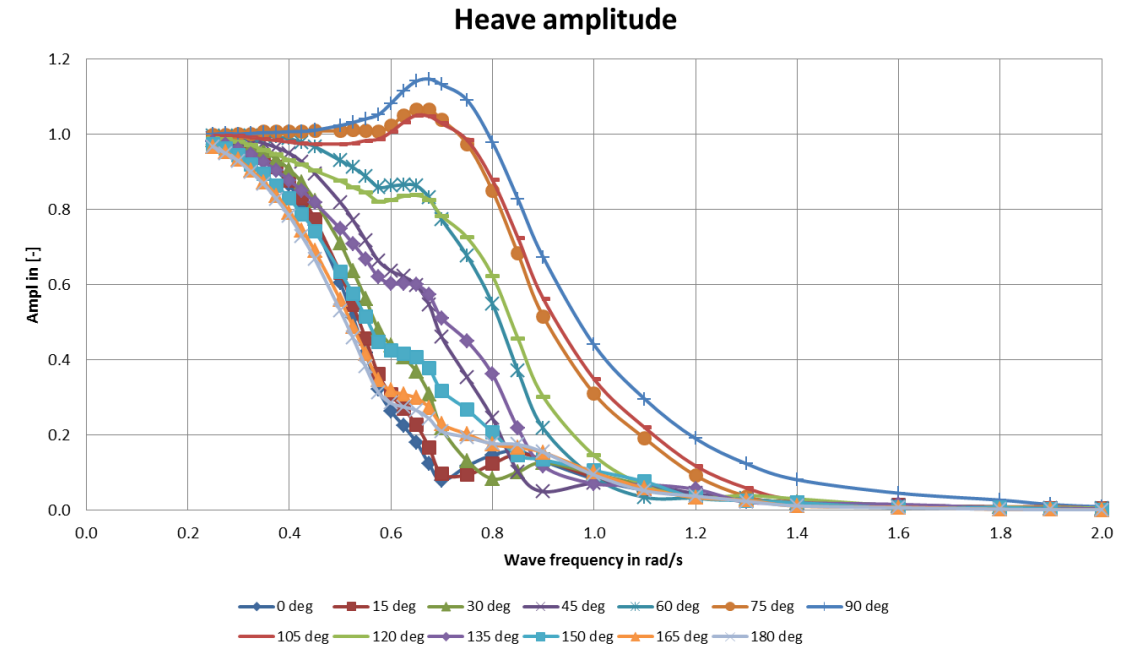

(b) including tank action

Figure D.3: RAOs for heave with the tuned tank in a regular wave

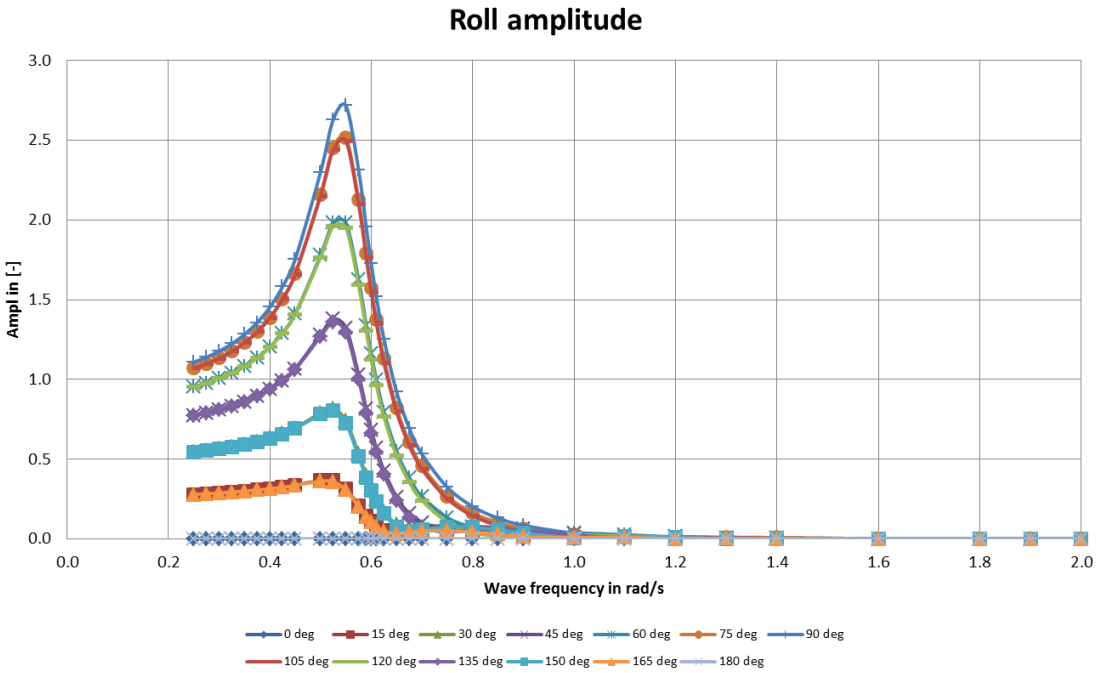

(a) excluding tank action

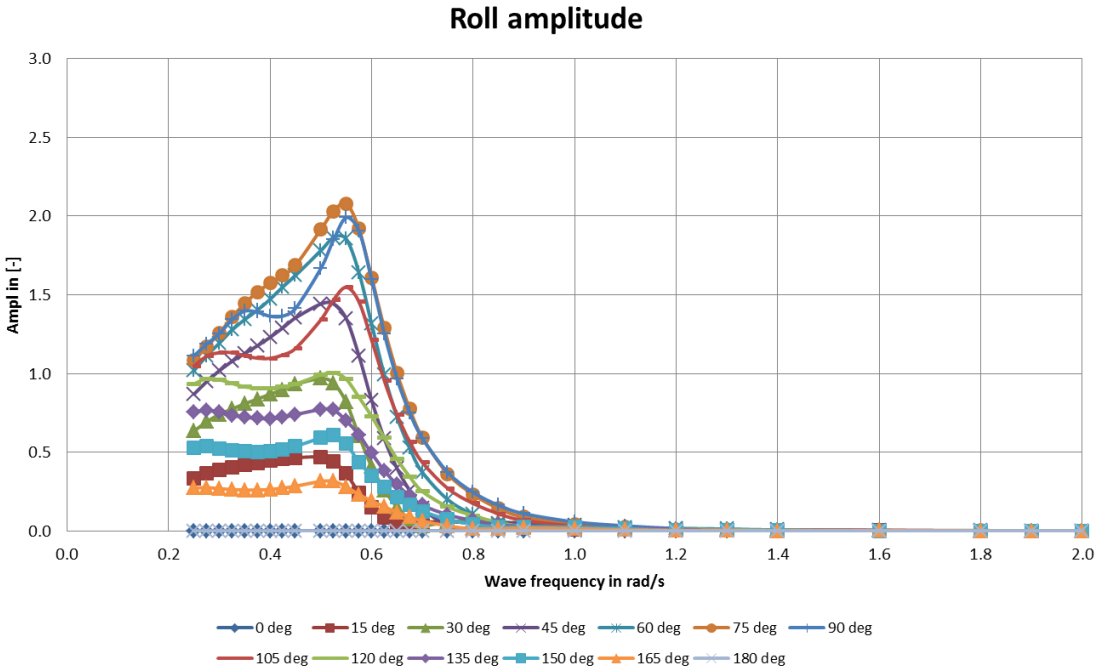

(b) including tank action

Figure D.4: RAOs for roll with the tuned tank in a regular wave

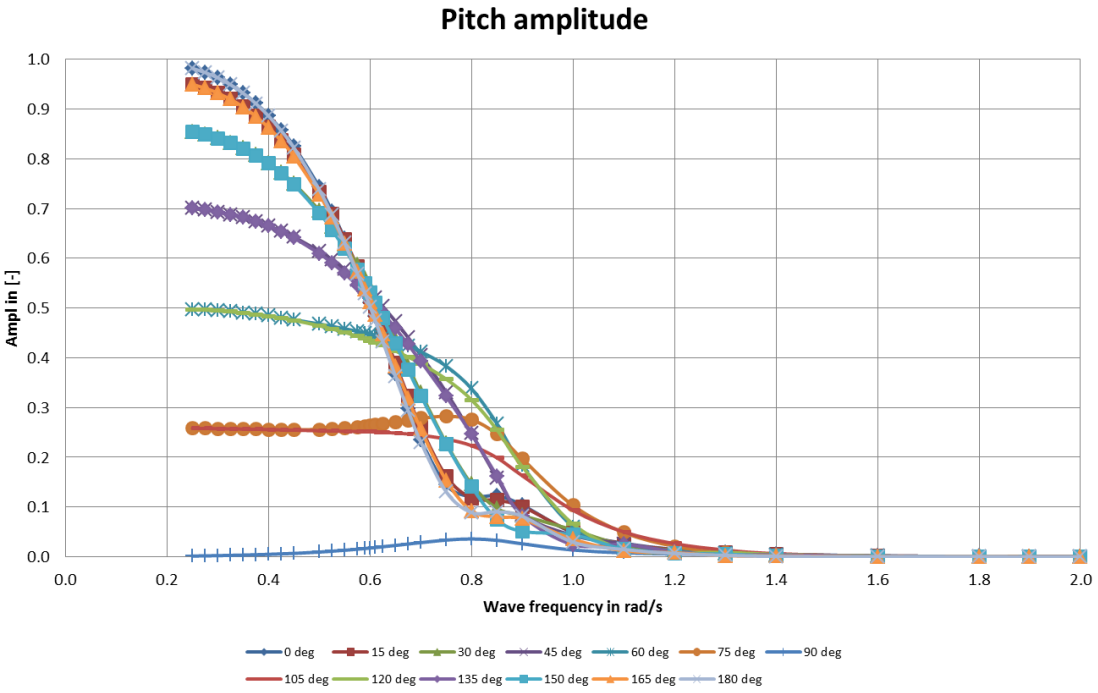

(a) excluding tank action

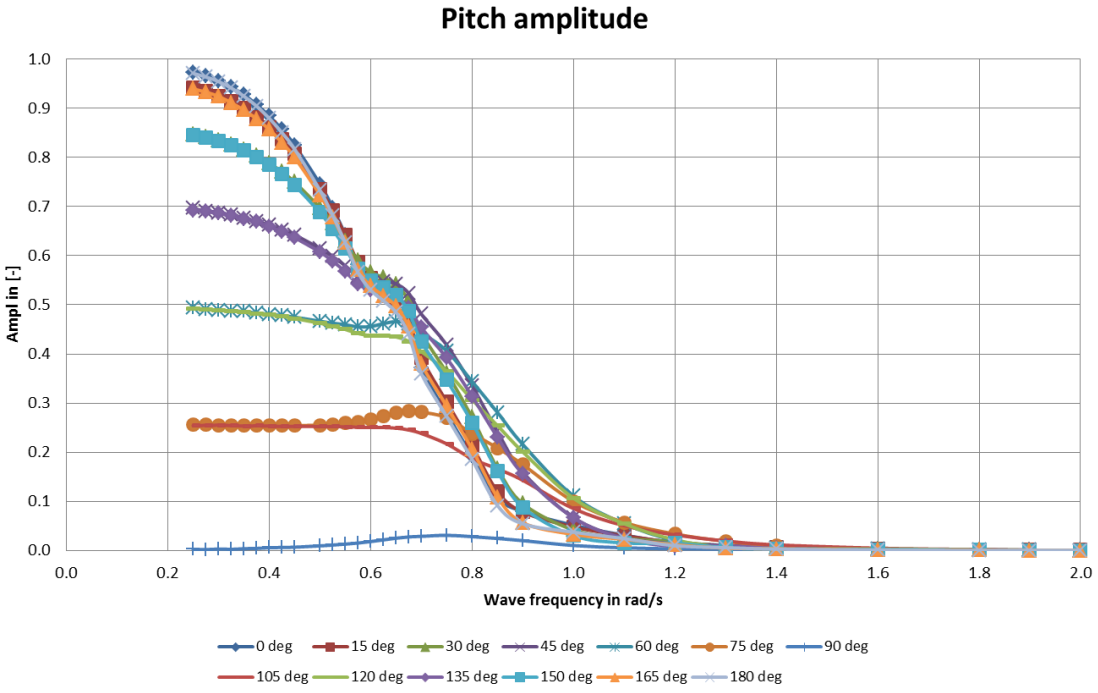

(b) including tank action

Figure D.5: RAOs for pitch with the tuned tank in a regular wave

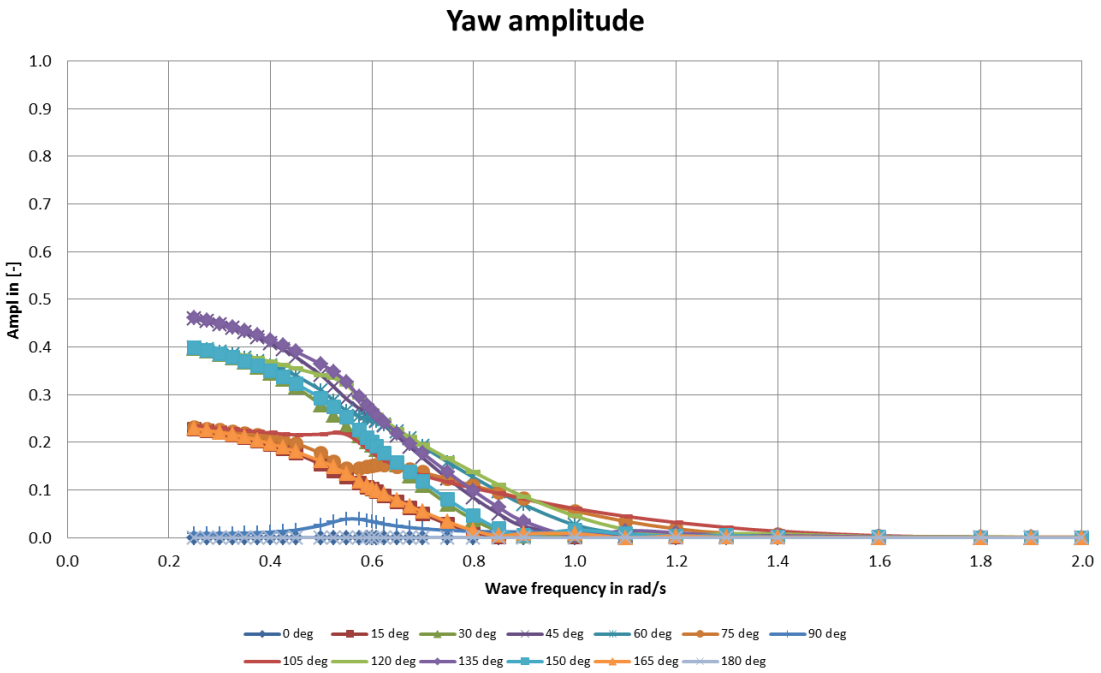

(a) excluding tank action

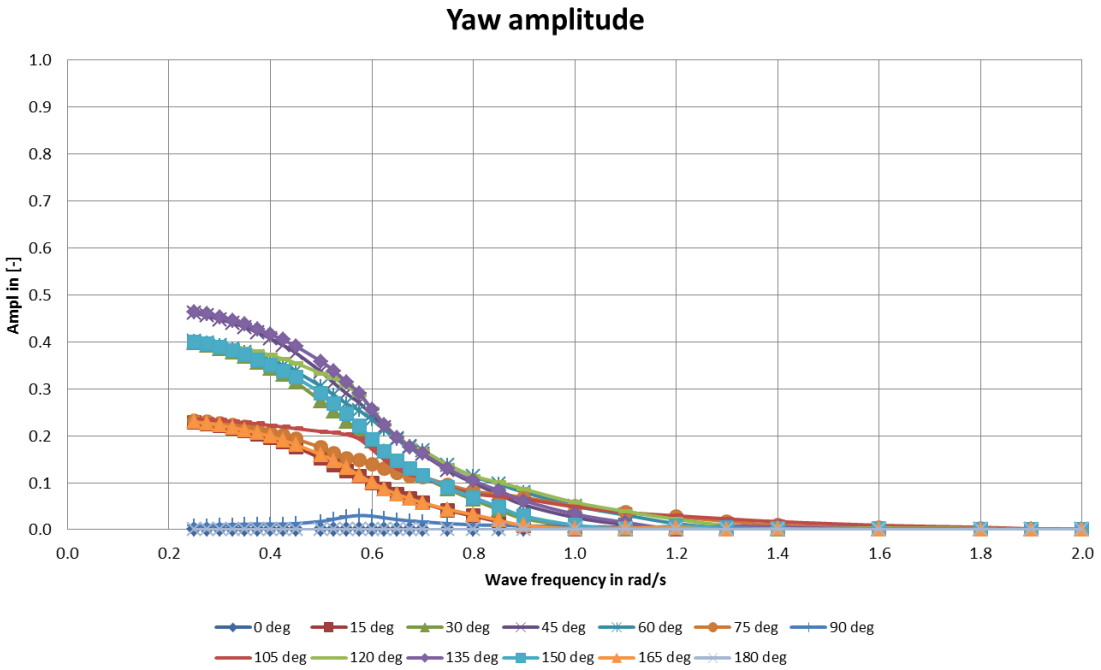

(b) including tank action

Figure D.6: RAOs for yaw with the tuned tank in a regular wave